# SEASONAL METABOLISM OF BROWN ADIPOSE TISSUE AND BRAIN MITOCHONDRIA IN THE THIRTEEN-LINED GROUND SQUIRREL (*Ictidomys tridecemlineatus*)

A Thesis
SUBMITTED TO THE FACULTY OF
UNIVERSITY OF MINNESOTA
BY

Mallory Anne Ballinger, B.S.

IN PARTIAL FULFILLMENT OF THE REQUIREMENTS
FOR THE DEGREE OF
MASTER OF SCIENCE

Matthew T. Andrews

August 2015

**Acknowledgements**

I would like to acknowledge and thank the chair of my Master's committee, Dr. Matthew Andrews, and the other members of my committee, Dr. Marshall Hampton and Dr. Ahmed Heikal. I would also like to thank the Integrated Biosciences Graduate Program, the UMD Department of Biology, and the University of Minnesota Center for Mass Spectrometry and Proteomics for their assistance and resources. Lastly, I am very appreciative of Mr. James Bjork and Dr. Christine Schwartz, for their patience, guidance, and technical assistance in the laboratory.

**Abstract**

During the hibernation season, thirteen-lined ground squirrels (*Ictidomys tridecemlineatus*) regularly cycle between bouts of torpor and interbout arousal (IBA). This presents a unique seasonal change in energy requirements in both the brain and brown adipose tissue (BAT). We hypothesized that brain and BAT mitochondria undergo a seasonal change in function to accommodate the variable energy demands of hibernation. To test this hypothesis, we examined mitochondrial bioenergetics of brain and BAT in thirteen-lined ground squirrels across five time points: summer, fall, torpor, IBA and spring. Through various molecular and functional analyses, we found significant increases in mitochondrial oxidative capacities of both brain and BAT during torpor and IBA. Overall, brain and BAT mitochondrial bioenergetics are not static across the year, and our studies suggest that these two tissues function efficiently during the hibernation season, when extreme physiological changes are occurring. These studies provide improved understanding of the overall energy requirements of a hibernator.

## Table of Contents

## List of Tables

## List of Figures

## List of Figures (continued)

# CHAPTER 1: Introduction

## SECTION 1.1: HIBERNATION

Evolution of Hibernation

Energy flow is central to the history and existence of life. Throughout the 3-4 billion year saga of life on Earth, biological systems have incorporated and evolved elaborate techniques to both harness and utilize the energy provided by the sun. Therefore, one of the major goals of integrated science is to understand the parameters of energy flow throughout the biosphere and its biological systems.

Certainly, one of the most important events in vertebrate evolution was the acquisition of endothermy - the ability of an organism to use metabolic heat production to elevate core body temperature above ambient temperature (Kemp, 2006). Within endothermy, some mammals have evolved to a state of homeothermy, where they maintain a constant body temperature (approximately 35-38$^{o}$C) despite continuous temperature variations in their environment (Lyman et al., 1982; Melvin & Andrews, 2009; Ruf & Geiser, 2014). The ability to maintain a constant body temperature has contributed to the evolutionary success of mammals, allowing this group to invade and inhabit unoccupied niches and become distributed worldwide (Kemp, 2006; Melvin & Andrews, 2009).

Despite the tremendous evolutionary advantage of homeothermy, it is energetically costly to maintain when environmental conditions become unfavorable (i.e. low external temperatures, scarcity of food and energy resources, etc.; Ruf & Geiser, 2014; Lyman et al., 1982). To combat these unfavorable conditions, natural selection has

favored mammals that adapt and respond to these environmental fluctuations via heterothermy (Geiser & Körtner, 2010; Geiser, 1998). Heterotherms are able to conserve energy by substantially reducing body temperature and metabolic rate; hence, they enter a state of torpor (Ruf & Geiser, 2014; Lyman et al., 1982).

Torpor is a highly successful adaptation that discrete mammals employ to cope with periods of variable nutritional and climatic conditions (Melvin & Andrews, 2009). Various degrees of torpor are observed over a phylogentically wide range of mammals (Melvin & Andrews, 2009). All three of the major divisions of the class Mammalia (Prototheria, Metatheria and Eutheria) contain hibernators, despite their relatively distant evolutionary relationship (Carey et al., 2003). Two general patterns of torpor are widely recognized. The first of these, daily torpor, lasts only a few hours and body temperature is usually maintained between 10-25$^{o}$C (Carey et al., 2003). Prolonged torpor, or hibernation, is the second common pattern of torpor, and will be the primary adaptation mechanism examined in this thesis. This biological adaptation is the product of tens of millions of years of evolution and results from the selective expression of the genes common to all mammals (reviewed in Carey et al. (2003). The hibernation phenotype is also variable across species, with the arctic ground squirrel (*Urocitellus parryii*) on the extreme end of the spectrum with body temperatures recorded below 0$^{o}$C (Barnes, 1989).

Mammalian hibernation encompasses a unique energy flow system that transitions between both homeothermy and heterothermy (Ruf & Geiser, 2014; Geiser & Körtner, 2010; Geiser, 1998; Lyman et al., 1982). In general, when hibernators are exposed to low ambient temperatures, they alter their physiological states to conserve

energy, which includes: 90% reduction of their basal metabolic rate; significant decrease in body temperature (body temperature drops between 0-10$^{o}$C); substantial declines in heart rate, oxygen consumption and carbon dioxide production; and physical inactivity for 10-14 days (Carey et al., 2003; Geiser, 2004; Lyman et al., 1982; Ruf & Geiser, 2014; Storey & Storey, 2010). Thus, mammalian hibernation has traditionally been regarded as a crucial adaptation that permits reduced energy expenditure during unfavorable conditions, such as periods of low ambient temperatures, food shortages, etc. (Bieber et al., 2014). The enormous reduction of energy expenditure during hibernation is widely viewed as the key to survive these life-challenging conditions (Melvin & Andrews, 2009).

Model System: Thirteen-Lined Ground Squirrel

The thirteen-lined ground squirrel (*Ictidomys tridecemlineatus*) is a small, obligate hibernator, and is the research organism used for the studies reported in this thesis. It is found across a wide range of latitudes, from southern Canada to the Gulf of Mexico. In northern habitats, with long winters and limited food resources, ground squirrels breed only once a year (late spring) and then hibernate in underground burrows from October to April (Laursen et al., 2015). Throughout its circannual cycle, the thirteen-lined ground squirrel transitions between states of homeothermy and heterothermy. Homeothermy is mainly characterized by constant normothermic body temperature, such as the summer, where ground squirrels are physically preparing for the upcoming hibernation season by greatly increasing white adipose stores (Carey et al.,

2003). During this state of hyperphagia, ground squirrels double or even triple their body weights in the preceding months (Carey et al., 2003). In early autumn, while the squirrels are still active, their food consumption drops dramatically and they begin to go through test bouts where they drop their body temperature to room temperature periodically (Schwartz et al., 2015; Figure 1.1).

As ground squirrels transition out of homeothermy and into heterothermy (i.e. hibernation), their physiology changes dramatically. The physiological characteristics of the thirteen-lined ground squirrel during hibernation include body temperatures ranging from 2-10$^{o}$C, oxygen consumption that holds at 2-3% of the aroused condition, and heart rate as low as 3-10 beats per minute, compared to 300-400 beats per minute when the animal is awake and active (Andrews, 2007). Hypoxemia is thought to be avoided during torpor as metabolic rate declines in concert with perfusion levels during entry into and maintenance of torpor to match oxygen delivery with demand (Hindle & Martin, 2013). The torpid state is not continually maintained throughout the hibernation season, but rather is interrupted by a series of interbout arousals (IBAs) during which the animal rapidly rewarms to the aroused state (Hampton et al., 2010; Figure 1.1). The spontaneous arousal from torpor to IBA takes an average of 2.8 hours in the thirteen-lined ground squirrel (Hampton et al., 2010; Figure 4A). IBAs occur every 1-2 weeks and are characterized by rapid whole body re-warming and a resumption of normothermic metabolic activity for 12-24 hours (Hampton et al., 2013). During this transition out of torpor, oxygen consumption increases 50-fold, heart rate explodes from less than 10 beats per minute to over 400 beats per minute, and body temperature increases from 5 to 37$^{o}$C

(Hampton et al., 2010). After an IBA, the animals return into a state of torpor, with January and February containing the longest average torpor bouts (Schwartz & Andrews, 2013). Spring represents the post-hibernation time point, where animals transition from heterothermy to homeothermy, with body temperature, heart rate, and metabolism returning back to normothermic rates (Carey et al., 2003; Figure 1.1). Additionally, thirteen-lined ground squirrels emerge much thinner compared to when they began hibernating, and they begin preparing for the reproductive season.

Metabolism and Fuel Selection

With two different homeostatic changes during the circannual cycle (active homeothermy and winter heterothermy), thirteen-lined ground squirrels utilize different fuel substrates during different times of the year. Amid spring, summer, and fall active time points, when food is readily available, energy enters the metabolic cycle in the form of carbohydrates. During hibernation, the main pathway for energy production shifts from glucose utilization to lipid consumption (Storey & Storey, 2004). Thirteen-lined ground squirrels rely on stored lipid as their primary fuel source during hibernation, evidenced by the absence of feeding, a reduction in white adipose tissue mass, and a respiratory quotient of 0.7 (Andrews, 2004; Andrews, 2007). In fact, the switch from a carbohydrate-based metabolism to one that relies on stored fat has been the subject of intense study over the last several years (Andrews et al., 1998; Andrews, 2004; Buck et al., 2002; Carey et al., 2003; MacDonald & Storey, 2005).

Furthermore, the heart and brain of hibernating ground squirrels preferentially use lipid-derived ketones as fuel (Andrews et al., 2009). More specifically, at low body temperatures, glucose and the ketone D-β-hydroxybutyrate are both transported across the blood-brain-barrier, but D-β-hydroxybutyrate is used preferentially, thus highlighting the strict conservation of carbohydrates (Andrews et al., 2009). In the heart, for example, both substrates are catabolized, but only carbon atoms derived from D-β-hydroxybutyrate enter the tricarboxylic acid (TCA) cycle (Andrews et al., 2009). This is due to increased expression of pyruvate dehydrogenase kinase, isoform 4 in the heart which blocks conversion of the glycolytic product pyruvate to acetyl-CoA; whereas catabolism of D-β-hydroxybutyrate results in two molecules of acetyl-CoA that directly enter the TCA cycle (Andrews et al., 2009; Buck et al., 2002; Russeth et al., 2006). In addition, lipid mobilized from white adipose tissue may signal when lipid stores are sufficient for entry into torpor and/or initiate the switch from carbohydrate to lipid-based catabolism (Melvin & Andrews, 2009).

## Section 1.1 Figures & Tables

**Figure 1.1. Circannual cycle of a thirteen-lined ground squirrel.** Body temperature was measured using a surgically implanted transmitter. The dashed lines represent the ambient (environmental) temperature. Homeothermy is characterized by constant normothermic body temperature, such as spring and summer, where ground squirrels are physically preparing for the upcoming hibernation season by greatly increasing white adipose tissue stores. During early fall, while the squirrels are still active, their food consumption drops dramatically and they begin to go through test bouts where they drop their body temperature to room temperature periodically. Heterothermy is characterized by hibernation, where during torpor, changes in body temperature, heart rate and oxygen consumption decrease immensely. Periodic interbout arousals (IBAs) are observed as regular spikes in body temperature despite a constant ambient temperature of 5°C during hibernation.

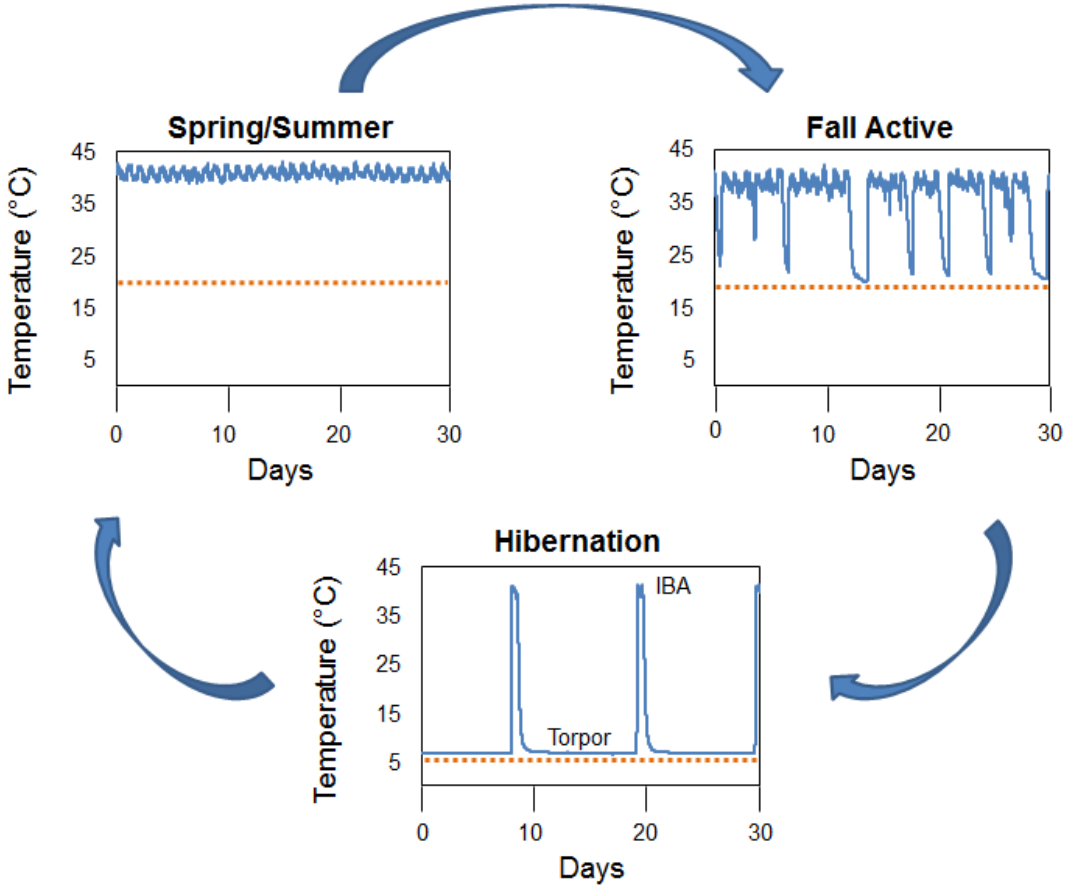

## SECTION 1.2: INTRODUCTION TO MITOCHONDRIA

The content presented in Section 1.2 is largely derived from Nelson et al. (2008).

### Introduction

Energy enters an organism through various sources (e.g. fats, carbohydrates, protein) and is converted into chemical energy (i.e. ATP) via oxidative phosphorylation for various cellular processes. Mitochondria are the site for oxidative phosphorylation in eukaryotic cells, and are the center of the final stages of cellular respiration in which the energy of oxidation drives the synthesis of ATP (Figure 1.2). Mitochondria have both an outer and inner membrane, and the inner membrane bears the components of the respiratory system and ATP synthase. Additionally, the mitochondiral matrix, enclosed by the inner membrane, contains the pyruvate dehydrogenase complex and the enzymes of the TCA cycle, the fatty acid β-oxidation pathway, and other pathways of fuel oxidation (except for glycolysis, which takes place in the cytosol). Specific transporters carry pyruvate and fatty acids into the matrix for access to the machinery of the TCA cycle (Figure 1.2).

Oxidative phosphorylation involves the reduction of oxygen to water with electrons donated by reducing equivalents, such as NADH and $FADH_2$. This is all accomplished through various mitochondrial enzymes and proteins associated with metabolic processes. Oxidative phosphorylation begins with the entry of electrons into the electron transport system (ETS), and these electrons mostly funnel through the universal electron acceptors, NADH and $FADH_2$.

Electron Transport System

The electron transport system is a series of enzymes associated with the inner membrane of mitochondria that catalyze the transfer of electrons derived from the oxidation of energetic substrates (Figure 1.3). Each electron transfer releases free energy (and heat), which is used to pump protons from the mitochondrial matrix to the space between the inner and outer mitochondrial membranes, thereby generating a proton gradient. This gradient is used to synthesize ATP (or heat), which can be used to power energetic reactions in the cell.

Four main complexes (complex I-IV) and ATP synthase (complex V) make up the ETS (Figure 1.3; Table 1.1). Complex I (NADH dehydrogenase) is the largest complex (~980 kDA) with 45 subunits (Carroll et al., 2006; Efremov et al., 2010; Table 1.1). It receives electrons from NADH, and then passes the electrons to ubiquinone while pumping four protons into the intermembrane space (Figure 1.3). Complex II (succinate dehydrogenase) is the smallest complex of the ETS (Table 1.1), and obtains electrons directly from the TCA cycle. Specifically, as succinate goes to fumarate, $FADH_2$ is produced and delivers the electrons to complex II (Figure 1.3). Electrons from complex II are then passed to ubiquinone without the simultaneous pumping of protons into the intermembrane space. In fact, unlike complexes I, III and IV, complex II does not contribute to the proton gradient, and as a result, more ATP is generated from NADH (2.5 ATP) than $FADH_2$ (1.5 ATP). Electrons from ubiquinone are transferred to complex III (cytochrome bc1 complex), which then passes electrons to cytochrome c while pumping four protons into the intermembrane space (Figure 1.3). Lastly, cytochrome c

hands the electrons to complex IV (cytochrome oxidase). In this final step, oxygen is reduced to water and as a result, two protons are pumped out of the matrix and into the intermembrane space. The proton gradient formed from electron transfer through the electron transport system can be used to synthesize ATP via complex V (ATP synthase). Briefly, protons flow back into the matrix through complex V, resulting in ATP formation which can then be used for various cellular processes (Figure 1.3).

Measuring Bioenergetic Properties of the ETS

The rate of oxidative phosphorylation in isolated mitochondria can be estimated by measuring the rate of oxygen consumption through the various ETS complexes. Chance & Williams (1955) termed these rates of oxygen consumption as *state 3* and *state 4* respiration rates. *State 3* respiration is defined as ADP-stimulated respiration of isolated, coupled mitochondria. It is a near-maximal state of oxygen consumption and ATP synthesis, and is measured in the presence of saturating concentrations of oxygen, energetic substrates and ADP. S*tate 3* is obtained when there is an increase in oxygen consumption with the addition of ADP in the presence of excess substrate. *State 4* respiration is the maximal respiration rate of isolated mitochondria that has no influence on ATP synthesis. In fact, it is termed the "non-phosphorylating" respiration rate because it does not generate ATP; instead, it is the maximal rate of respiration in the presence of excess substrate and can be obtained by inhibiting ATP synthase with oligomycin or other ATP synthase inhibitors.

Moreover, to assess the integrity of the mitochondrial inner membranes of isolated mitochondrial fractions, the respiratory control ratio (RCR) can be measured. The RCR of isolated mitochondria is the ratio between *state 3* and *state 4*, and is an indicator of coupling efficiency between substrate oxidation and ATP synthesis (Chance & Williams, 1955; Zhang et al., 2012). A high ratio is indicative of well-coupled mitochondria, while a low ratio is indicative of damaged or uncoupled mitochondria.

## Section 1.2 Figures & Tables

**Figure 1.2. Metabolic pathways associated with mitochondria.** Fuel derived from fatty acids or glucose enter mitochondria through various transporters. Once inside mitochondria, fatty acid derivatives are metabolized through β-oxidation pathways. Alternatively, glucose derivatives enter mitochondria through pyruvate. 1) Metabolic entities derived from β-oxidation for pyruvate metabolism can enter the tricarboxylic acid (TCA) cycle as acetyl-CoA. 2) The TCA cycle consists of various enzymes that breakdown (catabolize) substrates and pass the derived electrons to either NADH or $FADH_2$. 3) NADH and $FADH_2$ pass electrons onto the electron transport system for oxidative phosphorylation. ATP and heat are generated by the electron transport system and can be used for various cellular processes.

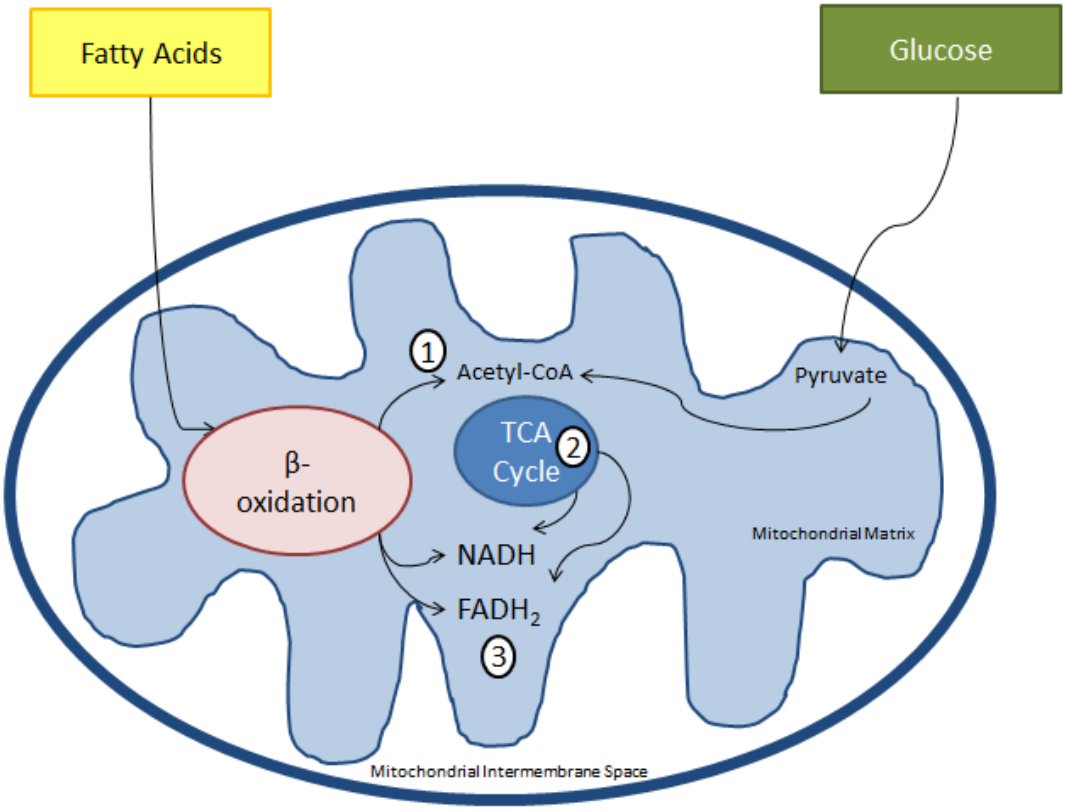

**Figure 1.3. Electron transport system in isolated mitochondria.** The electron transport system (ETS) is a series of enzymes associated with the inner membrane of mitochondria that catalyze the transfer of electrons derived from the oxidation of energetic substrates. Each electron transfer releases free energy (and heat) which is used to pump protons. NADH is oxidized by complex I and succinate by complex II. Electrons from these substrates are transferred to the mobile carrier ubiquinone, which transfers them to complex III, and subsequently to complex IV via cytochrome c (Cy C). Approximately 40% of free energy released by substrate oxidation is used by complexes I, III and IV to pump protons from the matrix to the intermembrane space. When activated, protons flow from the intermembrane space through ATP synthase (complex V) into the matrix, stimulating substrate oxidation and ATP synthesis.

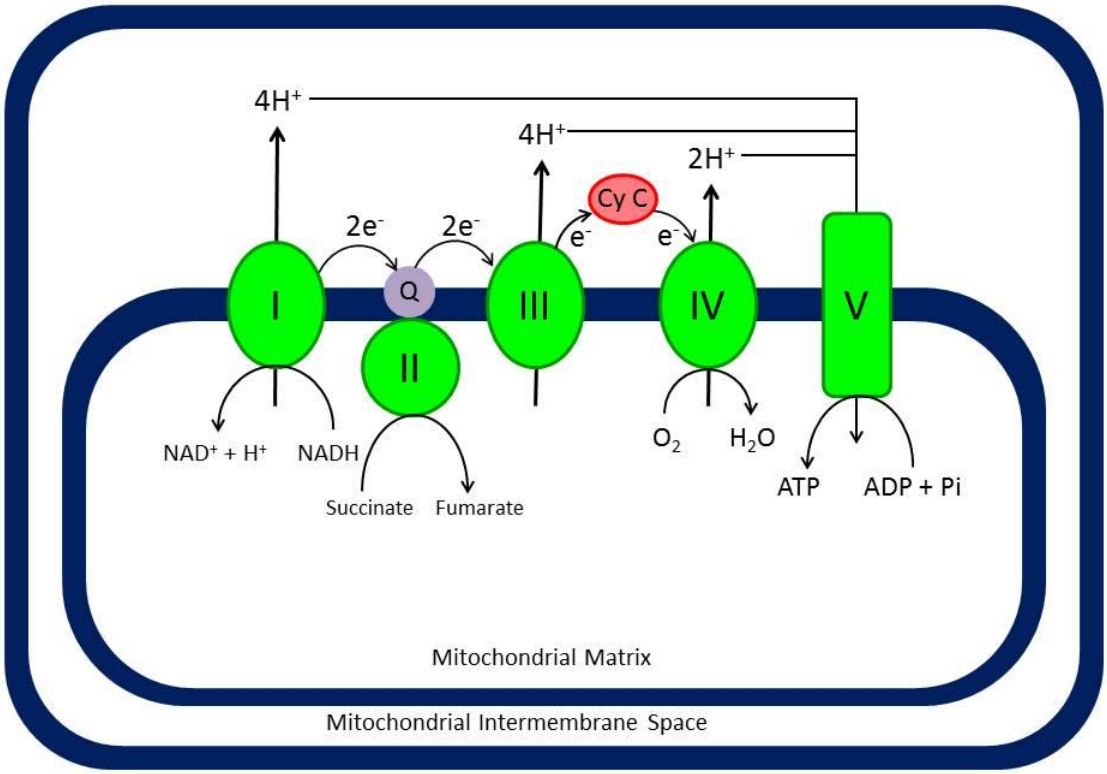

**Table 1.1. The protein components of the electron transport system (ETS).** The number of subunits and subunits encoded by mitochondrial DNA are listed for the five enzyme complexes of the ETS. (*Adapted and modified from* Nelson et al. (2008).

| The Protein Components of the Electron Transport System (ETS) | | |
|---|---|---|
| Enzyme Complex/Protein | Number of subunits | Number of subunits encoded by mitochondrial DNA (genes) |
| I NADH Dehydrogenase | 45 | 7 *(ND1, ND2, ND3, ND4L, ND4, ND5, ND6)* |
| II Succinate Dehydrogenase | 4 | 0 |
| III Cytochrome bc1 complex | 11 | 1 *(Cyt b)* |
| IV Cytochrome oxidase | 13 | 3 *(COI, COII)* |
| V ATP Synthase | 8 | 2 *(ATPase6, ATPase8)* |

## SECTION 1.3: BROWN ADIPOSE TISSUE

Introduction

Brown adipose tissue (BAT) specializes in the burning of fat, and is responsible for adaptive, nonshivering thermogenesis in mammals (Cannon & Nedergaard, 2004; Nicholls & Locke, 1984). The thermogenic activity of BAT is mediated by $\beta_3$-adrenergic receptors through the stimulation of norepinephrine released from the sympathetic nervous system (De Meis, 2003; Cannon & Nedergaard, 2004). $\beta_3$-adrenergic receptors are coupled to G-proteins, which upon activation, promotes an increase of lipolysis (Breitwieser, 2002; Chaudhry & Granneman, 1999; Lowell & Spiegelman, 2000; Nicholls & Locke, 1984; Silva, 2006). The release of fatty acids promotes the uncoupling of mitochondria through activation of uncoupling protein 1 (UCP1; Boss et al., 1998; Breitwieser, 2002; Chaudhry & Granneman, 1999; Fedorenko et al., 2012; Lowell & Spiegelman, 2000; Nicholls & Locke, 1984; Nicholls & Rial, 1999; Silva, 2006). This is associated with an increase of the mitochondrial respiration rate as protons leak across the inner mitochondrial membrane (Boss et al., 1998; Lowell & Spiegelman, 2000; Nicholls & Locke, 1984; Nicholls & Rial, 1999; Silva, 2006; Skulachev, 1998).

UCP1 is a BAT-specific transport protein of the inner mitochondrial membrane (Aquila et al., 1985; Bouillaud et al., 1986; Cannon & Nedergaard, 2004; Heaton et al., 1978; Ridley et al., 1986). It is present in all placental mammals (Cannon & Nedergaard, 2004; Nicholls & Locke, 1984), and is a six-transmembrane protein that has a tripartite structure (Nedergaard et al., 2001). UCP1 is activated by long-chain fatty acids and inhibited by purine nucleoside di- and triphosphates (Fedorenko et al., 2012; Locke et al.,

1982). It is responsible for uncoupling mitochondrial respiration from oxidative phosphorylation, thereby allowing energy that would otherwise be converted to ATP to be released as heat (Cannon & Nedergaard, 2004; Fedorenko et al., 2012; Figure 1.4).

BAT Function in Hibernation:

Overall, BAT has evolved to maximize the combustion of fat to generate heat in a short amount of time (Cannon & Nedergaard, 2004). Heat generation is especially advantageous during hibernation, as it plays a vital role in endogenous rewarming of animals during arousal from torpor via non-shivering thermogenesis (Cannon & Nedergaard, 2004). In fact, the highest rate of BAT activity occurs during periodic arousals from torpor, referred to as interbout arousals (IBAs), where the animal rapidly rewarms to an aroused state in about 2.8 hours (Hampton et al., 2010; Figure 1.5A). Moreover, this heat production during arousals occurs very quickly; the animal's body temperature increases 20$^{o}$C in less than one hour while simultaneously circulating warm blood throughout the body at normothermic rates (Schwartz et al., 2015; Figure 1.5B).

The interplay between mitochondria and thermogenesis in BAT is evidenced by the elevated levels of UCP1 transcripts during hibernation (Hampton et al., 2013). Specifically, Hampton et al. (2013) found a significant increase in UCP1 transcripts in torpor and IBA compared to spring, thus further validating the importance of BAT's thermogenic ability during hibernation. However, this thermogenic capacity and activity of BAT is probably not necessary during spring or summer (i.e. homeothermy); therefore, it is hypothesized that both BAT mitochondrial regulation and function change

seasonally. Metabolism in most other tissues can essentially be halted to conserve energy during hibernation, but maintenance of BAT function at a reduced level is critical due to its heat generation needed for arousals. Most mitochondrial metabolic studies in hibernators have been conducted on the liver, which shows metabolic suppression during hibernation (reviewed in Staples (2014). Nevertheless, the liver is not a highly metabolic tissue, whereas BAT contributes significantly to whole organism metabolic rate - especially during hibernation (Staples, 2011). Therefore, how does the mitochondrial metabolism of BAT change throughout the year?

Many aspects of BAT thermogenesis during arousal have been investigated (reviewed in Cannon & Nedergaard (2004), yet there has been very little investigation of mitochondrial metabolism in BAT throughout the circannual cycle of a natural hibernator (reviwed in Staples & Brown (2008) and Staples (2014). Most investigations on hibernator BAT do not contain a thorough investigation of mitochondrial bioenergetics between homoeothermic and heterothermic periods (Burlington et al., 1969; Chaffee et al., 1966; Chaffee et al., 1964; Hook & Guzman, 1941; Houstěk et al., 1975; Malatesta et al., 2001; McKee & Andrews, 1990; Nedergaard & Cannon, 1984). Thus, one goal of this thesis is to interrogate the function of BAT mitochondria across the circannual cycle using integrated approaches from gene expression to function. The BAT transcriptome of the thirteen-lined ground squirrel has recently been generated (Hampton et al., 2013), providing inferences on molecular mechanisms of BAT mitochondria. However, mRNA levels are not always correlated closely with protein abundance and function in living systems (Abreu et al., 2009; Foss et al., 2011; Gry et al., 2009; Nie et al., 2007; Pascal et

al., 2008; Yin et al., 2013). Therefore, we estimate changes in the mitochondria by producing the mitoproteome, in parallel with measurement of functional mitochondrial bioenergetics and comparison of BAT transcription. Comparing mRNA expression and the proceeding products of BAT mitochondria across the year provides insight into organelle biology (Lotz et al., 2014), in addition to elucidating the underpinnings underlying functional adaptations in BAT mitochondria in a mammalian hibernator.

## Section 1.3 Figures & Tables

**Figure 1.4. Electron transport system of brown adipose tissue mitochondria.** The electron transport system (ETS) is a series of enzymes associated with the inner membrane of mitochondria that catalyze the transfer of electrons derived from the oxidation of energetic substrates. Each electron transfer releases free energy (and heat) which is used to pump protons. NADH is oxidized by complex I and succinate by complex II. Electrons from these substrates are transferred to the mobile carrier ubiquinone (Q), which transfers them to complex III, and subsequently to complex IV via cytochrome c (Cy C). The inner mitochondrial membrane of mammalian brown adipose tissue contains little ATP synthase (complex V) and, uniquely, significant amounts of uncoupling protein 1 (UCP1). When activated, protons flow from the intermembrane space through UCP1 into the matrix, stimulating substrate oxidation and heat production, but no ATP synthesis.

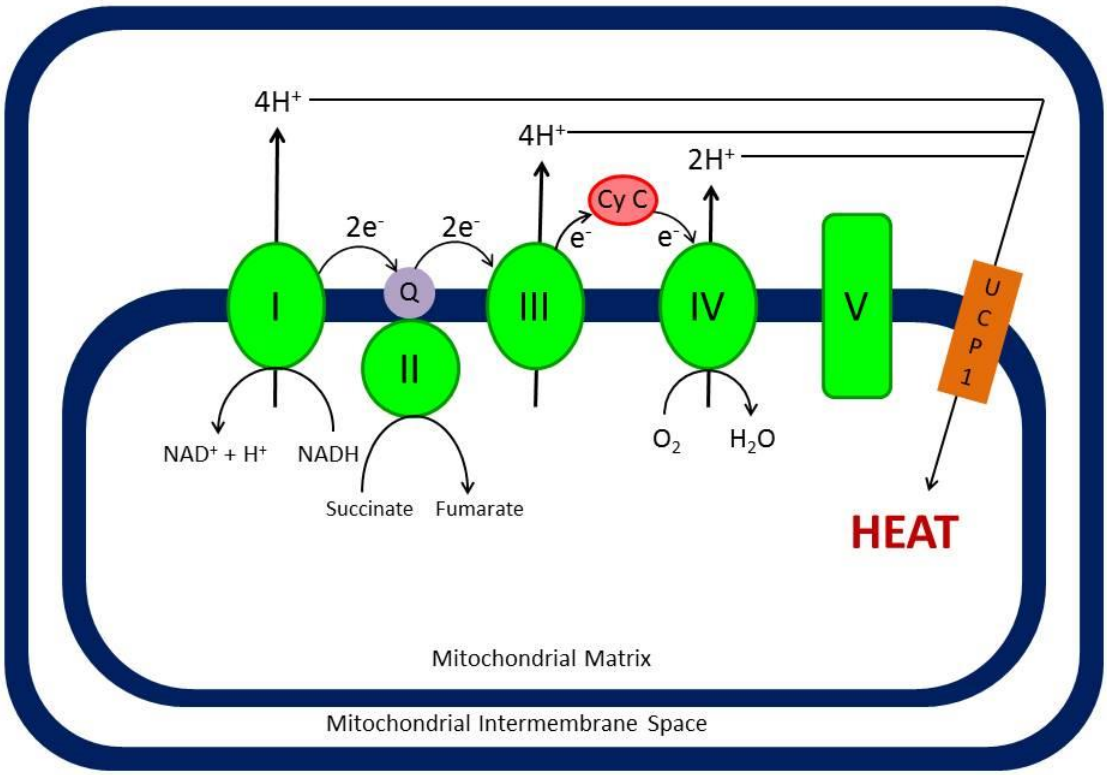

**Figure 1.5. The physiological parameters of arousal.** Body temperature and heart rate were measured using a surgically implanted transmitter. (A) Rapid increases in body temperature and (B) simultaneous increases in heart rate (red) and core body temperature (black) during arousal from torpor. Figure (A) is modified from Schwartz et al., *in review.*

**A**

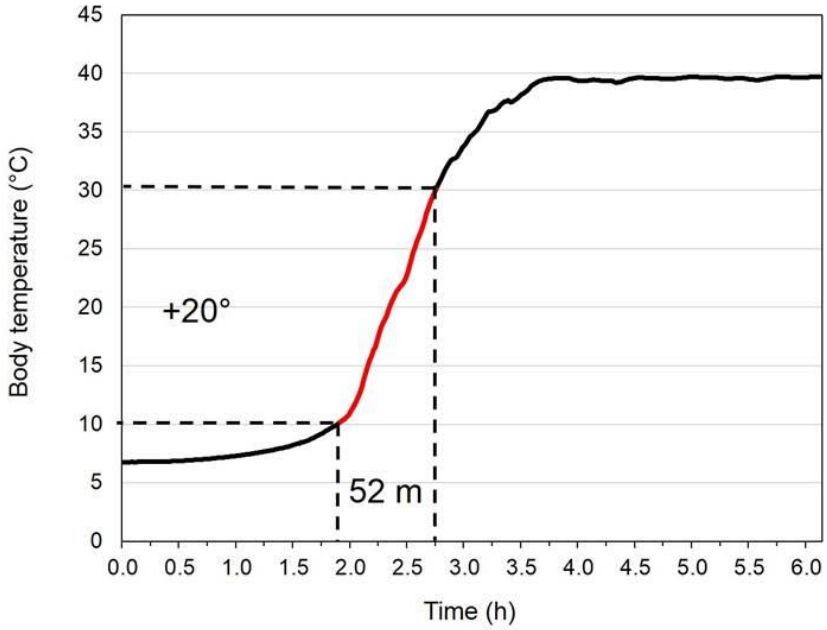

**B**

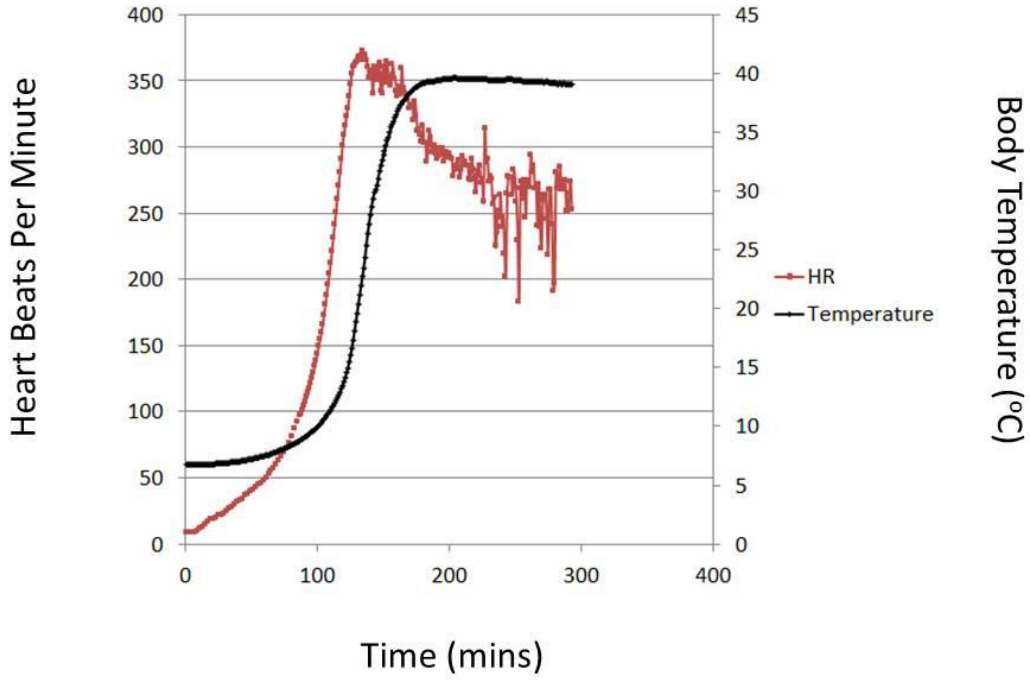
Heart Beats Per Minute
400
350
300
250
200
150
100
50
0
0
100
200
300
400
Time (mins)
45
40
35
30
25
20
15
10
5
0
HR
Temperature
Body Temperature (°C)

## SECTION 1.4: WHOLE BRAIN

### Introduction

Brown adipose tissue is not the only organ that has intricately evolved in a hibernator. The brain is also exposed to extreme fluctuations in body temperature, heart rate, metabolism, and oxygen consumption during hibernation. Specifically, cerebral blood flow in thirteen-lined ground squirrels is reduced by 90% during torpor (Frerichs et al., 1994). Rewarming episodes represent periods of intense metabolic activity, high oxygen demand and restoration of perfusion to ischemic regions (Hindle & Martin, 2013). Therefore, the energy demands and plasticity of the brain in a natural hibernator is of great interest.

### Neuroprotection in Hibernator's Brain

Despite the ischemic- and reperfusion-like levels during hibernation, no neurological damage is seen in any brain region of the ground squirrel (Frerichs et al., 1994; Ma et al., 2005). In fact, hibernation was initially proposed as a model for resistance to ischemic brain injury due to the extreme levels of cerebral blood flow that occurs during torpor (Frerichs et al., 1994). Reports on neuroprotective features of a hibernator's brain include: depressed metabolic rate to match the ~90% reduction of cerebral perfusion in torpor (Frerichs et al., 1994); mechanisms for effective synapse stabilization and re-establishment during brief euthermic periods (Dave et al., 2012); and maintenance of cellular homeostasis at low body temperature (van Breukelen & Martin, 2002). Additionally, oxygen delivery to the brain is enhanced during arousal, as

hemoglobin with high oxygen affinity is present during hibernation (Drew et al., 2004; Maginniss & Milsom, 1994). Enhanced antioxidant defense, along with enhanced oxygen delivery, may provide significant protection to the brain during arousal from torpor (Drew et al., 2004).

Furthermore, melatonin receptor signaling may also aid in neuroprotection of the hibernator brain. Mammals arousing from hibernation and daily torpor produce the hormone melatonin (Florant et al., 1984; Larkin et al., 2015; Stanton et al., 1986). The timing of the increase in circulating melatonin suggests that it could be playing a protective role during this extreme physiological transition (Tan et al., 2005). Melatonin is known to be protective, both as an antioxidant and through receptor-mediated mechanisms (Pandi-Perumal et al., 2008; Tan et al., 2007). Melatonin receptor signaling has been shown to provide protection through increasing survival signaling (Wang et al., 2012), decreasing apoptotic signaling (Radogna et al., 2007), and protecting mitochondria (Dragicevic et al., 2011; Radogna et al., 2008). Melatonin can freely pass through the blood brain barrier (Reiter et al., 2010) and is an excellent candidate for protection during arousal from torpor, particularly in the brain. Melatonin receptors are found throughout the mammalian brain, and are notably present in the suprachiasmatic nucleus of the hypothalamus in nearly all mammals studied, including ground squirrels (Bittman et al., 1994; Von Gall et al., 2002).

Energy Demand in Hibernator's Brain

There is evidence that some vital regions of the brain stay active year round in the thirteen-lined ground squirrel (Bratincsak et al., 2007; Drew et al., 2007), necessitating at least some low baseline energy demand during torpor. However, reducing or eliminating function in non-vital brain areas serves to conserve energy and promotes neuroprotection (Dave et al., 2012). Cortical electroencephalogram recordings during torpor indicate that there is little to no activity occurring during this time (Walker et al., 1977). This is supported by the finding that synaptic connections are significantly reduced in some areas of the forebrain during torpor (von der Ohe et al., 2007). Similarly, changes in dendritic spines and other synaptic structures resulting in reduced connectivity have been shown in torpor as well (Magariños et al., 2006; Popov et al., 1992; Popov & Bocharova, 1992; von der Ohe et al., 2006). However, importantly, synaptic connectivity and electrical activity in the brain are regained by IBA (von der Ohe et al., 2007; Walker et al., 1977), indicating that extensive synaptic restructuring is occurring during arousal. Synaptic plasticity and maintenance is energy-costly and requires extensive ATP production (Harris et al., 2012). Therefore, this translates into a major shift in energy demand that is occurring between torpor and IBA.

Brain Metabolism

During hibernation, the brain prefers to use ketone bodies produced by the liver over glucose as the main source of energy (Andrews et al., 2009; Schwartz et al., 2013). Metabolism in most other tissues can essentially be halted to conserve energy during

hibernation (reviewed in Staples (2014); however, maintenance of brain function at some reduced level is critical because it is the regulator of metabolic rate and of the hibernation phenotype (Drew et al., 2007; Pamenter, 2014). Mitochondria are integral to orchestrating the extreme changes in energy demand in the brain during hibernation, as their responses to hibernation contribute significantly to whole-organism metabolism (Staples, 2011). Despite this importance, little investigation has been done on the mitochondrial metabolism of the brain in a natural hibernator. Previous work has shown that there is no difference in brain mitochondrial respiration rates between torpor and IBA (Gallagher & Staples, 2013), but there has not been any investigation into whether mitochondria change seasonally. Therefore, another aim of this thesis is to investigate the mitochondrial metabolism of the thirteen-lined ground squirrel brain across the circannual cycle. By measuring mitochondrial metabolism throughout the year, our goal is to gain insight into the mechanisms and adaptations the ground squirrel brain employs to maintain function during extreme physiological challenges and shifts in energy demand.

## SECTION 1.5: KNOWLEDGE GAP

Current Knowledge Gap and Outstanding Questions

The metabolic feats hibernators employ are compelling, and these extreme dynamics of metabolism have motivated scientists to understand how hibernators utilize the energy available to them. One way scientists have been approaching this goal is through the investigation of mitochondrial metabolism. Because mitochondria are the primary sites for oxygen consumption, ATP production, and heat production, they are logical targets in attempting to understand how tissue-specific metabolism changes throughout the circannual cycle. However, despite the numerous mitochondrial studies associated with hibernation metabolism, little is known about the mitochondrial metabolic changes of a hibernator throughout the year.

Additionally, there are outstanding questions seeking answers and warrant further investigation. How do different environmental cues during the year (e.g. food availability, temperature) affect mitochondrial metabolism in different tissues of a mammalian hibernator? Does mitochondrial metabolism differ between spring and winter seasons when different fuel substrates are available and utilized by mitochondria? For example, how do mitochondria adapt to when fatty acids and ketones from lipid stores are the primary fuel source during hibernation, or when carbohydrates are the primary fuel source during homeothermy (Carey et al., 2003)? Do mitochondria in different tissues metabolize fuels at different rates across different seasons? Overall, there is a knowledge gap in regards to mitochondrial metabolism of a hibernator; more

specifically, there is very little known how each tissue functions through its mitochondria throughout different seasons of the year.

This lack of knowledge is accredited to the conventional approaches employed to study mitochondrial metabolism. These approaches have been one-dimensional by solely investigating mitochondrial function in primarily one type of tissues. For example, with extensive investigation of liver mitochondria, most studies have been done to determine differences associated between torpor and IBA, or between winter heterothermy and the summer active state (Staples & Brown, 2008; Staples, 2014). Liver has been shown to be suppressed during hibernation, but what about tissues that contribute significantly to whole-organism metabolism? While these studies attempt to understand the energy flow and thermodynamics associated with liver mitochondria, they have come short of the realistic expectation of understanding whole organismal mitochondrial metabolism due to the corporation of only one mitochondrial method – measurement of respiration rates. Measurements of mitochondrial respiration rates alone do not fully aid in understanding the metabolism associated with hibernation. Additional dynamics associated with mitochondria, such as mitoproteomics, also need to be employed in other tissues. These additional dynamics include identifying proteins that are present and abundant in the mitochondria across the year.

To better understand this unique adaptation, an integrative approach is needed to thoroughly understand the mitochondrial metabolism associated with hibernation. The functions of mitochondria greatly influence the dynamics of various biological levels. By

employing an integrative approach, a more complete metabolic measurement of mammalian hibernation can be constructed.

# CHAPTER 2: Materials and Methods

## SECTION 2.1: ANIMALS AND COLLECTION POINTS

Animal Capture and Care:

All procedures were approved by the University of Minnesota Institutional Animal Care and Use Committee (Protocol #1103A97712 ). Wild thirteen-lined ground squirrels, *Ictidomys tridecemlineatus*, were live-trapped on private property with permission near Paynesville, Minnesota by slowly pouring water into burrows and capturing the animal in a butterfly net when it emerges. Following capture, animals were housed in the AAALAC-accredited Animal Care Facility located in the University of Minnesota Duluth School of Medicine. Squirrels were kept individually in plastic top-load rat cages filled with aspen shavings. The squirrels were kept at room temperature in a 12:12 light/dark cycle at 23$^{o}$C and fed standard rodent chow (Purina, #5001) and water *ad libitum.* During the hibernation season (~November-March), the squirrels were moved into an artificial hibernation chamber and kept in constant darkness at 5-7$^{o}$C with no food provided.

Experimental Collection Points: (*Synopsis was modified from* Schwartz et al. (2013).

Five collection points were used to uncover the most meaningful comparisons in ground squirrel mitochondria across the circannual cycle: pre-hibernation (summer active and fall active), torpor, interbout arousal (IBA), and post-hibernation (spring active). The summer active collection point provides a time point when the animals are physically preparing for the hibernation season, as they are in a state of hyperphagia. During this

time, ground squirrels are able to consume over 25 g of food per day (Schwartz et al., 2015). The animals used for the summer active collection point were sacrificed in August. The fall collection point provides a time when the animals are already physically prepared for hibernation, having doubled or even tripled their body weights in the preceding months (Carey et al., 2003; Schwartz et al., 2015). This time point represents an opportunity to examine how brown adipose tissue (BAT) and brain mitochondria prepare for the upcoming hibernation season. Ground squirrels can potentially have begun shallow torpor bouts in October (Russell et al., 2010). However, all the animals used for this collection point were active at the time of collection and were sacrificed in September and October. The torpor and IBA collection points provide the two extremes of the hibernation cycle. The animals used for the torpor collection point were around day four in a torpor bout and had shown no sign of arousals. All animals used for the IBA collection point aroused naturally and spontaneously, were observed as awake and active, and were torpid the previous day. The hibernation collection point animals (torpor and IBA) were sacrificed in December, January, and February, when average torpor bout length is longest (Schwartz et al., 2013). The spring active time point provides an opportunity to examine the period of recovery after the completion of an entire hibernation season. Spring active animals were collected in April and May.

An equal number of males and females were sacrificed at each collection point. Animal state at each collection point was verified by rectal body temperature and behavior (Torpor: 6-8$^{o}$C/inactive; Active/IBA: 35-37$^{o}$C/active). All animals were deeply anesthetized with 5% isoflurane and killed by decapitation prior to tissue collection.

BAT samples were taken from the axillary pads. Whole BAT axillary pads were dissected from the surrounding tissues, cleaned of any contaminating tissue, and immediately placed in ice-cold mitochondria isolation buffer (MIB; ♦1). Whole brain was removed from the skull and the meninges and blood vessels surrounding the brain were removed. The brain was immediately placed in ice-cold MIB (♦1).

Additional animals were used for the experiments associated with Chapter 5. For the hibernation time point, animals toward the end of a torpor bout were targeted for drug administration. Summer animals were wild-caught in mid-May, so they did not undergo hibernation in the lab. These animals were kept in captivity for approximately one month prior to the beginning of the experimental protocol. For the summer group, animals were lightly anesthetized with isoflurane. All animals were administered 30 mg/kg luzindole or equivalent volume of vehicle intraperitoneally. The squirrels were then returned to their home cage for undisturbed arousal. Both hibernating and summer squirrels were sacrificed two hours after drug administration, which was the approximate time to mid-arousal with the more invasive rectal temperature reading. Animals were killed by decapitation prior to tissue collection. Whole brain was removed from the skull and the meninges and blood vessels surrounding the brain were removed. The brain was immediately placed in ice-cold MIB (♦1).

## SECTION 2.2: MITOCHONDRIAL ISOLATION

BAT

Isolation of mitochondria via differential centrifugation was adapted and modified from (Cannon & Nedergaard, 2008; Li & Graham, 2012; Silva & Oliveira, 2012). Left axillary BAT pads were blotted and weighed for determination of wet mass. The right and left axillary pads were then minced on ice and homogenized with ten passes in 30 mL MIB + bovine serum albumin (BSA; ♦2) using a rotating loose fitting Teflon pestle. The homogenate was filtered through three layers of sterile gauze and centrifuged at 1,000 × *g* for 10 minutes at 4°C. Floating lipid was aspirated from the supernatant, which was transferred to a new pre-chilled centrifuge tube and centrifuged at 500 × *g* for 10 minutes at 4°C. Any additional floating lipid was aspirated from the supernatant, which was transferred to a new pre-chilled centrifuge tube and centrifuged at 10,500 × *g* for 10 minutes at 4°C. The supernatant was decanted, and any lipid adhering to the tubes was carefully removed using KimWipes. The pellet was re-suspended in 30 mL ice-cold Wash Buffer (WB) + BSA (♦3) and centrifuged at 12,000 × *g* for 10 minutes at 4°C. The supernatant was decanted and the mitochondrial pellet was re-suspended in 30 mL ice-cold WB (♦4) and centrifuged at 12,000 × *g* for 10 minutes at 4°C. The final mitochondrial pellet was aliquoted and transferred to two pre-chilled Eppendorf tubes. One tube of purified mitochondria was frozen at -80°C until further proteomics analyses, while the second tube was kept on ice until assayed for mitochondrial respiration (maximum 6 hours). The protein concentrations of isolated mitochondria were determined by bicinchoninic acid (BCA) protein assay (Pierce BCA assay – Thermo

Scientific, #23255, 23277) according to the manufacturer's protocol, using BSA as a standard. Mitochondrial respiration measurements were performed directly after the mitochondrial isolation at 25°C.

Brain

Mitochondrial isolation was performed on whole brains via differential centrifugation (adapted and modified from established protocols (Li & Graham, 2012; Palmeira & Rolo, 2012; Silva & Oliveira, 2012). The brain was minced on ice and homogenized with ten passes in 30 mL MIB + BSA (♦2) using a rotating loose fitting Teflon pestle. The homogenate was filtered through three layers of sterile gauze and centrifuged at 1,000 × *g* for 10 minutes at 4°C. Floating lipid was aspirated from the supernatant, which was transferred to a new pre-chilled centrifuge tube and centrifuged at 500 × *g* for 10 minutes at 4°C. Any additional floating lipid was aspirated from the supernatant, which was transferred to a new pre-chilled centrifuge tube and centrifuged at 10,500 × *g* for 10 minutes at 4°C. The supernatant was decanted, and any lipid adhering to the tubes was carefully removed using KimWipes. The pellet was re-suspended, including the fluffy synaptosomal layer (Silva & Oliveira, 2012), in 30 mL WB + BSA (♦3) and centrifuged at 12,000 × *g* for 10 minutes at 4°C. The supernatant was decanted and the mitochondrial pellet was re-suspended, including the fluffy synaptomosomal layer (Silva & Oliveira, 2012), in 30 mL ice-cold WB (♦4) and centrifuged at 12,000 × *g* for 10 minutes at 4°C. The final mitochondrial pellet was transferred to a pre-chilled Eppendorf tube and kept on ice until assayed (maximum 6 hours). The protein

concentrations of isolated mitochondria were determined via BCA protein assay (Thermo Scientific, #23255) according to the manufacturer's instructions, using BSA as a standard. Mitochondrial bioenergetics analyses were performed directly after mitochondrial isolation.

## SECTION 2.3: *IN VITRO* MITOCHONRIAL RESPIRATION

Clark-type Oxygen Electrode:

A Clark-type oxygen electrode is the traditional instrument for measuring mitochondrial respiration on isolated mitochondria (Severinghaus & Astrkup, 1986). A major benefit of using a Clark-type oxygen electrode is that a variety of inhibitors and substrates can be added with isolated mitochondria, all in one run (Table 2.1). Thus the respiratory activity of the individual electron transport system complexes can be assessed (Silva & Oliveira, 2012; Zhang et al., 2012).

Calibration:

The reaction chamber of a Clark-type oxygen electrode (from Hansatech Instruments) was equilibrated at room temperature by adding 1 mL $dH_2O$. After a plateau of 100% oxygen was reached, zero oxygen was measured by adding a pinch of dithionite into the chamber. Once the plateau of zero oxygen was reached, the calibration was saved and was able to be used for 24 hours.

BAT

*In vitro* mitochondrial respiration rates were measured using a Clark-type oxygen electrode from Hansatech Instruments, in 0.5 or 1 mL of respiration buffer (♦5), at 25$^{o}$C while undergoing constant stirring (Li & Graham, 2012; Silva & Oliveira, 2012; Zhang et al., 2012). Unless otherwise stated, all compounds were dissolved in $dH_2O$.

Mitochondria were added in a final concentration of 0.5 mg protein $mL^{-1}$. Maximal flux through various segments of the electron transport system (ETS) were determined under non-phosphorylating (*state 4*; Chance & Williams (1955) conditions with the addition of ADP (200 nM), using specific substrates and inhibitors (Table 2.1; Zhang et al., 2012). Flux through complexes I-IV was measured using 5 mM Glutamate/Malate (G/M). Succinate (SUC, 5 mM) and Glycerol-3-Phosphate (G3P, 5 mM) were added to stimulate flux through complexes II-IV and complexes III-IV, respectively. Ascorbate (Asc, 5 mM) and *N,N,N', N',*-tetramethyl-*p*-phenylenediamine (TMPD, 10 mM) were added subsequently to measure flux through complex IV. Rotenone (2 mM, dissolved in ethanol; an ETS complex I inhibitor) was added to the mitochondrial suspension before SUC to prevent reverse electron flow. Malonate (10 mM) was added before the addition of G3P to inhibit complex II, and Antimycin A (2 μM) was added before the addition of Asc/TMPD to inhibit complex III. At the end, oligomycin (1 μg $mL^{-1}$, dissolved in ethanol; an ATPase inhibitor) was added to ensure *state 4* respiration rates were being measured (Figure 2.1).

Brain

*In vitro* mitochondrial respiration rates were measured using a Clark-type oxygen electrode from Hansatech Instruments in 0.5 mL of respiration buffer (♦5) at 25°C while undergoing constant stirring (Li & Graham, 2012; Silva & Oliveira, 2012; Zhang et al., 2012). Unless otherwise stated, all compounds were dissolved in $dH_2O$.

Mitochondria were added in a final concentration of 0.5 mg protein $mL^{-1}$. Maximal flux through various segments of the ETS were determined under phosphorylating (*state 3*; Chance & Williams, 1955) conditions with the addition of ADP (200 nM), using specific substrates and inhibitors (Zhang et al., 2012). Flux through complexes I-IV was measured using 5 mM G/M. SUC (5 mM) and G3P (5 mM) were added to stimulate flux through complexes II-IV and complexes III-IV, respectively. Rotenone (2 mM, dissolved in ethanol; an ETS complex I inhibitor) was added to the mitochondrial suspension before SUC and G3P were introduced to prevent reverse electron flow. All substrate oxidation rates were allowed to reach both steady *state 3* and steady *state 4* (non-phosphorylating) respiration rates (Chance & Williams, 1955; Divakaruni & Brand, 2011; Figure 2.1). To assess the integrity of the mitochondrial inner membranes of our isolated mitochondrial fractions, we measured the respiratory control ratio (RCR). RCR is the ratio between *state 3* and *state 4*, and is an indicator of coupling efficiency between substrate oxidation and ATP synthesis (Chance & Williams, 1955; Zhang et al., 2012).

## Section 2.3 Figures & Tables

**Figure 2.1. Oxygen consumption trace of isolated BAT and brain mitochondria.** The differences between uncoupled mitochondria (BAT mitos) and coupled mitochondria (Brain mitos) are evidenced in the oxygen consumption trace, using a Clark-type oxygen electrode (Hansatech Instruments). After the addition of G/M, BAT mitos obtain a *state 4* respiration rate ("non-phosphorylating" or "non-ATP producing" respiration rate). Two additions of ADP do not affect the respiration rate associated with BAT mitos (i.e. there is no change in the oxygen consumption rate). *State 4* respiration rate is confirmed with the addition of oligomycin, an ATPase inhibitor. Again, no changes in the oxygen consumption rate are observed after the addition of oligomycin. Contrarily, brain mitos are a coupled system, indicated by the following trace. After the addition of G/M and ADP, there is an increase in the oxygen consumption rate, and this increase in rate is referred to as *state 3* respiration rate ("phosphorylating" or "ATP-producing" respiration rate). Once most of the ADP has been phosphorylated, the oxygen consumption rate decreases, reflecting *state 4* respiration rate. The integrity of coupled mitochondria can be assessed by measuring the ratio between *state 3* and *state 4*, or the respiratory control ratio. Abbreviations: G/M, glutamate/malate; BAT, brown adipose tissue; Mitos, mitochondria.

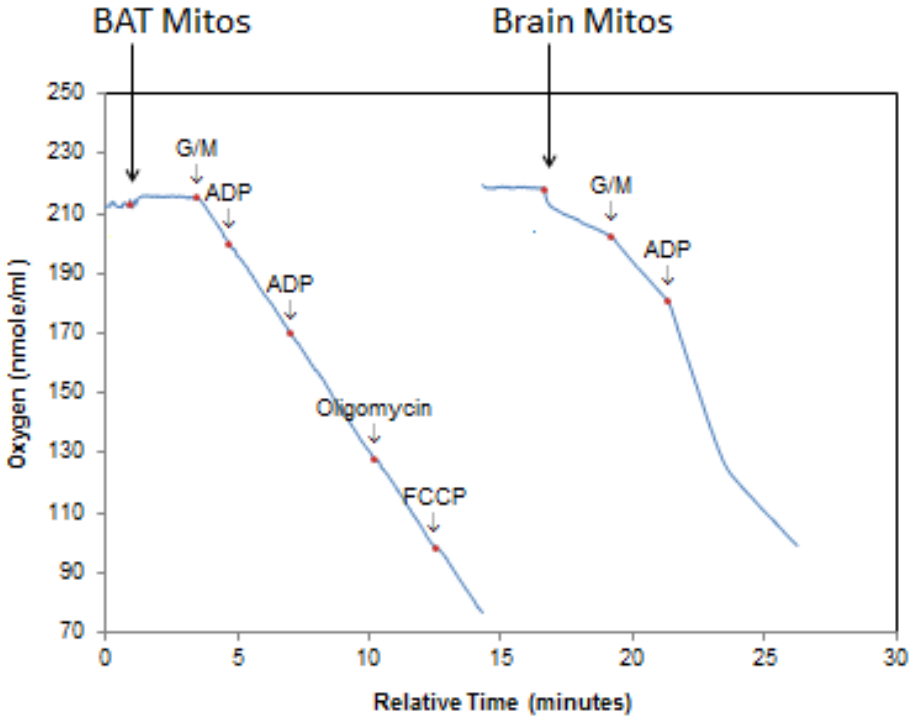

**Table 2.1: Substrates and inhibitors used during mitochondrial respiration assay (*modified from* Silva & Oliveira (2012) and Zhang et al. (2012).**

| Name | Classification | Place of Action |
|---|---|---|
| Antimycin A | Inhibitor | Complex III |
| Ascorbate | Co-substrate | Complex IV (by donating electrons to cytochrome *c*) |
| Glutamate + Malate (G/M) | Substrates | Measures oxygen consumption rate from combined ETC complex I, III and IV. Electrons from NADH generated from glutamate oxidation by glutamate dehydrogenase enter the respiratory chain via complex I |
| Glycerol-3-Phosphate (G3P) | Substrate | Complex III (via glycerol-phosphate cycle by glycerol-3-phosphate dehydrogenase) |
| Malonate | Inhibitor | Inhibition of succinate oxidation |
| Oligomycin | Inhibitor | Complex V |
| Rotenone | Inhibitor | Complex I |
| Succinate (SUC) | Substrate | Complex II |
| TMPD | Reducing co-substrate | By-passing electrons to Complex IV (via cytochrome *c*), as an artificial electron mediator |

## SECTION 2.4: BAT MITOPROTEOMICS VIA iTRAQ

Protein Extraction and iTRAQ® Labeling:

All proteomic experiments were performed at the University of Minnesota Center for Mass Spectrometry and Proteomics, Minneapolis, MN. Frozen isolated BAT mitochondria from spring ($n$ = 3), IBA ($n$ = 3) and torpor ($n$ = 2) were used for iTRAQ® proteomics. The mitochondria were reconstituted in phosphate buffer saline, vortexed briefly, then sonicated at 30% amplitude for 7 seconds with a Branson Digital Sonifier 250 (Branson Ultrasonics, Danbury, CT). Each sample was placed in a Barocycler NEP2320 (Pressure Biosciences, Inc., South Easton, MA) and cycled between 35 kpsi for 30 seconds and 0 psi for 15 seconds for 40 cycles at 37°C. The samples were alkylated with 8 mM methyl methanethiosulfonate at room temperature for 15 minutes. Two aliquots of each sample were taken for protein concentration determination via Bradford assay. Afterwards, 100 µg aliquot of each sample was transferred to a new 1.5 mL microfuge tube and brought to the same volume with protein extraction buffer plus 8 mM methyl methanethiosulfonate. All samples were trypsin digested overnight for 16 hours at 37°C, and then frozen at -80°C for 0.5 hours and dried in a vacuum centrifuge. Each sample was cleaned with a 4 mL Extract Clean™ C18 SPE cartridge from Grace-Davidson (Deerfield, IL). Elutants were vacuum dried and re-suspended in dissolution buffer (♦6) to a final concentration of 2 µg/µl. One set of 8-plex iTRAQ® reagents was used for labeling the 8 samples in the experiment. 40 µg of each sample was labeled with iTRAQ® reagent per manufacturer's protocol (AB Sciex, Foster City, CA). Equal amounts of protein were combined from one male and one female for each time point.

The peptides derived from the three spring samples were labeled with 113, 114, and 115; the three IBA samples were labeled with iTRAQ® reagents 116, 117, and 118; and iTRAQ® 119 and 121 were used to label the two torpor samples. After labeling, the samples were multiplexed together and vacuum-dried. The multiplexed samples were cleaned with a 4 mL Extract Clean™ C18 SPE cartridge, and the elutants were dried in a vacuum centrifuge.

Liquid Chromatography and Tandem Mass Spectrometry (LC-MS/MS)

The iTRAQ® labeled samples were re-suspended in Buffer A (♦7) and fractionated offline by high pH C18 reversed-phase chromatography (Yang et al., 2012). A Shimadzu Promenance HPLC (Shimadzu, Columbia, MD) was used with a C18 XBridge column, 150 mm × 2.1 mm internal diameter, 5 µm particle size (Waters Corporation, Milford, MA). The flow rate was 200 µl/min. with a gradient from 2-35% Buffer B (♦8) over 60 minutes, followed by 35-60% over 5 minutes. Fractions were collected every 2 minutes and UV absorbance was monitored at 215 nm and 280 nm. Peptide-containing fractions were divided into two equal numbered groups, "early" and "late". Concatenated samples were dried in a vacuum centrifuge, re-suspended in load solvent (98:2:0.01, water:acetonitrile:formic acid) and 1-1.5 µg aliquots were run on a Velos Orbitrap mass spectrometer (Thermo Fisher Scientific, Inc., Waltham, MA) as previously described (Lin-Moshier et al., 2013), with the exception that the HCD activation energy was 20 mseconds.

Bioinformatic and Statistical Analyses:

The MS/MS spectra were searched using a customized ground squirrel database generated from the NCBI annotated thirteen-lined ground squirrel genome merged with RNA-seq-data generated in the lab (Hampton et al. 2013), along with the contaminants database using Paragon Alogirithm (V. 4.5.0.0 ) search engines in ProteinPilot™ (V. 4.5, ABSciex, Foster City, CA). The precursor mass window was set to sub-ppm, and MS/MS error tolerance was set at 0.1 Da with up to one missed tryptic cleavage. 8-plex iTRAQ® peptide labeling and cysteine methyl methanethiosulfonate alkylation were set as fixed modifications. The search effort was thorough, and the identification focus was set for biological modifications. All peptides were identified with at least a 95% confidence interval value (CI value) as specified by the Paragon Algorithm in ProteinPilot™, and less than a 1% false discovery rate (FDR) based on forward/reverse database searches. Relative quantification of proteins was determined by ProteinPilot™ in a normalized $\log_{10}$-based relative iTRAQ® ratio format, with iTRAQ® 113, 114 and 115 as the reference denominators. Proteins were considered differentially expressed relative to the reference denominator if they had at least 2 unique peptides, an experiment-wide FDR of no more than 1%, and a p-value $\leq 0.001$. ProteinPilot™ defines p-value as a measure of the certainty that the average ratio randomly differs from 1. Significant differences must be present in two or three of the samples in each time point, and show the same trend. Differentially expressed proteins were submitted into the Database for Annotation, Visualization and Integrated Discovery (DAVID; Huang et al.,

2009), and literature searches to highlight proteins associated with various mitochondrial functions.

## SECTION 2.5: BRAIN BIOENERGETICS

Membrane Potential and Proton Leak:

Proton leak, as defined by the mitochondrial respiration rate in the presence of an ATP synthase inhibitor (i.e. oligomycin; Divakaruni & Brand, 2011), is undeniable in mitochondria (Nicholls, 1974). Proton leak kinetics can be quantified by simultaneously measuring respiration (Clark et al., 1953) and mitochondrial membrane potential (Nicholls, 1974) as both are titrated using respiratory inhibitors. Proper quantification of proton conductance requires measurement of the respiration used to drive proton leak at a defined membrane potential (Divakaruni & Brand, 2011). Mitochondrial respiration under *state 4* conditions is used to drive the leak of protons across the mitochondrial inner membrane (Barger et al., 2003).

For the determination of proton leak kinetics, simultaneous measurements of oxygen consumption and membrane potential ($\Delta\Psi_m$) were required (Palmeira & Rolo, 2012; Serviddio et al., 2010). Oxygen consumption was determined by the Clark-type oxygen electrode, while membrane potential was determined by a tetraphenylphosphonium ($TPP^+$) sensitive electrode (Hansatech Instruments). Initially, rotenone (2 mM; dissolved in ethanol) was added to inhibit complex I, and oligomycin (1 $\mu g\ mL^{-1}$, dissolved in ethanol) was added to inhibit ATP synthase. Mitochondria were added to the chamber at a final concentration of 0.5 $mg\ mL^{-1}$ at 25°C. A $TPP^+$ sensitive electrode and a AgCl reference electrode (Hansatech Instruments) were inserted into the oxygen chamber to measure external [$TPP^+$]. The $TPP^+$ electrode was calibrated by

making three additions of $TPP^+$ (1 mM); each addition increased external [$TPP^+$] by 1 μM. After calibration, *state 4* respiration was induced by the addition of 10 mM succinate. The kinetics of proton leak were determined by inhibiting succinate oxidation stepwise by titrating 0.3 mM malonate until a complete inhibition was obtained, and then measuring this effect on $\Delta\Psi_m$.

$\Delta\Psi_m$ was calculated from external [$TPP^+$] using a modified Nernst equation, adapted and modified from Barger et al. (2003) and Serviddio et al. (2010):

$$\Delta\Psi_m = -59 \log \left\{ \frac{[TPP^+]_{added} - [TPP^+]_{external}}{(0.001)(\text{mg protein})([TPP^+]_{external})} \right\}$$

$[TPP^+]_{external}$ is the concentration of $TPP^+$ outside of the mitochondria, and the value 0.001 represents the internal volume of the mitochondria (taken as 1.1 μL mg $protein^{-1}$; Palmeira & Rolo, 2012).

Calcium Loading Capacity:

Mitochondrial calcium loading capacity is a measure of the total amount of calcium that mitochondria are capable of accumulating from the incubation medium before releasing it back to the medium via the mitochondrial transition pore (Zhou et al., 2001). For estimation of calcium loading capacity, rotenone (2 mM; dissolved in ethanol) and oligomycin (1 μg $mL^{-1}$, dissolved in ethanol) were initially added to inhibit complex I and ATP synthase, respectively. Mitochondria were added to the chamber at a

final concentration of 0.5 mg $mL^{-1}$ at 25°C. A calcium electrode (filled with 10mM $CaCl_2$; Hansatech Instruments) was calibrated by sequential additions of $CaCl_2$ solution (e.g. 20 mM, 20 mM, 40 mM, 80 mM, and 100 mM (total 260 mM). Once calibrated, succinate (10 mM) was added to stimulate approximately *state 4* respiration. The estimation of calcium loading capacity was determined after calcium loading halted in the mitochondrial suspension (i.e. mitochondria released calcium back into the medium). This $Ca^{2+}$-induced mitochondrial $Ca^{2+}$ release indicates the opening of the mitochondrial transition pore, which was confirmed by adding cyclosporin A (1 μM), a specific inhibitor of the mitochondrial pore (Broekemeier et al., 1989), to block the $Ca^{2+}$ release (Zhou et al., 2001). The calcium loading capacity is expressed as μmoles of $Ca^{2+}$ per mg of mitochondrial protein (Zhou et al., 2001).

## SECTION 2.6: MtDNA COPY NUMBER

Mitochondrial DNA (mtDNA) and Nuclear DNA (nuDNA) Quantification via qPCR:

Genomic DNA was isolated from frozen cerebral cortex samples from $n = 6$ IBA and spring, using QIAmp DNA Blood Mini Kit (Qiagen, #51104). Cerebral cortex was chosen for analysis as it is the largest region of the brain, thus giving a better representation of mitochondrial abundance present throughout the whole brain. Samples were taken from animals with similar seasonal timing as the animals used for functional analyses. Prior to DNA precipitation, samples were sonicated to ensure unbiased DNA extraction of nuclear DNA (Malik et al., 2011). Primer sequences from unique mitochondrial segments and single copy nuclear genes were previously designed following the protocol of Malik et al. (2011), and synthesized by Integrative DNA Technologies. Primer regions are as follows:
ND1 (F: 5'-TGTCCCAATCTTAGTAGCCATAGCCTT-3'; R:5'-TGCGTCAGCAAATGGTTGGAGT-3') and B2M (F: 5'-ATACCCGGCACCCGGCTGAG-3'; R:5'-AGAGAGGTCCGACTGCTCGACT-3').

Amplicons were then purified using QIAquick PCR purification kit (Qiagen, #28104). Quantitative PCR (qPCR) was performed with the individual mitochondrial and nuclear primers on the RotorGene3000 (Qiagen), and was carried out in accordance with the Lutfalla & Uze (2006) procedure, changing initial denaturing/enzyme activation at 95°C for 10 minutes and primer annealing temperature at 60°C. Using qEvaGreen Master Mix (qARTA Bio, Inc.), crossing threshold (Ct) values were derived following the procedures of Hampton et al. (2011). Log transformation of the serial dilutions to

their Ct values generated a standard curve that was used to compare the log transformed Ct values of the unknown qPCR samples. Mitochondrial DNA copy numbers were assessed relative to the single copy nuclear gene fragments in the same qPCR run. These values were used to calculate the ratio of ND1:B2M, or mitochondrial to nuclear DNA.

## SECTION 2.7: DATA ANALYSES

Statistical analysis on BAT and brain data were carried out using JMP Pro 11 statistical software. All data presented as means ± standard error (SE), and $P < 0.05$ was considered statistically significant in all cases.

BAT:

Significant differences in BAT pad mass and mitochondrial respiration data between groups were determined using a one-way analysis of variance (ANOVA). Significant results were further analyzed using a Tukey's HSD test to find means that were significantly different from each other.

Brain:

Differences in seasonal respiration rates were determined using a one-way ANOVA. Significant results were further analyzed using a Tukey's HSD test to find means that were significantly different from each other. Differences in respiration rates, proton leak kinetics, calcium loading capacity and mtDNA copy number between hibernating (torpor and IBA) and spring animals were calculated using a Student's T-Test.

## SECTION 2.8: SOLUTIONS INDEX

**♦1 Mitochondrial Isolation Buffer (MIB)**

250mM Sucrose
5mM HEPES
1mM EGTA
pH ~7.2-7.4 (using NaOH); store and use at 4$^{o}$C.

**♦2 Mitochondrial Isolation Buffer + Bovine Serum Albumin (MIB + BSA)**

250mM Sucrose
5mM HEPES
1mM EGTA
0.1% fatty acid free bovine serum albumin (BSA)
pH ~7.2-7.4 (using NaOH); store and use at 4$^{o}$C.

**♦3 Wash Buffer + Bovine Serum Albumin (WB + BSA)**

250mM Sucrose
5mM HEPES
0.1% fatty acid free bovine serum albumin (BSA)
pH ~7.2-7.4 (using NaOH); store and use at 4$^{o}$C.

**♦4 Wash Buffer (WB)**

250mM Sucrose
5mM HEPES
pH ~7.2-7.4 (using NaOH); store and use at 4$^{o}$C.

**♦5 Respiration Buffer**

135mM sucrose
65mM KCl
5mM $KH_2PO_4$
5mM HEPES
2.5mM $MgCl_2$
pH 7.2-7.4 (using NaOH); store at 4$^{o}$C.

**♦6 Dissolution Buffer**

0.5M triethylammonium bicarbonate
pH 8.5
Made, stored and used at University of Minnesota – Center for Mass Spectrometry and Proteomics (UM-CMSP).

**♦7 Buffer A**

20mM ammonium formate
in 98:2 water:acetonitrile
pH 10
Made, stored and used at UM-CMSP.

**♦8 Buffer B**

20mM ammonium formate,
10:90 water:acetonitrile
pH 10
Made, stored and used at UM-CMSP.

# CHAPTER 3: Interrogation of Brown Adipose Tissue Mitochondria in a Mammalian Hibernator: from Gene Expression to Function

* This chapter is included in the following manuscript, which will be submitted for publication in a peer-reviewed journal: Ballinger, M.A., Hess, C., Napolitano, M.W., Bjork, J.A. and Andrews, M.T. (*in preparation)* Interrogation of Brown Adipose Tissue Mitochondria in a Mammalian Hibernator: from Gene Expression to Function.

## SECTION 3.1: RESULTS

BAT Mass and Recruitment

Qualitatively, we have observed in the laboratory that axillary brown adipose tissue (BAT) pad mass in thirteen-lined ground squirrels increases in size prior to the hibernation season. To further investigate these qualitative observations, the masses of left axillary BAT pads were measured immediately after excision. Means of BAT mass ± standard error (SE) for spring (SP), fall (FA), torpor (TOR), and interbout arousal (IBA) were 0.41 ± 0.03, 0.89 ± 0.05, 1.17 ± 0.05, and 0.98 ± 0.07, respectively. BAT mass was significantly lower in SP compared to FA, TOR and IBA (one-way ANOVA, $P < 0.0001$, Figure 3.1). TOR also showed significantly higher BAT masses compared to FA (one-way ANOVA, $P = 0.0066$). The axillary pads begin to increase in mass during FA in preparation for hibernation, and are largest during the hibernation season (TOR and IBA).

In addition to the overall morphology of BAT, mitochondrial abundance in brown adipose tissue has been determined via mitochondrial DNA (mtDNA) to nuclear DNA (nuDNA) ratio measurements across the circannual cycle (Figure 3.2). Similar to wet mass results, SP animals had the lowest mtDNA copy number when compared to FA, TOR and IBA states (one-way ANOVA, $P < 0.05$), thus further validating the overall decrease in BAT mitochondrial abundance during SP. Our mtDNA copy number results do not support previous studies indicating that there is no difference in mitochondrial abundance between hibernation and post-hibernation periods (Hindle & Martin 2014). However, not only did this previous study use different primers, but they also did not take into account the possibility that mitochondrial biogenesis and recycling (Gomes et al.,

2011; Liesa & Shirihai, 2013; Youle & van der Bliek, 2012) may require weeks post-hibernation to see any noticeable effects. This assumption is supported when comparing genes associated with mitochondrial biogenesis and the BAT transcriptome. For example, calcineurin (Kelly & Scarpulla, 2004) and *PGC1α* (Li et al., 2011) are positively correlated with mitochondrial biogenesis and show significantly higher mRNA expression in BAT during hibernation (Hampton et al., 2013).

This trend in BAT mass was initially observed in uncoupling protein 1 (UCP1) mRNA levels, with UCP1 transcripts significantly higher in TOR and IBA compared to spring (Hampton et al., 2013). However, the level of UCP1 mRNA can show a dramatic response (Cannon & Nedergaard, 2004). The turnover rate of UCP1 protein is slow because of its requirement of mitochondrial synthesis (Cannon & Nedergaard, 2004); thus, there is also a long time delay before modifications in UCP1 mRNA levels lead to corresponding modifications in amounts of UCP1 protein (Cannon & Nedergaard, 2004). Therefore, UCP1 mRNA is a less feasible indicator of BAT recruitment. Instead, the most physiologically relevant measure of BAT recruitment, and the best reflection of the actual thermogenic capacity change occurring during hibernation, is through the quantitation of UCP1 protein directly (Cannon & Nedergaard, 2004). The protein quantitation of UCP1 was determined via Western blot analysis (Figure 3.3). Although not significant, the same trend identified in BAT pad mass and mtDNA copy number was also observed measuring UCP1 protein, with the hibernation time points containing the most UCP1 protein in brown adipose tissue (Figure 3.3).

BAT Mitochondrial Respiration

Individual complexes of the electron transport system (ETS) in BAT mitochondria were interrogated across the circannual cycle of the thirteen-lined ground squirrel. Based on fuel utilization and selective inhibitors, no significant differences were identified at complexes I or IV; but significant differences were observed at complexes II and III. Fueled with succinate (SUC), complex II of isolated mitochondria from SP had significantly lower respiration rates compared to FA, TOR and IBA (one-way ANOVA; $P < 0.0001$, $P = 0.0028$, and $P = 0.0007$, respectively; Figure 3.4). Complex III, fueled with glycerol-3-phosphate (G3P), had significantly higher respiration rates in IBA compared to FA (one-way ANOVA, $P = 0.0465$; Figure 3.4).

In addition, complex I (fueled with glutamate/malate (G/M) showed the lowest rates of respiration, most likely due to the large size (~980 kDA) and the 45 subunits that make up complex I (Carroll et al., 2006; Efremov et al., 2010). Contrarily, complex IV (fueled with ascorbate/TMPD (Asc/TMPD) showed the highest respiration rates, likely due to the fast shuttle of electrons through complex IV. These results suggest that complexes II-III may be playing key roles in mitochondrial metabolism during SP than complexes I and IV.

In general, rates at complexes II-IV are highest (non-significant) during the hibernation season (Figure 3.4). In fact, we did not see any differences between torpor and IBA at any of the four complexes. High respiration rates during the hibernation season suggest fuel preference of fatty acids, as they are the driving force behind the thermogenic ability of BAT necessary for hibernation (Cannon & Nedergaard, 2004).

Higher rates also suggest an increase in the delivery of reducing equivalents (such as NADH and $FADH_2$) in BAT during hibernation, which are produced readily from lipid metabolism.

Additional investigation has been done on the effects of temperature on mitochondrial metabolism, using succinate as a fuel. There were no significant differences at any temperature (5, 13, 21, 29, and 37$^{o}$C) between SP, TOR and IBA (Figure 3.5). This suggests that unlike liver mitochondria in thirteen-lined ground squirrels, BAT mitochondria are able to function and respire at high rates regardless of temperature. For $Q_{10}$ analyses, average respiration rates at each temperature were calculated for each state (TOR, IBA, and SP). For most biological reactions, $Q_{10}$ typically falls between 2 and 3 suggesting that temperature changes alone (passive effects) are adequate to explain reductions in metabolism (Staples & Brown, 2008; Guppy & Withers, 1999; Snapp & Heller, 1981). When $Q_{10}$ is greater than 3, active processes are also involved in regulating metabolic suppression (Staples & Brown, 2008; Geiser, 1988). Based on $Q_{10}$ analyses, the greatest $Q_{10}$ values were obtained at the lower temperatures (Ballinger et al., *in preparation*). For the hibernation season, TOR $Q_{10}$ values were between 2 and 2.6 and IBA values were between 2 and 2.7 (Ballinger et al., *in preparation*). For SP, respiration rates were only available for 5 and 13$^{o}$C and were 3.0 and 2.6, respectively (Ballinger et al., *in preparation*). These results suggest that passive thermal effects are primarily responsible for metabolic suppression in BAT mitochondria. In mitochondria isolated from SP animals, there is greater reliance on

active processes for function at lower temperature. Furthermore, these results suggest there could be intrinsic regulation present in HIB mitochondria that is not present in SP.

BAT Mitoproteomics

Overall, 778 BAT mitochondrial proteins were identified in the thirteen-lined ground squirrel across the hibernation and spring time points. The top mitochondrial proteins are encoded by many transcripts that were also highly expressed in the BAT transcriptome, such as UCP1 (Figure 3.6; Hampton et al., 2013). Of the 778 total proteins, 106 were differentially expressed according to the criteria outlined in the Materials and Methods section (Appendix A). In this proteomic study, the hibernation time point (HIB) is a combination of data from torpor TOR and IBA. 56 proteins showed highest expression in HIB compared to SP, while 48 proteins showed highest expression in SP compared to HIB (Appendix A). UCP1 did not make the differential expression cut-off criteria; however, it did show the same trend as the BAT transcriptome and Western blot analyses, with UCP1 showing highest protein levels in HIB.

The HIB time point also had the largest number of differentially expressed proteins, with TOR having the most highly expressed proteins compared to SP. The majority of proteins that showed the highest level in SP are highest compared to IBA, and not TOR. This was surprising because both SP and IBA are euthermic time points; however, the IBA time point is surrounded by extended periods of hypothermic torpor and thus, may require a different set of proteins that allow for the rapid increase in oxygen consumption and body temperature associated with the IBA (Vermillion et al.,

manuscript submitted for publication). It is thought that IBAs are required to allow for critical protein synthesis and biomolecule replenishment and repair (Andrews, 2007).

Functional Analysis of Mitoproteomics

To further analyze the differentially expressed proteins, DAVID functional annotation clustering was used (Huang et al., 2007). As expected, both data sets (highest expression in HIB and highest expression in SP) contained the highest enrichments for mitochondrial located proteins (Tables 3.1 & 3.2). Not only do these top enrichments validate our mitochondrial isolation, but they also inform us on the important localities of proteins between HIB and SP. For example, the HIB time point had the highest enrichment for proteins that are found in the mitochondrial membranes, while SP proteins had the highest enrichment for the mitochondrial matrix. This is evident to hibernation requiring increased fatty acid transport for the increased lipid metabolism present in BAT (Cannon & Nedergaard, 2004; Carey et al., 2003).

*Proteins showing highest expression in HIB.* Overall, pathways that showed highest enrichment of BAT mitochondrial proteins during HIB dealt with lipid oxidation and fatty acid metabolism (Table 3.1). Fatty-acyl CoA mitochondrial transport proteins, such as CPT1B, CPT2, and SLC25A20, had highest expression during HIB. These proteins are also important in the carnitine shuttle. There is also more efficient mitochondrial protein trafficking during HIB as the inner membrane translocase was enhanced by more abundant motor and associated proteins (TIMM50 and TIMM44). Additionally, β-oxidation of fatty-acyl CoA was also enriched for (CPT1B, CPT2,

ACADS, ECHS1, DECR1, CRAT, HSD17B4, HADHA, HADHB). Hibernation also favors isocitrate metabolism compared to spring, with isocitrate conversion to α-ketoglutarate being enhanced (IDH3B, IDH3G, IDH2) and NADH shuttling into the ETS. In fact, Hindle and Martin (2014) see the same enhancement of catabolism of isocitrate during HIB, and validated this observation through an IDH3 assay where they showed ~80% increase in IDH3 in IBA compared to summer active animals. Additionally, coenzyme binding proteins (D2HGDH, AIFM1, ACADS, IDH3B, DECR1, OGDH, HADHB) are also enhanced during HIB in BAT mitochondria, allowing for essential metabolic enzymatic reactions to proceed (i.e. TCA cycle and β-oxidation).

*Proteins showing highest expression in SP*. Unlike HIB, where fatty acid metabolism and β-oxidation proteins are enriched, the SP time point contains mitochondrial proteins enriched for acetyl-CoA and pyruvate metabolism (Table 3.2). This further validates the switch in metabolism from lipid to carbohydrate in SP (Eddy & Storey 2004; Carey et al. 2003). Further recognition of this metabolic switch is through the enrichment of TCA cycle enzymes (Table 3.2). Unlike in HIB, where CS and IDH enzymes are enhanced, succinate metabolism is enriched (SDHA and SDHB). Additionally, citrate to isocitrate (ACO2) is enhanced in SP, and these observations were also seen by Hindle and Martin (2014). Lastly, fatty acid binding is decreased during SP, evidenced again by the decrease in lipid metabolism outside of hibernation.

## Section 3.1 Figures & Tables

**Figure 3.1. Seasonal wet axillary BAT pad mass.** BAT pad mass was measured from the left axillary pad between SP, FA, TOR, and IBA time points ($n$ = 6). Means of BAT mass ± SE for SP, FA, TOR, and IBA were 0.41 ± 0.03, 0.89 ± 0.05, 1.17 ± 0.05, and 0.98 ± 0.07, respectively. BAT mass was significantly lower in SP compared to FA, TOR, and IBA (one-way ANOVA, $P < 0.0001$). TOR also showed significantly higher BAT masses compared to FA ($P = 0.0066$). Time points that are not connected by the same letter are significantly different (Tukey's HSD). Data are individual animals represented by an individual symbol. Abbreviations: SP, spring; FA, fall; TOR, torpor; IBA, interbout arousal; SE, standard error.

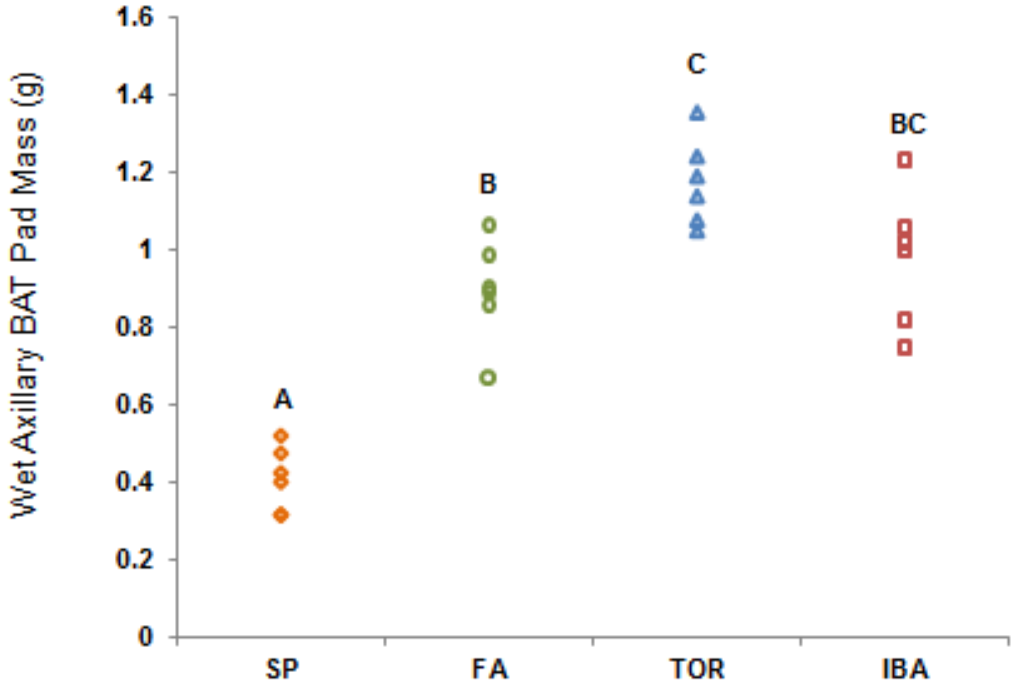

**Figure 3.2. Seasonal mitochondrial DNA (mtDNA) to nuclear DNA (nuDNA) ratios in BAT.** Ratios of mitochondrial genes (*ND1* and *COX2*) to nuclear genes (*B2M* and *ACTA*) were quantified via qPCR in ground squirrel brown adipose tissue ($n$ = 6). Ratio of ND1/B2M (A) showed a significant increase in mtDNA copies from SP to FA (one-way ANOVA, $P < 0.05$). Ratio of COX2/ACTA (B) showed a significant increase in mtDNA copies from SP to TOR (one-way ANOVA, $P < 0.05$). Data are presented as mean ± SE. Time points that are not connected by the same letter are significantly different (Tukey's HSD). Abbreviations: SP, spring; FA, fall; TOR, torpor; IBA, interbout arousal; SE, standard error.

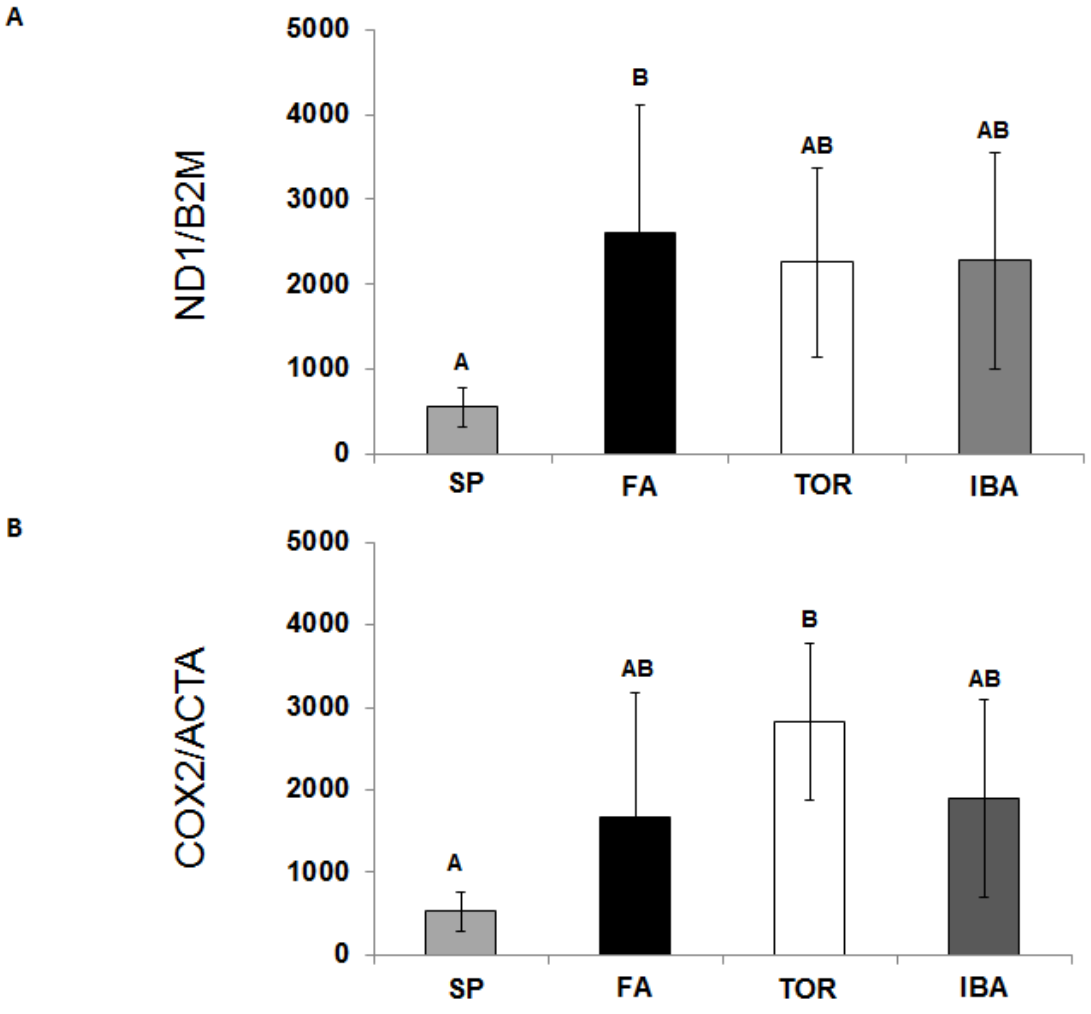

**Figure 3.3. Representative Western blot (A) and densitometry (B) of UCP1.** The expression of UCP1 protein was determined via Western blot analysis. 15 µg of BAT protein homogenate was loaded in each lane ($n$ = 2). Image J was used to measure the density of the ~30 kDa band from Western blots using anti-UCP1 antibody. Bands from each of the two blots were normalized to a common lane (Ctl) with 15 µg pooled BAT homogenate. No significant differences in UCP1 abundance were observed. Error bars are SE. Abbreviations: SP, spring; FA, fall; TOR, torpor; IBA, interbout arousal; Ctl, control; UCP1, uncoupling protein 1.

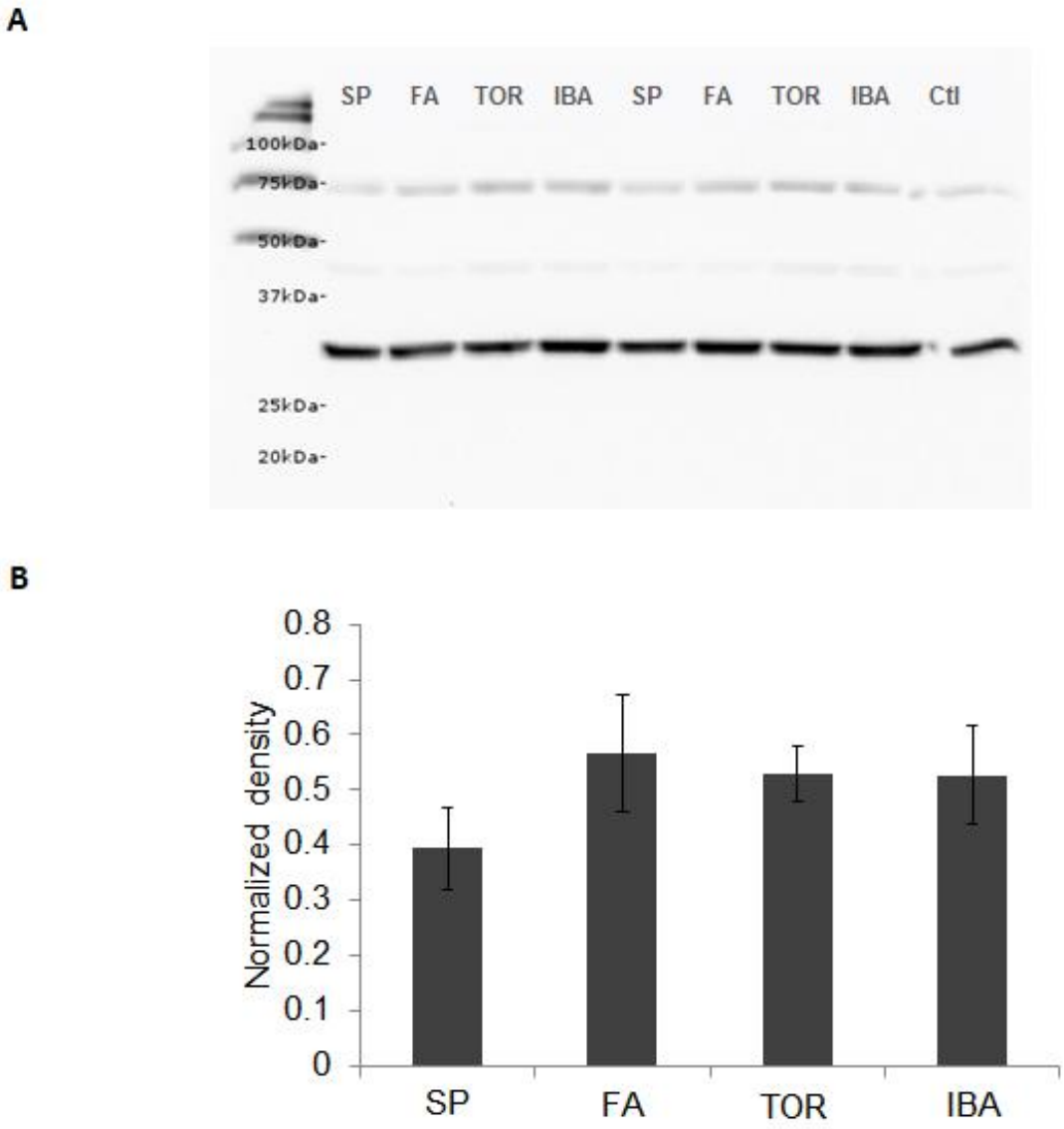

**Figure 3.4. Seasonal respiration rates in isolated BAT mitochondria.** BAT mitochondria were isolated from SP, FA, TOR, and IBA ground squirrels. *State 4* (non-phosphorylating; maximal) respiration rates were measured at complexes I-IV. *State 4* rates were significantly higher in hibernation (TOR and IBA) compared to SP at complex II (one-way ANOVA, $P < 0.05$). *State 4* rates were also significantly lower in FA compared to IBA at complex III (one-way ANOVA, $P < 0.05$). Time points at each complex that are not connected by the same letter are significantly different (Tukey's HSD). Data are means ± SE. Number of animals (n) for each group is listed at the bottom of the respective bar. Abbreviations: SP, spring; FA, fall; TOR, torpor; IBA, interbout arousal; SE, standard error.

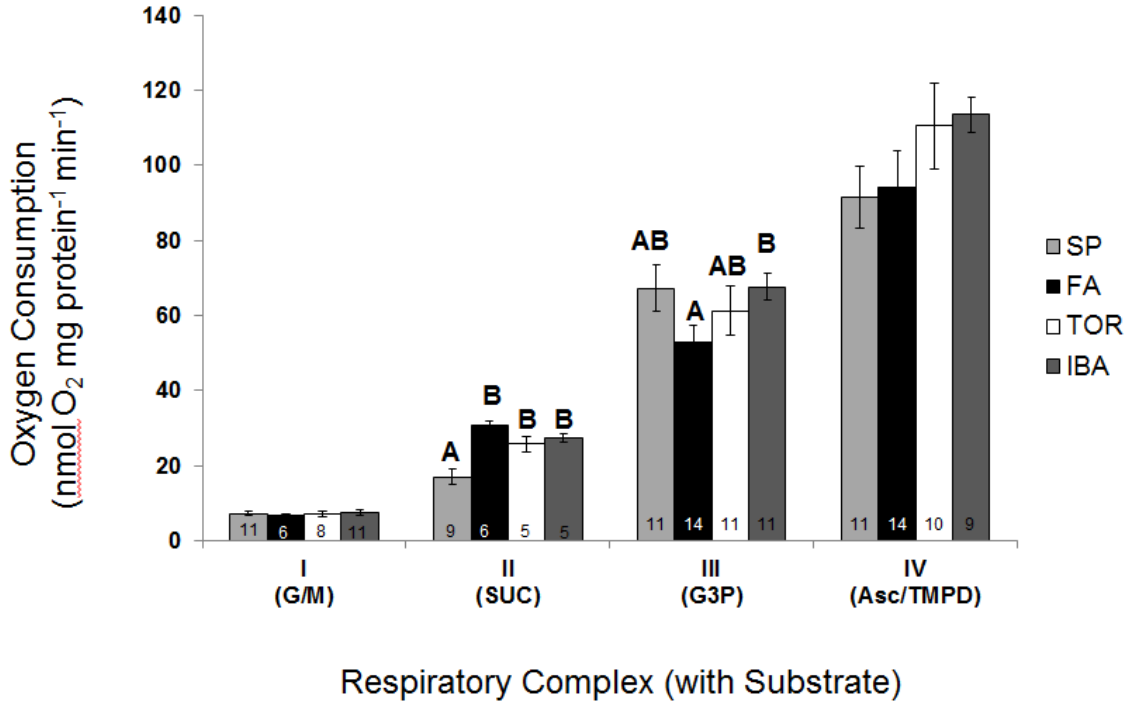

**Figure 3.5. Respiration rates of BAT mitochondria at different temperatures.** BAT mitochondria were isolated from SP, TOR, and IBA ground squirrels. *State 4* (non-phosphorylating; maximal) respiration rates were measured at complex II, using succinate as a fuel only, at six different temperatures (5, 13, 21, 29, 37°C). There were no significant differences observed between time points at any temperature. Data are means ± SE. $n$ = 6 for each time point at each of the five temperatures (except for SP, which only had $n$ = 2 for 21°C and $n$ = 2 for 29°C). Abbreviations: SP, spring; TOR, torpor; IBA, interbout arousal; SE, standard error.

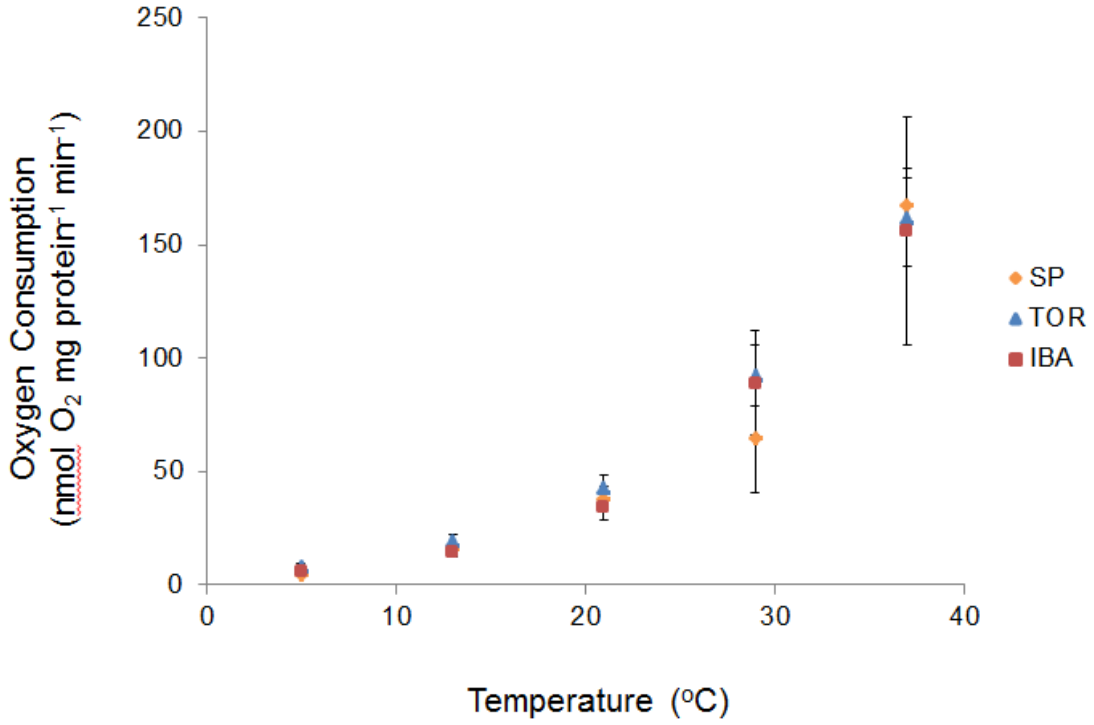

**Figure 3.6. Comparison of BAT transcripts (A) and mitochondrial proteins (B).** Top 20 most abundant BAT transcripts found in mitochondria (A) were compared to the top 20 most abundant BAT mitochondrial proteins (B). Abbreviations: ACAA2, 3-ketoacyl-CoA thiolase; ACADL, acyl-CoA dehydrogenase; ACADS, short-chain specific acyl-CoA dehydrogenase; ACADVL, very long-chain specific acyl-CoA dehydrogenase; ACO2, aconitate hydratase; ATP5B, ATP synthase, beta polypeptide; ATP5A1, ATP synthase, alpha subunit 1; ADCK3, aarF domain containing kinase 3; ACADM, acyl-CoA dehydrogenase; ACSL1, acyl-CoA synthetase long-chain family member 1; CS, citrate synthase; ECH1, enoyl CoA hydratase 1; ETFA, electron-transfer-flavoprotein, alpha polypeptide; HADHA, trifunctional protein, alpha subunit; HADHB, trifunctional protein, beta subunit; HSPD1, heat shock 60kDa protein 1; HSPA9, heat shock 70kDa protein 9; HSDL2, hydroxysteroid dehydrogenase like 2; IDH3B, isocitrate dehydrogenase 3 beta; IMMT, inner mitochondrial membrane protein; LRPPRC, leucine-rich PPR-motif containing; MDH, malate dehydrogenase; NDUFS, NADH dehydrogenase, Fe-S protein; OGDH, oxoglutarate dehydrogenase; PC, pyruvate carboxylase; SDHA, succinate dehydrogenase complex, subunit A; UCP1, uncoupling protein 1; UQCRC2, ubiquinol-cytochrome c reductase core protein II; UQCRC1, ubiquinol-cytochrome c reductase core protein I.

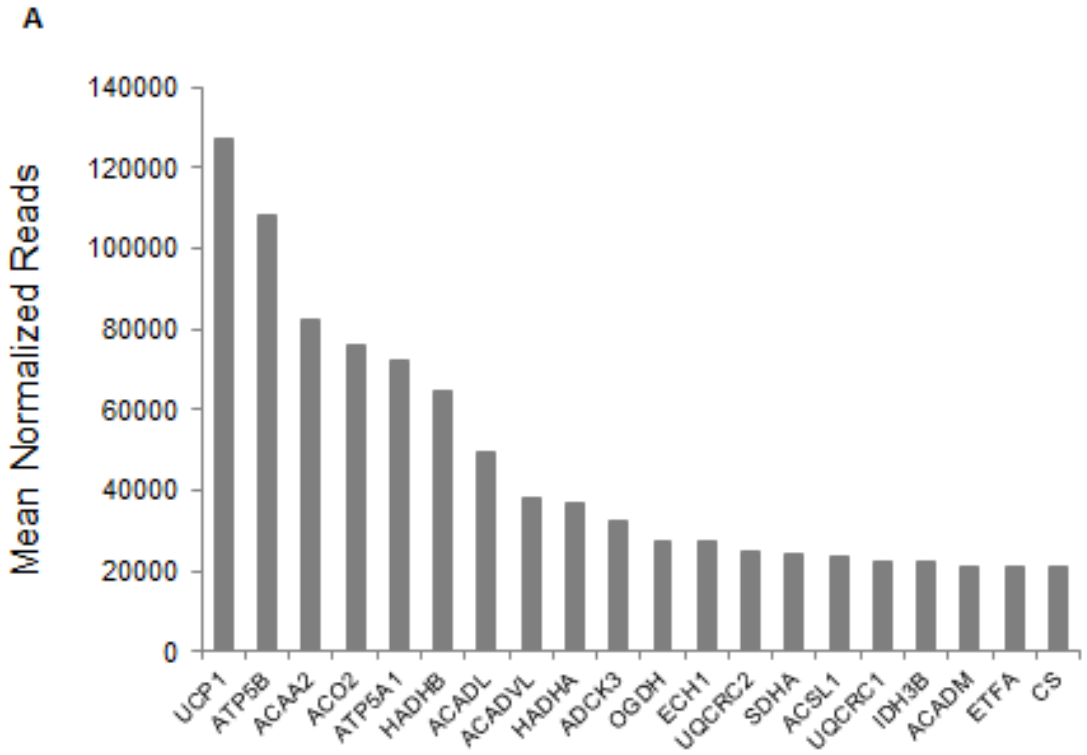

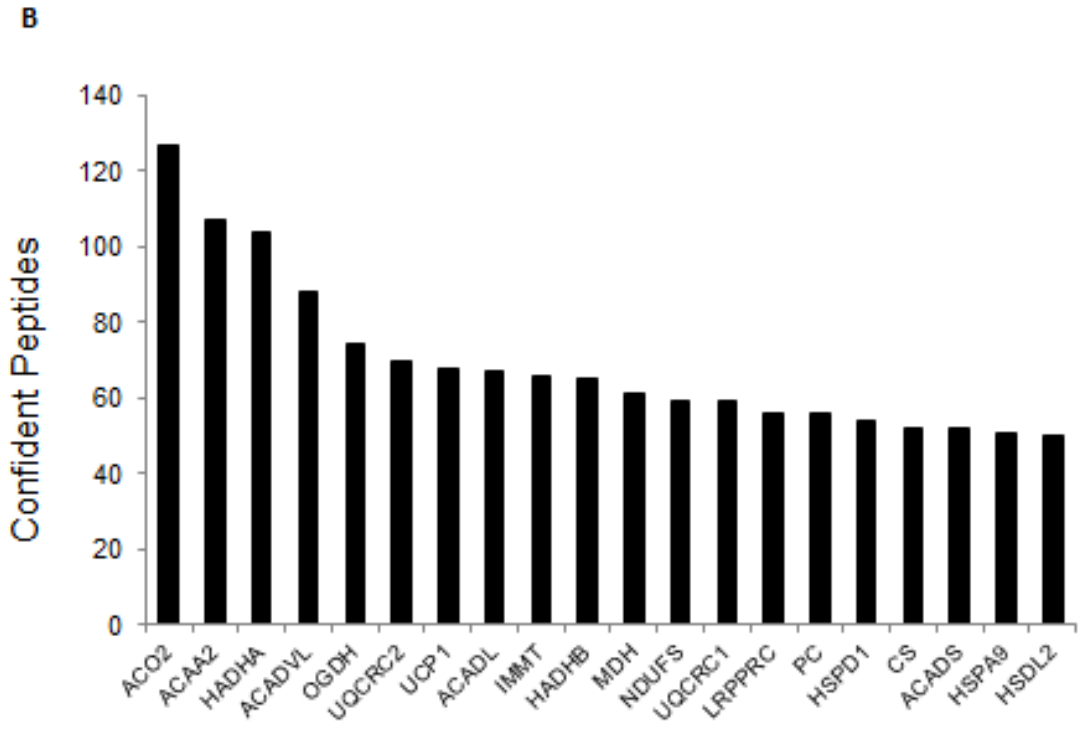
B
Confident Peptides
140
120
100
80
60
40
20
0
ACO2
ACAA2
HADHA
ACADVL
OGDH
UQCRC2
UCP1
ACADL
IMMT
HADHB
MDH
NDUFS
UQCRC1
LRPPRC
PC
HSPD1
CS
ACADS
HSPA9
HSDL2

**Table 3.1. Differentially expressed BAT proteins showing highest expression in hibernation.**

| Annotation Terms | Score | Genes* |
|---|---|---|
| **Subcellular Location** | | |
| Mitochondrial Membrane | 24.04 | *CKMT1B, CPT2, SAMM50, NLRX1, TIMM50, OGDH, HADHA, HADHB, GOT2, SLC25A20, ACSL1, MTCH2, DNAJC11, HADH, CPT1B, ACAA2, ABCB8, IMMT, AK2, CRAT, VDAC2, SLC25A11, NNT, PHB2, PMPCA, PMPCB, PC* |
| Mitochondrial Matrix | 11.13 | *PDPR, ACADS, CYCS, CS, AK3, ECHS1, IDH3B, OGDH, VDAC2, HADHA, HADHB, GOT2, IDH3G, PITRM1, HADH, PMPCA, PDHX, PMPCB, PC* |
| **Mitochondrial Import** | | |
| Fatty Acid Transport | 2.50 | *GOT2, CPT1B, SLC25A20, CPT2* |
| Ion Transport | 2.50 | *CPT1B, SLC25A20, CPT2, NNT, AMACR, VDAC2* |
| Transmembrane Transport | 2.50 | *CPT1B, SLC25A11, SLC25A20, CPT2, ABCB8, MTCH2, TIMM50, VDAC2* |
| **Mitochondrial Metabolism** | | |
| Fatty acid Metabolism/ β-oxidation | 10.39 | *ACAA2, CPT1B, CPT2, ACSL1, ACADS, ECHS1, CRAT, HSD17B4, HADH, HADHA, HADHB, DECR1* |
| TCA Cycle | 4.13 | *IDH3G, CS, IDH2, IDH3B, OGDH, PCK2, PC* |
| Isocitrate Metabolic Process | 4.13 | *IDH3G, IDH2, IDH3B* |
| Aerobic Respiration | 4.13 | *NNT, IDH3G, CYCS, CS, IDH2, IDH3B, OGDH* |
| **Binding and Carrier Activity** | | |
| Conenzyme Binding | 10.00 | *D2HGDH, AIFM1, ACADS, IDH3B, DECR1, OGDH, HADHB, NNT, IDH3G, IDH2, HADH, PDHX* |
| NAD Binding | 4.13 | *NNT, IDH3G, IDH2, IDH3B, HADHA, HADHB* |
| Fatty Acid Binding | 2.77 | *ACADS, HADHA, HADHB* |
| FAD Binding | 1.50 | *D2HGDH, AIFM1, ACADS* |
| Adenyl Nucleotide Binding | 1.45 | *CPT1B, D2HGDH, ABCB8, IDH3G, ACSL1, CKMT1B, AIFM1, ACADS, AK3, NLRX1, AK2, PC* |

Enrichments by DAVID. "Score" denotes DAVID enrichment score (significance set > 1.3).
(*represents gene abbreviations for mitochondrial proteins.)

**Table 3.2. Differentially expressed BAT proteins showing highest expression in spring.**

| Annotation Terms | Score | Genes* |
|---|---|---|
| **Subcellular Location** | | |
| Mitochondrial Membrane | 6.33 | *GPD2, GCDH, SHMT2, SUCLG1, NDUFA7, ACAT1, SLC25A12, ACADVL, SDHA, SDHB, SLC25A3, ETFDH, HSPD1* |
| Mitochondrial Matrix | 17.01 | *BCKDHA, GCDH, SHMT2, ACO2, SUCLG2, SUCLG1, LARS2, ACAT1, ACADVL, DBT, ACSS1, LONP1, MUT, IVD, ALDH4A1, HSPD1, PCCB, OAT, ETFB, LRPPRC, PCCA, ACSM5, ETFA* |
| **Mitochondrial Metabolism** | | |
| Acetyl-CoA Metabolism | 5.15 | *SDHA, SDHB, ACSS1, ACO2, SUCLG2, MLYCD, SUCLG1* |
| Succinate Metabolism | 5.15 | *SDHA, SDHB, ACO2, SUCLG2, SUCLG1, SDHA, SDHB* |
| Fatty Acid Metabolism | 3.31 | *ACADVL, GCDH, ALDH7A1, ACAT1, ALDH9A1, ACSS1* |
| Pyruvate Metabolism | 3.31 | *ALDH7A1, ACAT1, ALDH9A1* |
| **Binding and Carrier Activity** | | |
| Conenzyme Binding | 6.06 | *SDHA, ACADVL, DBT, GCDH, ALDH6A1, IVD, ETFDH, ACAD10, ETFA* |
| FAD Binding | 6.06 | *GPD2, SDHA, ACADVL, GCDH, IVD, ETFDH, ACAD10, ETFB, ETFA* |
| Adenyl Nucleotide Binding | 4.06 | *ACTB, GCDH, SUCLG2, LARS2, ACSS3, ACSF2, SDHA, ACADVL, TRAP1, ACSS1, LONP1, IVD, ETFDH, HSPD1, PCCB, EHD2, ACAD10, PCCA, ACSM5, ETFA* |
| **Electron Transport System** | | |
| OXPHOS | 3.33 | *SLC25A12, SDHA, SDHB, NDUFA7, ETFDH, ETFB, ETFA* |

Enrichments by DAVID. "Score" denotes DAVID enrichment score (significance set > 1.3).
(*represents gene abbreviations for mitochondrial proteins.)

## SECTION 3.2: DISCUSSION

### Introduction

Brown adipose tissue plays a crucial role and undergoes maximal activity when participating in non-shivering thermogenesis. This important function occurs frequently as thirteen-lined ground squirrels readily arouse from torpor to IBA numerous times throughout the hibernation season. The major thermogenic function and characteristics of BAT are primarily due to mitochondria containing UCP1 that short-circuits the electron transport system and thereby produces heat. This thermogenic capacity and activity of BAT is probably not necessary during spring or summer; therefore, it is presumed that both BAT mitochondrial recruitment and function change seasonally. Here, we investigated BAT morphology, mitochondrial proteomics, and mitochondrial function to evaluate components essential for BAT function during heterothermic and homothermic states. We also traced our findings back with the BAT transcriptome (Hampton et al., 2013) to develop an understanding of how gene and protein expression correlate with function in brown adipose tissue mitochondria.

### Increase of BAT Mitochondrial Abundance Allows for Enhanced Metabolic Activity

Brown adipose tissue mass is reduced in the spring but increases during fall in preparation for hibernation. This trend is also evidenced by large proteome differences between the two homeothermy states in BAT compared to other tissues (Grabek et al., 2015). BAT recruitment is also observed by increased mitochondrial membrane proteins (Cannon & Nedergaard, 2004). Unlike previous studies (Hindle & Martin, 2014), we

were able to detect many of the mitochondrial membrane proteins due to our proteomics technique utilizing a barocycler (see Materials and Methods (Chapter 2) for details). Rather than abundant changes in ETS proteins, structural mitochondrial proteins (e.g. membrane transporters) are increased in hibernation (Hindle & Martin, 2014). This increase in membrane transporters allows BAT mitochondria to have an increase in fatty acid handling during hibernation (Grabek et al. 2015; Hindle & Martin, 2014).

During hibernation, BAT mitochondria rely on numerous lipid reserves for fuel that are present throughout the hibernation season (Grabek et al., 2015). This is observed by increased reducing equivalents (i.e. NADH and $FADH_2$) being produced during torpor and IBA shuttling into the ETS, along with an increase in fatty acid handling. The increase in lipid utilization and its resulting reducing equivalents allows for an increase in mitochondrial metabolism and efficiency during hibernation. This observation is supported at the transcriptome and proteome levels as transcripts and proteins for ubiquinone are enhanced in TOR and IBA. For example, *COQ10A* transcript is significantly higher in IBA compared to spring (Hampton et al., 2013). COQ10B has higher expression in HIB in the mitoproteome, and Hindle and Martin (2014) show COQ5 protein being highly expressed in HIB as well.

The enhancement of reducing equivalents from lipid metabolism during hibernation is also observed at the functional level, as respiration rates of BAT mitochondria at three of the four complexes are high during TOR and IBA. These high respiration rates allow heat to be produced in large quantities efficiently to aid in arousal. In fact, there is no difference in respiration rates between TOR and IBA, suggesting that

BAT mitochondria are primed and ready during hibernation to produce heat once norepinephrine signal is present. Unlike the suppression in respiration rates of liver mitochondria during torpor (reviwed in Staples (2014), BAT mitochondria show no suppression of respiration during torpor at any temperature. Furthermore, BAT respiration retains one-third of its optimum activity during hibernation in the thirteen-lined ground squirrel, while the kidney and white adipose tissue reduce their metabolism to a minimum (Hook & Guzman, 1941).

Spring Contains Enhanced Mitochondrial Protein and Function

Whereas lipid metabolism is the primary fuel selection during hibernation, the spring time point is characterized by an increase in carbohydrate metabolism (Carey et al., 2003). This is supported by the mitoproteome, in which SP is less enriched in fatty acid metabolism, and more enriched for acetyl-CoA and succinate metabolism. However, we see suppression of respiration rates at complex II in SP, using succinate as a fuel. In general, succinate metabolism is relatively simple, requiring only transport across the inner mitochondrial membrane and oxidation by ETS complex II (Staples, 2014). Metabolism of pyruvate derivatives, such as glutamate/malate, is more complex, and includes oxidation through the TCA cycle. Suppression of BAT mitochondrial respiration in SP is more modest with these substrates (i.e. complex I) than it is with succinate, suggesting that much of the suppression occurs at complex II.

The observed suppression of succinate-fueled respiration in spring may be caused by ETS complex II inhibition via oxaloacetate, a TCA cycle intermediate (Staples, 2014).

Upon investigating succinate-fueled respiration at complex II at different temperatures between SP, TOR and IBA, we do not see the same suppression during SP. This suggests that the mitochondrial metabolic activity involving the TCA cycle may not be enhanced during SP in brown adipose tissue (Chaffee et al., 1964). Overall, these functional differences in spring and hibernation suggest seasonally distinct regulation of TCA cycle intermediates. It is noteworthy that the observed seasonality will produce the most metabolically meaningful differences in concentrations of isocitrate, succinate and oxaloacetate, all able to exert allosteric or competitive effects on the activity of respiratory complex II (Armstrong & Staples, 2010; Brown et al., 2013; Chung et al., 2011; Hindle & Martin, 2014; Staples, 2014).

Furthermore, the SP time point has an increase in handling the reducing equivalent $FADH_2$, which can be generated by the glycerol phosphate shuttle. The glycerol phosphate shuttle contains two components, the cytosolic glyercol-3-phosphate dehydrogenase (GDP1) and the mitochondrial form (GDP2). The glycerol phosphate shuttle and its corresponding enzymes are found highest in mammalian BAT; supporting cytosolic ATP generation by NADH reoxidation (Chaffee et al., 1966; Ohkawa et al., 1969). In BAT, all energy created by oxidative phosphorylation is dissipated as heat (Nicholls & Locke, 1984), and since BAT mitochondria have little ATP synthase, ATP production is important (Cannon, 1977; Mráček et al., 2013). In general, GDP2 converts glycerol to glycerol-3-phosphate, which leads to transport of $FADH_2$ into mitochondria via ubiquinone for respiration (Mráček et al., 2013; Houstěk et al., 1975). The mitoproteome shows an enhancement of GDP2, which is further supported by high

respiration rates at complex III in SP when fueled with glycerol-3-phosphate. Additionally, glycerol kinase, the enzyme that converts glycerol to glyercol-3-phosphate, is significantly higher in the spring than fall in the transcriptome, further suggesting an increase in $FADH_2$ handling during spring (Hampton et al., 2013). Moreover, the cytosolic form of the glycerol phosphate shuttle is favored during the fall in ground squirrels, thereby allowing an increase in lipid stores needed for hibernation (Hindle & Martin, 2014). This GDP2 to GDP1 switch is also evidenced by significantly decreased respiration rates at complex III in FA compared to IBA. Overall, the mitochondrial component of the glycerol phosphate shuttle is enhanced in the spring, which is likely an element of retained thermogenic capacity in spring BAT, despite reduced fatty acid metabolism and lipid reserves (Hindle & Martin, 2014).

Conclusions: Integration of BAT Transcriptome, Mitoproteome, and Function

Brown adipose tissue mitochondria play an important role in the adaptive thermogenesis portrayed by the thirteen-lined ground squirrel. Results from this study further validate the importance BAT mitochondria play during hibernation, as mitochondrial proteins for fatty acid handling and metabolism are enhanced during hibernation (Figure 3.8). In addition, functional analysis on mitochondrial bioenergetics also show increased respiratory capacity of BAT mitochondria during hibernation, all of which contributes to the massive and essential amount of heat generated by BAT for arousals (Figure 3.8).

Although the basis of this study measured *in vitro* mitochondrial dynamics, a more complete metabolic picture was constructed due to the integration of BAT transcriptome, mitoproteome and functional assessments. Despite the transcriptome giving us massive depth and coverage, mRNA levels are not always correlated closely with protein abundance in living systems (Yin et al., 2013; Gry et al., 2009; Nie et al., 2007; Foss et al., 2011; Pascal et al., 2008). Therefore, it was essential to estimate the changes in mitochondrial proteins in response to hibernation for a better understanding of the molecular mechanisms underlying functional adaptations in mitochondria. The results of this study suggest that the regulation of BAT function is not at the mitochondrial level. As we have shown, BAT mitochondria are primed to produce heat regardless of the season. Therefore, the overall control and regulation that allows BAT to be seasonally optimized for rapid and efficient heat production is most likely at the cellular level (Hampton et al., 2013; Hindle & Martin, 2014).

In the end, this study improves our understanding of the metabolic feats in a hibernator. Future studies should consist of identifying and characterizing novel protein isoforms, such as alternative splice variants, single amino acids variants, mutations, and post-translational modifications of mitochondrial proteins. Careful analysis of these amino acid variants may provide essential underpinnings into the hibernation phenotype and may aid in better understanding how BAT function is maintained throughout hibernation. Additionally, future functional studies involving various fuels, such as fatty acid derivatives, should be conducted to investigate if specific substrates at different temperatures play a role in the overall thermogenic capacity of BAT mitochondria across

the year. Even assessing coupled BAT mitochondria may provide mechanistic insight of BAT and may aid in understanding the overall mitochondrial metabolism of a natural hibernator.

## Section 3.2 Figures & Tables

**Figure 3.7. Mitochondrial model of BAT transcripts (A) and proteins (B) during hibernation.** The results of a previous study (Hampton et al. 2013) were used to construct a model of isolated BAT mitochondria during hibernation (torpor and IBA). (A) The genes shown in the model are mRNA that show highest expression during hibernation. (B) The proteins shown in the model show highest expression during hibernation. *UCP1 did not make the differential expression cutoff (see Materials and Methods for details); however, it does have the trend of being higher expressed during hibernation compared to spring. Abbreviations: ACADS, short-chain specific acyl-CoA dehydrogenase; ACSL1, long-chain-fatty-acid--CoA ligase 1; ADCK1, aarF domain containing kinase 1; COQ10A, coenzyme Q10 homolog A; CPT1A, carnitine palmitoyltransferase 1A; CPT2, carnitine O-palmitoyltransferase 2; CYC1, cytochrome c-1; DECR1, 2,4-dienoyl-CoA reductase; HADH, hydroxyacyl-coenzyme A dehydrogenase; HADHA, trifunctional enzyme subunit alpha; HADHB, trifunctional enzyme subunit beta; IDH2, isocitrate dehydrogenase; IDH3A, isocitrate dehydrogenase 3 alpha; NDUFA10, NADH dehydrogenase 1 alpha subcomplex, 10; NDUFA9, NADH dehydrogenase 1 alpha subcomplex, 9; NDUFAF2, NADH dehydrogenase 1 alpha subcomplex, assembly factor 2; NDUFV3, NADH dehydrogenase flavoprotein 3; OGDH, 2-oxoglutarate dehydrogenase; PDHX, pyruvate dehydrogenase protein X component; PDK4, pyruvate dehydrogenase kinase, isozyme 4; SLC25A20, mitochondrial carnitine/acylcarnitine carrier protein; TIMM50, translocase of inner mitochondrial membrane 50 homolog; SUCLA2, succinate-CoA ligase, ADP-forming, beta subunit; UCP1, uncoupling protein 1; UQCRC2, ubiquinol-cytochrome c reductase core protein II.

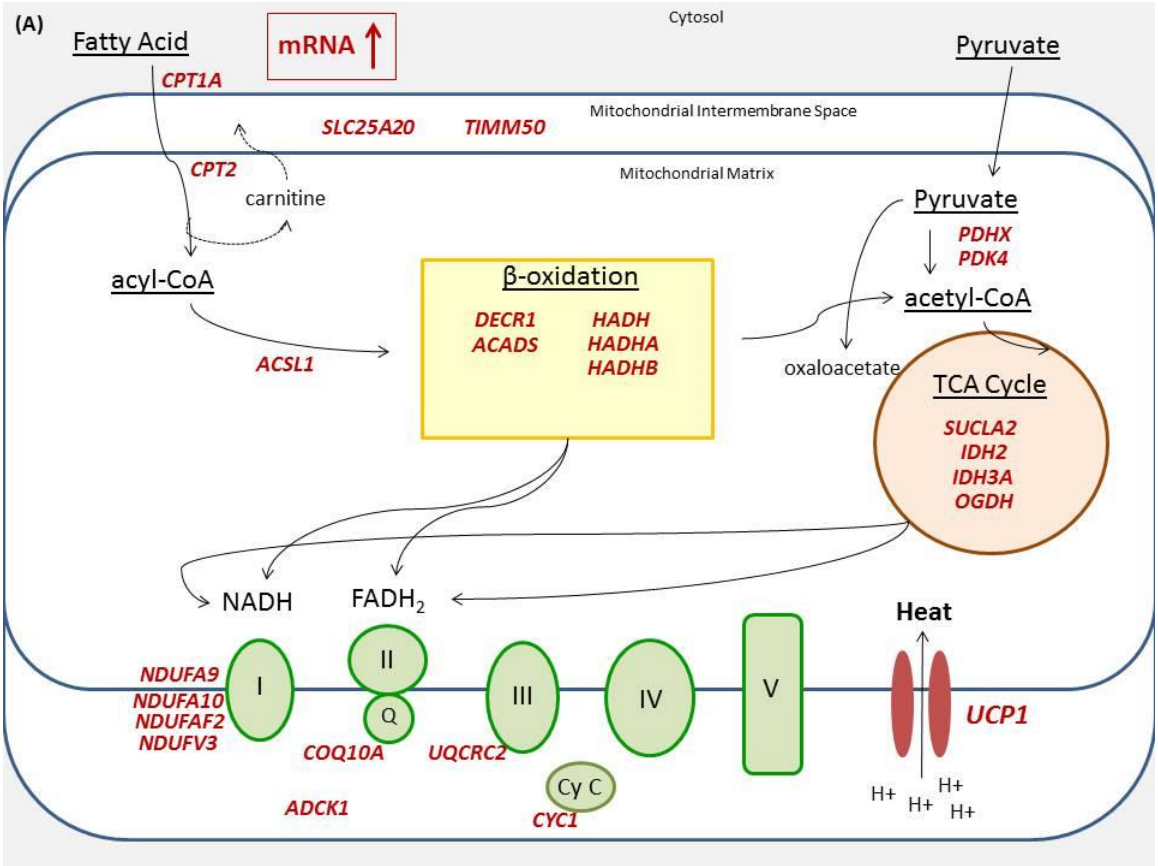

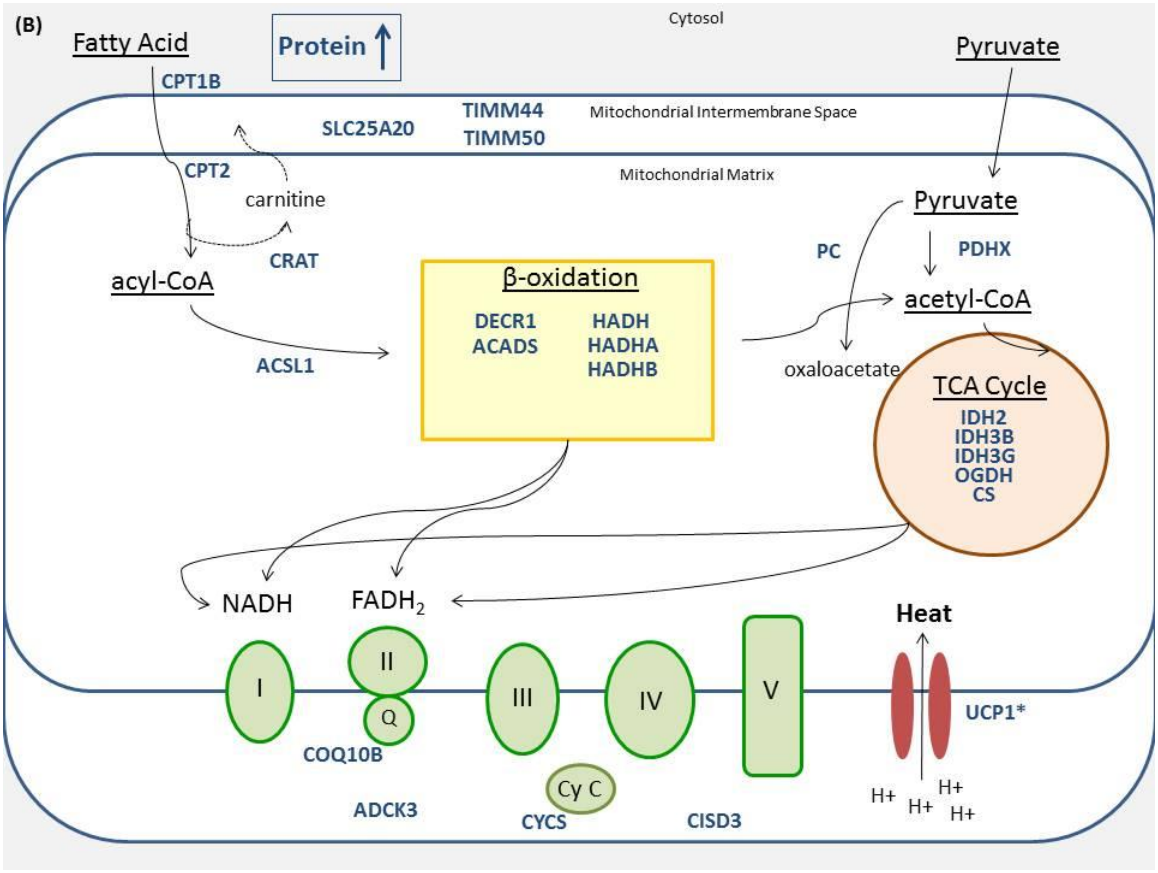
(B)
Fatty Acid
Protein
Cytosol
Pyruvate
CPT1B
SLC25A20
TIMM44
TIMM50
Mitochondrial Intermembrane Space
CPT2
carnitine
Mitochondrial Matrix
Pyruvate
CRAT
PC
PDHX
acyl-CoA
β-oxidation
acetyl-CoA
DECR1
ACADS
HADH
HADHA
HADHB
ACSL1
oxaloacetate
TCA Cycle
IDH2
IDH3B
IDH3G
OGDH
CS
NADH
FADH2
Heat
I
II
III
IV
V
Q
UCP1*
COQ10B
Cy C
ADCK3
CYCS
CISD3
H+
H+
H+
H+

**Figure 3.8. Mitochondrial model of BAT transcripts, proteins, and function during hibernation.** The results of this study were used to construct a functional model of isolated BAT mitochondria during hibernation (torpor and IBA). The genes shown in the model are both mRNA and protein that show highest expression during hibernation. 1) Increases in membrane and transport proteins during hibernation allow for an increase in fatty acid handling in BAT mitochondria. 2) Along with fatty acid handling, there is also an increase in mitochondrial metabolism associated with β-oxidation and TCA cycle are present during hibernation. This is evidenced by enhancements of both transcripts (Hampton et al. 2013) and proteins associated with the two pathways. This metabolic enhancement allows for an increase in reducing equivalents (i.e. NADH and $FADH_2$) to flow into the electron transport system (ETS), evidenced again by the increase in respiration during hibernation. 3) The increase in reducing equivalents shuttling through the ETS is indicated by enhanced respiration rates through the various complexes of the ETS during hibernation. This is shown through the increased maximal respiration rates of various ETS complexes during hibernation, along with an enhancement of proteins that aid in the transfer of electrons through the ETS (see Table 1). 4) The enhancements of all the various mitochondrial aspects (#1-3) allow for an increase in heat production via UCP1 during hibernation. This rapid and efficient heat production aids in the rewarming process of arousal from torpor to IBA. (UCP1 did not make the differential expression cutoff (see Materials and Methods for details); however, it does have the trend of being higher expressed during hibernation compared to spring.) Abbreviations: ACADS, short-chain specific acyl-CoA dehydrogenase; ACSL1, long-chain-fatty-acid--CoA ligase 1; CPT2, carnitine O-palmitoyltransferase 2; DECR1, 2,4-dienoyl-CoA reductase; HADH, hydroxyacyl-coenzyme A dehydrogenase; HADHA, trifunctional enzyme subunit alpha; HADHB, trifunctional enzyme subunit beta; IDH2, isocitrate dehydrogenase; OGDH, 2-oxoglutarate dehydrogenase; PDHX, pyruvate dehydrogenase protein X component; SLC25A20, mitochondrial carnitine/acylcarnitine carrier protein; UCP1, uncoupling protein 1.

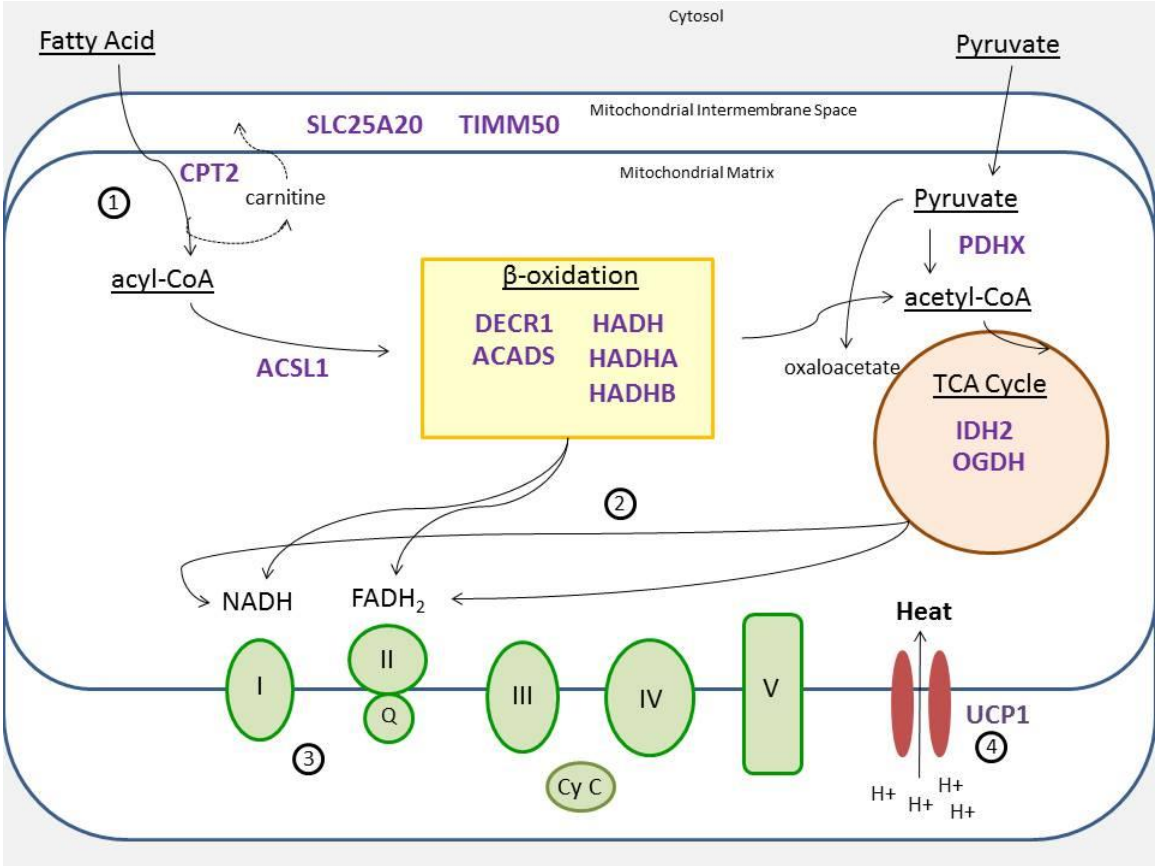

# CHAPTER 4: Enhanced Oxidative Capacity of Brain Mitochondria during Hibernation

* This chapter is included in the following manuscript, which will be submitted for publication in a peer-reviewed journal: Ballinger, M.A., Schwartz, C. and Andrews, M.T. (*in preparation)* Enhanced Oxidative Capacity of Brain Mitochondria during Hibernation.

## SECTION 4.1: RESULTS

Seasonal Respiration Rates:

To assess the mitochondrial bioenergetics of brain mitochondria in the thirteen-lined ground squirrel, *state 3* (phosphorylating) respiration rates were measured in isolated whole brain mitochondria. *State 3* respiration is defined as ADP-stimulated respiration of isolated, coupled mitochondria (Chance & Williams, 1955). It is a near-maximal state of oxygen consumption and ATP synthesis, and is measured in the presence of energetic substrates and ADP (Chance & Williams, 1955). Using three different substrates (glutamate/malate (G/M), succinate (SUC), and glycerol-3-phosphate (G3P), mitochondria from hibernating animals (HIB, torpor and IBA) had significantly higher *state 3* respiration rates at complexes I and II compared to spring (SP; T-test, $P < 0.05$; Figure 4.1). This same trend is also observed with complex III, where *state 3* respiration rates with G3P showed higher rates in HIB compared to SP, but this result is non-significant. Overall, these results suggest that complexes I and II play an important and different role during HIB than complex III. In addition, fueling complex III with G3P is indirect (Mráček et al., 2013; Houstěk et al., 1975), which is perhaps why we see low respiration rates at complex III (as complex III should have higher rates than complexes I and II).

Additionally, *state 4* (non-phosphorylating; maximal) rates were measured to assess respiratory control ratios (RCRs). *State 4* respiration is the maximal respiration rate of isolated mitochondria that has no influence on ATP synthesis (Chance & Williams, 1955). The RCR of isolated mitochondria is the ratio between *state 3* and *state*

*4*, and is an indicator of coupling efficiency between substrate oxidation and ATP synthesis (Chance & Williams, 1955; Zhang et al., 2012). The RCRs, using G/M, for SP, summer (SU), fall (FA), and HIB were 2.81 ± 0.35, 2.58 ± 0.74, 2.68 ± 0.58, and 2.79 ± 0.29 respectively. The observed RCRs indicate that the seasonal mitochondria used in this study were well coupled and not physically damaged.

Because SP and HIB show the most dramatic and significant differences, subsequent experiments were done only comparing these two time points.

Proton Leak Kinetics:

The kinetics of proton leak were also determined for isolated brain mitochondria by the simultaneous measurement of membrane potential ($\Delta\Psi_m$) and *state 4* respiration rates (see Materials and Methods (Chapter 2) for details). Proton leak kinetics were determined for both SP and HIB, and are summarized in Figure 4.2. Both time points were then plotted together to compare proton leak kinetics between seasons (Figure 4.3). Maximal leak-dependent respiration and membrane potential (the furthest points to the right in the Figure 4.3) were different between SP and HIB. Specifically, there was a significant increase in maximum $\Delta\Psi_m$ in HIB compared to SP (T-test, $P = 0.01$; Table 4.1). There were, however, no significant differences in maximal *state 4* respiration rates (Table 4.1). Additionally, there was also a significant increase in $\Delta\Psi_m$ in HIB compared to SP at the first addition of malonate (the second furthest points to the right in Figure 4.3; T-test, $P = 0.009$).

The highest $\Delta\Psi_m$ shared between SP and HIB was approximately 195 mV (Figure 4.3), and this shared $\Delta\Psi_m$ proton leak is higher in SP than HIB. In addition, SP had an overall higher proton leak compared to HIB, which is apparent when comparing the fit of the two curves. This suggests that proton permeability of the mitochondrial membrane is higher in SP than HIB. It also suggests that brain mitochondria during hibernation are more coupled to oxidative phosphorylation. Thus, brain mitochondria have an increase in ATP demand during hibernation, as supported by both high respiration rates (Fig. 4.1) and proton leak kinetics, as ATP demand decreases proton leak (Brand et al., 1994).

Calcium Loading Capacity:

A second parameter used to assess proton permeability and mitochondrial integrity is calcium loading capacity (Zhou et al., 2001). Isolated brain mitochondria of thirteen-lined ground squirrels were able to load significantly more calcium during SP compared to HIB (T-test, $P = 0.0002$; Figure 4.4). In the presence of cyclosporin A, mitochondria accumulated and retained all of the added $CaCl_2$ (see Materials and Methods (Chapter 2) for details). This increase in mitochondrial calcium accumulation during spring imposes a dual energetic demand on the mitochondrial proton circuit (Nicholls, 2005; Nicholls, 2009). The direct uptake of calcium into the mitochondrial matrix utilizes the proton circuit and directly competes with mitochondrial ATP synthesis (Nicholls, 2005; Nicholls, 2009). Therefore, storing calcium in the mitochondrial matrix would interfere with essential ATP production needed for hibernation, specifically, arousal from torpor to IBA. This is evidenced by low calcium loading capacity in HIB.

Additionally, elevations in cytoplasmic calcium will activate plasma membrane and endoplasmic reticulum $Ca^{2+}$ATPases with a resultant increase in ATP demand, which is suggested by the brain's physiology in hibernation.

mtDNA Copy Number:

An increase in ATP demand may be promoted by increasing the abundance of mitochondria in the specific tissue. Therefore, to assess mitochondrial abundance in the thirteen-lined ground squirrel brain, quantitative PCR (qPCR) was performed to measure mitochondrial DNA (mtDNA) copy number in frozen cerebral cortex tissues between non-hibernation (SP) and hibernation state (IBA), as shown by the mitochondria gene, *ND1* (NADH dehydrogenase, subunit 1) per the nuclear gene, *B2M* (beta-2-microglobulin) amplicons (Figure 4.5). The cerebral cortex was chosen as the representative brain tissue due to its size, as the cortex is the largest brain region, and thus, gives the best representation of mitochondrial abundance in the whole brain. No significant differences were observed in DNA copies between SP and IBA (T-test, $P = 0.141$), but a trend shows SP animals having a lower mtDNA copy number ratio compared to IBA (Figure 4.5).

## Section 4.1 Figures & Tables

**Figure 4.1. Seasonal respiration rates in isolated brain mitochondria.** Brain mitochondria were isolated and interrogated from thirteen-lined ground squirrels. *State 3* respiration rates were measured at complexes I – III. *State 3* rates were significantly higher in HIB compared to SP at complexes I and II (one-way ANOVA, $P < 0.05$). Time points at each complex that are not connected by the same letter are significantly different (Tukey's HSD). Data are means ± SE. Number of animals (n) for each group is listed at the bottom of the respective bar. Abbreviations: SP, spring; SU, summer; FA, fall active; HIB, hibernation (torpor and IBA); SE, standard error.

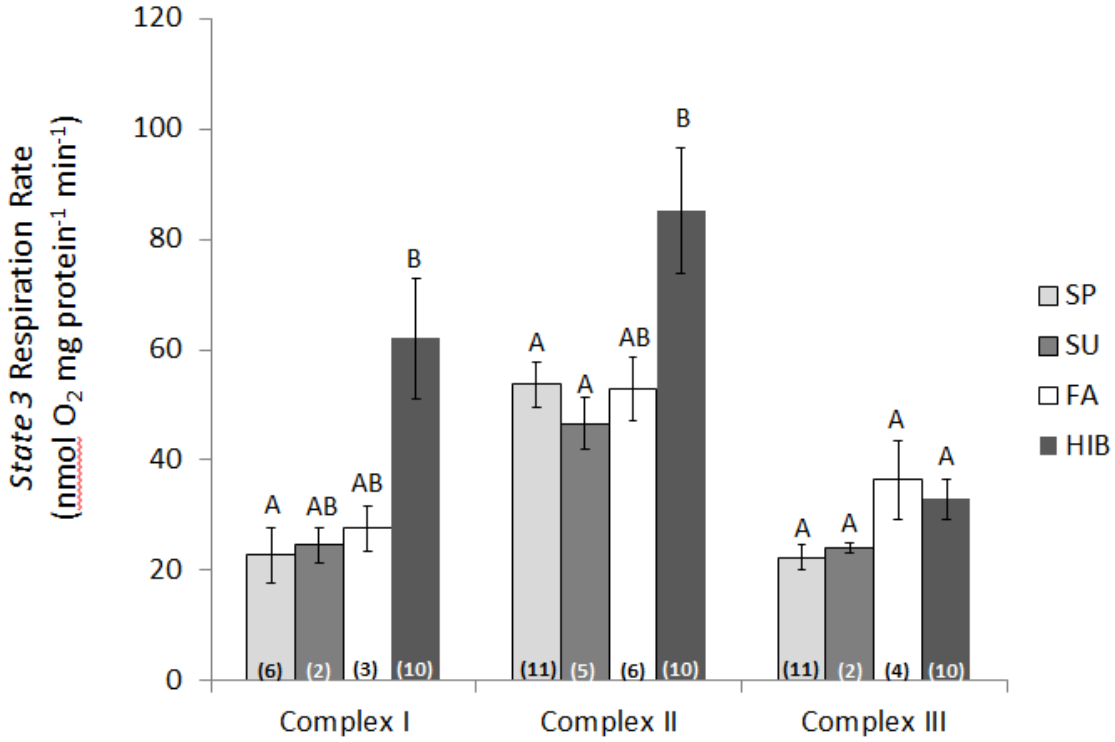

**Figure 4.2. Proton leak kinetics of brain mitochondria.** Maximal *state 4* conditions (respiration rate and membrane potential) are shown as the top right-most point. Proton leak kinetics were initiated by inducing *state 4* respiration with the addition of 10 mM succinate. The kinetics of proton leak were determined by inhibiting succinate oxidation stepwise by titrating 0.3 mM malonate until a complete inhibition was obtained, and then measuring this effect on $\Delta\Psi_m$. Values at each data point are means ± SE; $n$ = 6 for SP and $n$ = 13 for HIB (torpor and IBA). Abbreviations: SP, spring; HIB, hibernation; SE, standard error.

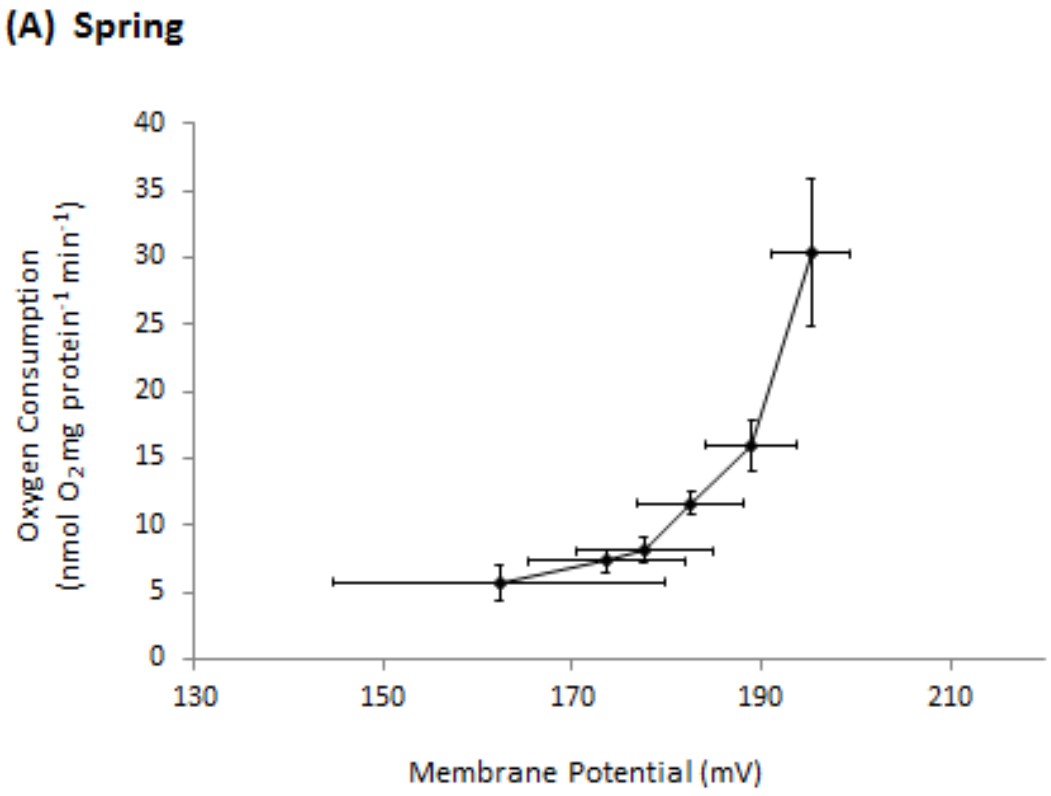

**(B) Hibernation**

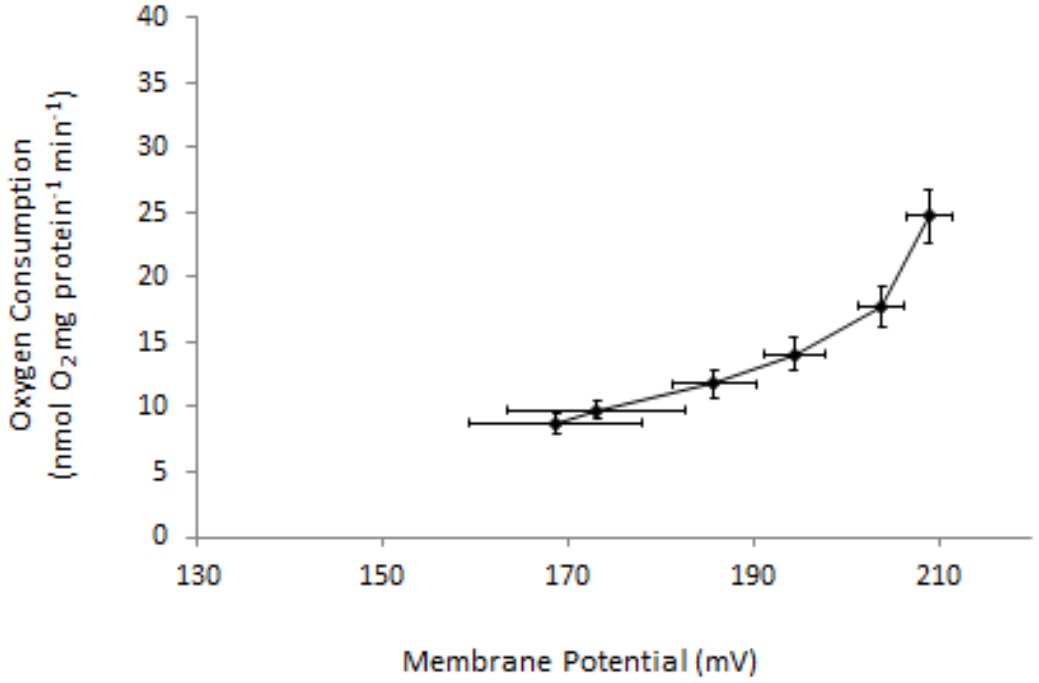

**Figure 4.3. Proton leak kinetics of brain mitochondria between spring and hibernation.** Maximal *state 4* conditions (respiration rate and membrane potential) are shown as the top right-most points. Proton leak kinetics were initiated by inducing *state 4* respiration with the addition of 10 mM succinate. The kinetics of proton leak were determined by inhibiting succinate oxidation stepwise by titrating 0.3 mM malonate until a complete inhibition was obtained, and then measuring this effect on $\Delta\Psi_m$. $\Delta\Psi_m$ was significantly higher in brain mitochondria from hibernating animals (T-test, $*P < 0.05$). *State 4* respiration was not significantly different between the two time points. Values are means (SE bars are omitted for clarity); $n = 6$ for SP and $n = 13$ for HIB (torpor and IBA). Abbreviations: SP, spring; HIB, hibernation; SE, standard error.

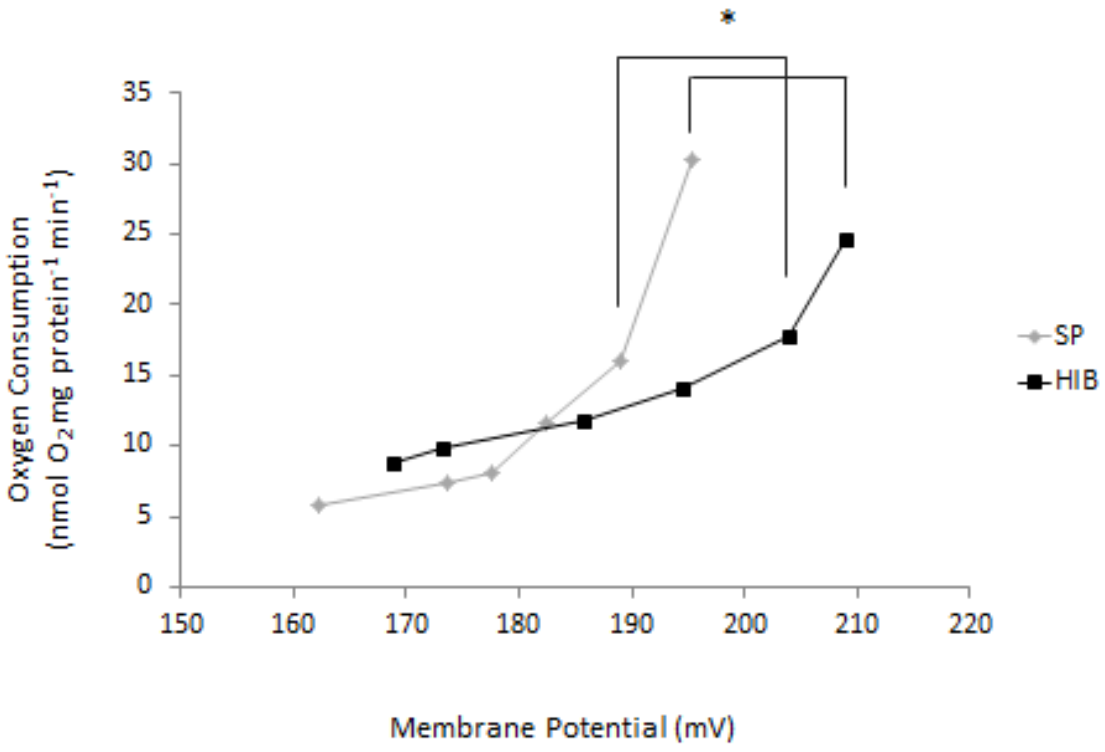

**Figure 4.4. Calcium loading capacity of brain mitochondria.** Assessment of calcium loading capacity was performed on isolated brain mitochondria from thirteen-lined ground squirrels. Briefly, $CaCl_2$ (10 mM) was titrated into the chamber upon addition of succinate (10 mM) to stimulate approximately *state 4* respiration (see Methods and Materials for details). The estimation of calcium loading capacity was determined after calcium loading halted in the mitochondrial suspension. Brain mitochondria from SP time point loaded more calcium than brain mitochondria from HIB time point (T-test, ***$P < 0.001$). Data presented are means ± SE. Abbreviations: SP, spring ($n = 6$); HIB, hibernation (torpor and IBA; $n = 13$); SE, standard error.

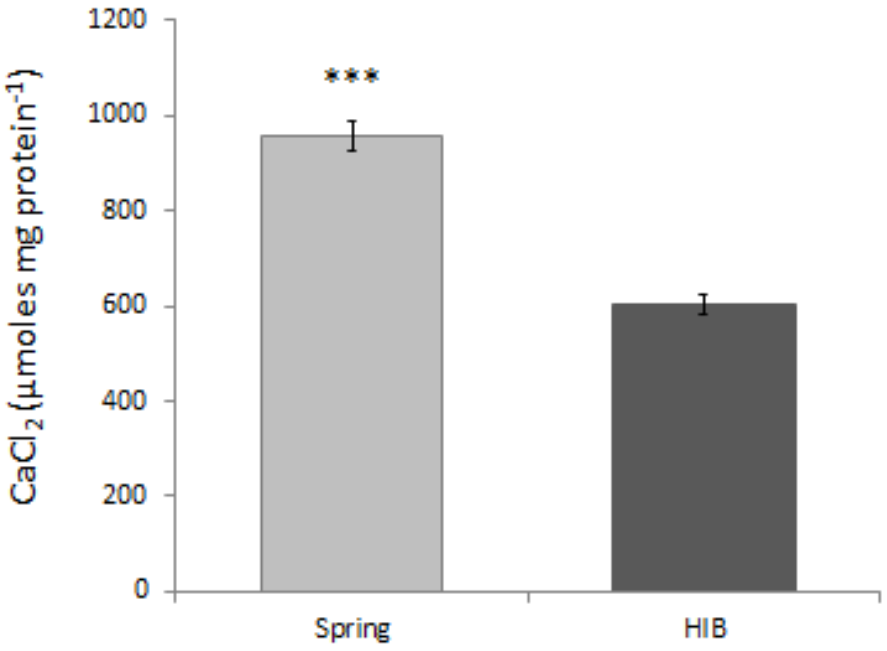

**Figure 4.5. Comparison of mtDNA copy number in brain cortex between spring and IBA.** The ratio of mitochondrial (ND1, NADH dehydrogenase, subunit 1) to nuclear (B2M, beta-2-microglobulin) DNA copies were quantified in brain cortex via qPCR. No significant differences were seen between the two time points (T-test, $P = 0.141$). Data presented are means ± SE. Abbreviations: SP, spring ($n = 6$); IBA, interbout arousal ($n = 6$); SE, standard error; qPCR, quantitative PCR.

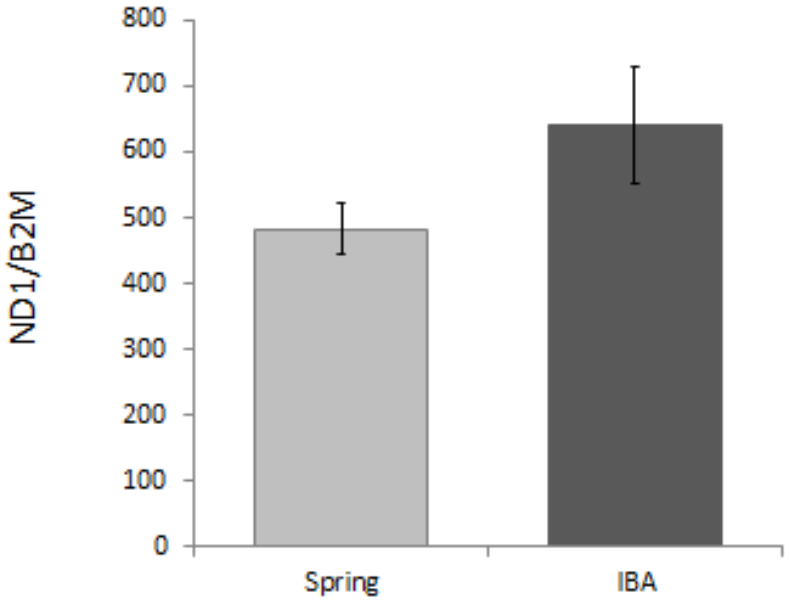

**Table 4.1. Proton leak kinetics of brain mitochondria.** Values are means ± SE. Significant differences between SP and HIB groups were determined using a Student's T-test, with $*P < 0.05$. *n*-values are in parentheses. Abbreviations: SP, spring; HIB, hibernation; SE, standard error.

| Group | *State 4* Respiration Rate (nmol $O_2$ mg protein$^{-1}$ min$^{-1}$) | Maximal Membrane Potential (mV) |
|---|---|---|
| SP | 33.3 ± 5.4 (6) | 195.2 ± 4.1 (6) |
| HIB | 24.7 ± 2.0 (13) | 209.0 ± 2.5 (13)* |

## SECTION 4.2: DISCUSSION

### Introduction

Despite enduring extreme oscillations in oxygen demand, cerebral blood flow, and body temperature during hibernation, some regions of the thirteen-lined ground squirrel brain stay active at a reduced level during torpor (Bratincsak et al., 2007; Drew et al., 2007). Moreover, synaptic plasticity and maintenance that occurs during hibernation is energy-costly and requires large amounts of ATP (Harris et al., 2012). Therefore, a major shift in energy demand is required for hibernation. As a site for oxygen consumption, aerobic metabolism, and ATP production, brain mitochondria were the primary investigation of this study. Here, we measured various mitochondrial bioenergetic properties of isolated brain mitochondria to determine metabolic function and potential molecular mechanisms underlying energy demand in the brain of the thirteen-lined ground squirrel.

### Brain Mitochondria are More Efficient during Hibernation

Brain mitochondria isolated from the thirteen-lined ground squirrel exhibit both high respiration rates and low proton leak during hibernation, suggesting a high and efficient rate of oxidative phosphorylation. Additionally, no differences were found in mitochondrial function between torpor and IBA, indicating that isolated brain mitochondria during hibernation are primed for rapid and efficient ATP production. Gallagher and Staples (2013) also saw no mitochondrial suppression in brain cortex between torpor and IBA in the thirteen-lined ground squirrel. A lack of mitochondrial

suppression in the brain during torpor is intuitive as the brain is a major metabolic tissue that signals important autonomic functions during hibernation, such as regulating metabolic rate (Drew et al., 2007; Shibao et al., 2007). In fact, high-energy phosphates in the brains of ground squirrels appear to be higher in torpor than IBA (Henry et al., 2007), suggesting that ATP is still being consumed at a reduced level during torpor.

Most of the brain energy is used for synaptic and ionic gradient maintenance (Boveris & Chance, 1973; Harris et al., 2012), and this requirement of ATP is significantly diminished during torpor (Dave et al., 2012). In the golden-mantled ground squirrel (*Callospermophilus lateralis*), entry into torpor is associated with 50-60% loss of synapses, although their protein abundance does not change (von der Ohe et al., 2007). However, ATP is required prior to and during arousal for synaptic reconstruction (von der Ohe et al., 2007). This ATP requirement is supported in this study as isolated brain mitochondria from hibernating animals show enhanced mitochondrial bioenergetics. Additionally, golden hamsters (*Mesocricetus auratus*)show no reduction in synaptic mitochondrial function during oxygen-glucose deprivation (Mielke, 2013). Furthermore, brain wave activity is regained during IBA, again suggesting that synaptic reconstruction is occurring during arousal (Walker et al., 1977). In fact, studies in golden hamsters indicate that energy charge in brain is maintained during arousal (Lust et al., 1989).

Calcium Regulation Plays Significant Role in Enhanced Mitochondrial Metabolism

Mitochondrial calcium sequestration is highly dependent of the proton motive force (Mitchell & Moyle, 1967; Nicholls & Ferguson, 2013), as the balance between

mitochondrial calcium uptake and calcium efflux mechanisms are dependent on the mitochondrial proton gradient (Pamenter, 2014). During hibernation, brain mitochondria sequester significantly less calcium into the mitochondrial matrix compared to mitochondria during spring. These results also correlate with the decreased proton leak exhibited by brain mitochondria during hibernation.

In addition to the supporting functional data presented here, there are also both transcriptomic and proteomic supporting data from thirteen-lined ground squirrel brain regarding calcium uptake. For example, Schwartz et al. (2013) saw significant increases in two calcium-binding genes (*SLC24A2* and *S100A6*) during hibernation in the cerebral cortex compared to spring. These two genes may play significant roles in binding and regulating calcium levels in the brain. Additionally, Hindle and Martin (2013) showed sorcin protein (soluble resistance-related calcium binding protein, SRI) to be in low abundance at cold temperatures (i.e. torpor) in the forebrain of the thirteen-lined ground squirrel. SRI may be implicated in $Ca^{2+}$ homeostasis by regulating intracellular $Ca^{2+}$ handling during torpor (Hindle & Martin, 2013).

Moreover, the disassembly of synapses occurring with each torpor bout in thirteen-lined ground squirrels is likely to complement channel arrest in order to reduce the potential for $Ca^{2+}$ buildup at cold body temperatures and detrimental excitotoxicity (Dave et al., 2012; Hindle & Martin, 2013). It has also been shown that neurons in Daurian ground squirrels (*Spermophilus dauricus*) are able to maintain lower levels of intracellular calcium concentrations compared to rats, and thus, are better at maintaining calcium homeostasis (Zhao et al., 2014). Lastly, both arctic ground squirrels and golden

hamsters show downregulation of NMDR (N-methyl-D-aspartate receptor) function during hibernation (Ross et al., 2006; Zhao et al., 2006), blunting excitotoxicity and calcium responses, such as mitochondrial dependent apoptosis (Larson et al., 2014; Lipton, 1999).

More Efficient Production of ATP Aids in Arousal

The various functional data accumulated in this experiment allude to the observation that this efficient production of ATP is necessary for the energetically demanding arousals from torpor throughout hibernation. In support of these functional observations, Epperson et al. (2010) identified upregulation of numerous mitochondrial proteins in the thirteen-lined ground squirrel brainstem during hibernation, also suggesting rapid ATP production upon arousal from torpor. Additionally, they also found a higher expression of some mitochondrial membrane proteins (NDUFS1, NDUFS3, NDUFV2, UQCRC1, UQCRH, ATP5A1, ATP5B, and VDAC2) earlier in torpor in the brainstem of thirteen-lined ground squirrels (Epperson et al., 2010). The higher winter copy number of proteins in oxidative phosphorylation (such as complex I) allow brain mitochondria to rapidly and efficiently produce ATP for arousal (Epperson et al., 2010). In addition to ground squirrel brain proteomics, hibernating bats also alter the expression pattern of mitochondrial membrane proteins during torpor, such as an increase in voltage-dependent anion channel 2 (*VDAC2*) during torpor (Zhang et al., 2014). Moreover, both species show consistent modifications to electron handling in the ETS, such as subunits of complexes I, III, and ATP synthase (Epperson et al., 2010; Zhang et

al., 2014). These proteins are enhanced during torpor when both metabolic rate and membrane temperatures are reduced in order to successfully handle torpor-arousal cycles (Epperson et al., 2010).

Neuroprotection against ROS Formation

Mitochondria produce superoxide as a by-product of oxidative metabolism, and are a major source of intracellular reactive oxygen species (ROS) production (Boveris & Chance, 1973; Brand, 2011; Murphy, 2009). High respiration rates and membrane potentials, observed in brain mitochondria during hibernation, promote the risk of producing ROS. Moreover, since mitochondrial superoxide production is steeply dependent on the proton motive force (Korshunov et al., 1997; Lambert & Brand, 2004; Liu, 1997), proton leak pathways may generally exist to minimize oxidative damage by mitigating the proton motive force and mitochondrial superoxide production (Divakaruni & Brand, 2011). This is known as the "uncoupling to survive" hypothesis (Brand, 2000). As evidenced in this study, no uncoupling is observed throughout hibernation in brain mitochondria. Additionally, it was recently proposed that ground squirrel brain contains neuronal uncoupling protein 1 (UCP1) to aid in local thermogenesis (Laursen et al., 2015). However, our study does not support the presence of UCP1 because we see no functional evidence of the uncoupling associated with this protein. In fact, our data show that the brain mitochondria are more tightly coupled in hibernation when compared to spring. If local thermogenesis was occurring through UCP1 in the brain during hibernation, the brain mitochondria should have shown the opposite pattern.

The use of uncoupling is perhaps unnecessary for hibernators due to their sweep of protective mechanisms. Mammalian hibernators exhibit a compelling ability to tolerate oxidative stress during hibernation by eliminating free radicals generated during repeated cycles of torpor and arousal (Storey, 2010). Specifically, both glutathione and ascorbate play protective roles in the brain of ground squirrels during arousal form torpor (Dave et al., 2012; Drew et al., 1999; Tøien et al., 2001). In addition to ascorbate and glutathione, melatonin also plays a protective role to brain mitochondria during hibernation. Melatonin-receptor mediated mechanisms have been shown to aid in mitochondrial performance of thirteen-lined ground squirrel brain during arousal from torpor (Schwartz et al., *in review*). Specifically, inhibition of melatonin receptor signaling reduced *state 3* respiration rates in brain mitochondria, thus suggesting melatonin aids in the mitochondrial performance of rapid production of ATP during arousal (Schwartz et al., *in review*). It is possible that melatonin production upon arousal from torpor functions to help brain mitochondria work more efficiently during a period of extreme energy need (Schwartz et al., *in review*).

## Conclusions

The brain is a major metabolic tissue that contributes to the overall energetic needs and metabolism of the thirteen-lined ground squirrel. Unlike other tissues, where tissue metabolism is suppressed during torpor, maintenance of brain metabolism at some reduced level is critical because it is the central regulator of hibernation (Drew et al., 2007). Despite the physiological challenges associated with torpor-arousal cycles

throughout hibernation, no long-term tissue damage is observed in the brain (Dave et al., 2012; Frerichs et al., 1994). This suggests an innate adaptation to protect and maintain function in the brain during extreme physiological challenge (Dave et al., 2012).

The results of this study suggest that brain mitochondria during the hibernation season are more efficient at oxidative phosphorylation than brain mitochondria during spring (Figure 4.6). This was evidenced by: increases in *state 3* respiration rates at various complexes of the ETS; decreases in mitochondrial proton leak during hibernation; and decreased calcium loading in hibernation. These results, along with previous findings, suggest that the hibernator brain contains a streamlined mechanism capable of efficient and rapid energy production and utilization during torpor and arousal cycles of hibernation (Epperson et al., 2010). This study provides additional insight into the overall metabolic system of the thirteen-lined ground squirrel. Moreover, it aids in the understanding of both mitochondrial and tissue metabolism, as before this study, very little investigation was done on brain tissue and mitochondrial metabolism in hibernators (Gallagher & Staples, 2013). Future studies should focus on the roles that temperature and substrate oxidation play on the enhanced metabolic activity of brain mitochondria during hibernation.

## Section 4.2 Figures & Tables

**Figure 4.6. A model of mitochondrial function during hibernation (A) and spring (B) of isolated brain mitochondria.** The results of both this study and previous studies were used to construct a functional model of isolated brain mitochondria during hibernation (torpor and IBA) and spring. (A) 1) Oxidative phosphorylation, and specifically, complexes of the electron transport system (ETS), are enhanced during hibernation. This is evidenced by increased *state 3* respiration rates of various ETS complexes during hibernation, along with an enhancement of proteins coding for the complexes (refer to (Epperson et al., 2010; Zhang et al., 2014). 2) Along with an increased in oxidative phosphorylation, there is also an increase in the proton conductance associated with oxidative phosphorylation. There is less proton leak in brain mitochondria during hibernation, thus allowing an efficient proton gradient to be formed for ATP synthesis. 3) Intracellular mitochondrial $Ca^{2+}$ loading is also decreased during hibernation, allowing for an increase in ATP production and a decrease in detrimental excitotoxicity responses (Hindle & Martin 2013). 4) Increases in mitochondrial metabolism associated with β-oxidation and TCA cycle are present during hibernation. This is evidenced by enhancements of both transcripts and proteins associated with the two pathways (Epperson et al., 2010; Schwartz et al., 2013; Zhang et al., 2014). This metabolic enhancement allows for an increase in reducing equivalents (i.e. NADH and $FADH_2$) to flow into the ETS, evidenced again by the increase in oxidative phosphorylation during hibernation. 5) The enhancements of all the various mitochondrial aspects (1-4) allow for an increase in ATP production during hibernation in brain mitochondria. This rapid and efficient ATP production aids in the energetic process of arousal from torpor to IBA. (B) The oxidative capacities of isolated brain mitochondria during spring are decreased (#1-4), which results in a less rapid and efficient production of ATP (5).

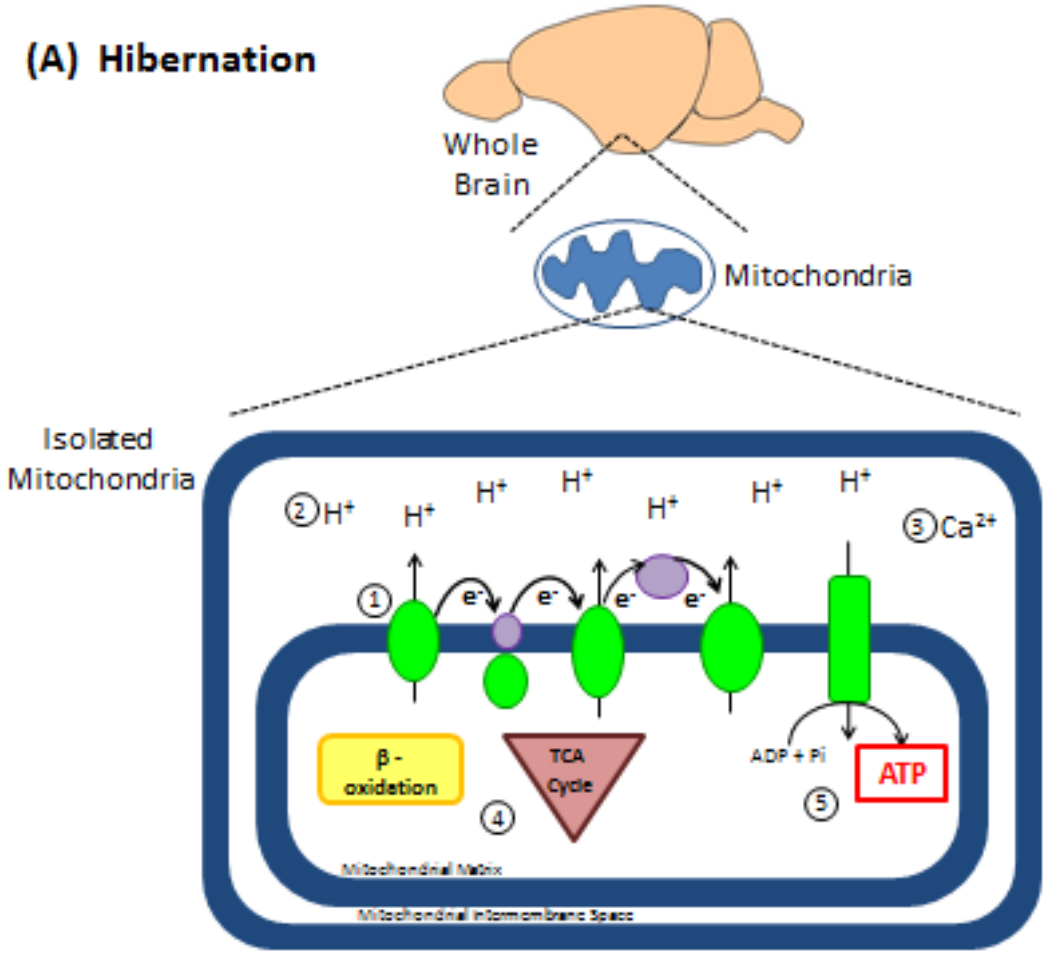
(A) Hibernation
Whole Brain
Mitochondria
Isolated Mitochondria
② H+
H+
H+
H+
H+
H+
H+
③ Ca2+
①
e-
e-
e-
e-
β - oxidation
TCA Cycle
④
ADP + Pi
ATP
⑤
Mitochondrial Matrix
Mitochondrial Intermembrane Space

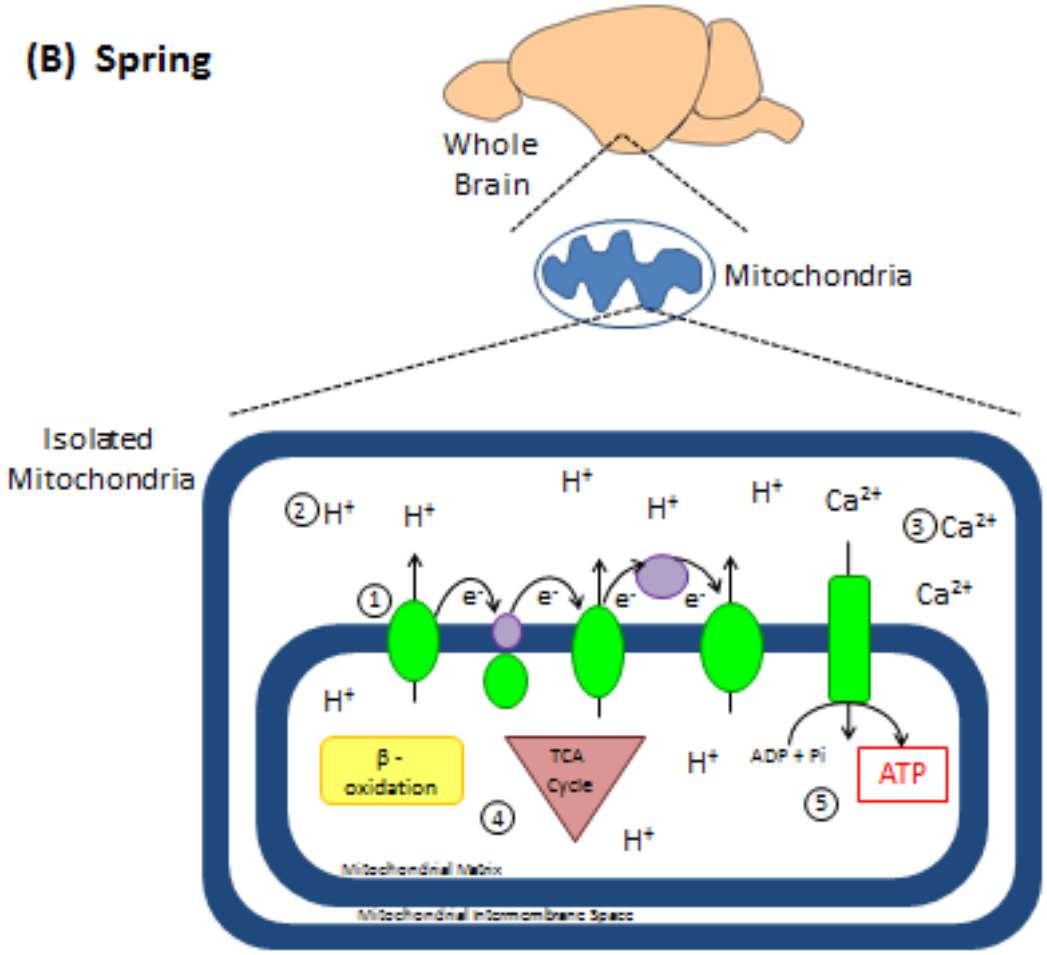
(B) Spring
Whole Brain
Mitochondria
Isolated Mitochondria
H+
Ca2+
e-
β - oxidation
TCA Cycle
ADP + Pi
ATP
Mitochondrial Matrix
Mitochondrial Intermembrane Space

# CHAPTER 5: Melatonin Receptor Signaling Contributes to Neuroprotection upon Arousal from Torpor

* This chapter is included in the following manuscript, which has been submitted for publication in a peer-reviewed journal: Schwartz, C., Ballinger, M.A. and Andrews, M.T. (*in revision)* Melatonin Receptor Signaling Contributes to Neuroprotection upon Arousal from Torpor in the Thirteen-Lined Ground Squirrel.

## SECTION 5.1: RESULTS

Mitochondrial Respiration

Melatonin increases in the pineal and serum of hibernating mammals during arousal from torpor (Florant et al., 1984; Larkin et al., 2015; Stanton et al., 1986) and has been shown to protect mitochondria (Acuna-Castroviejo et al., 2001). We used the melatonin receptor antagonist, luzindole, to examine the role of melatonin receptor-mediated protection of brain mitochondria in thirteen-lined ground squirrels during hibernation and summer. Summer was chosen as a time when the ground squirrels are not hibernating and melatonin levels during the day would be essentially undetectable.

To assess the effect of luzindole on the mitochondrial bioenergetics of brain mitochondria in the thirteen-lined ground squirrel, *state 3* (phosphorylating) respiration rates were measured in isolated whole brain mitochondria isolated from whole brains. *State 3* respiration is defined as ADP-stimulated respiration of isolated, coupled mitochondria (Chance & Williams, 1955). It is a near-maximal state of oxygen consumption and ATP synthesis, and is measured in the presence of energetic substrates and ADP (Chance & Williams, 1955). Using three different substrates (glutamate/malate (G/M), succinate (SUC), and glycerol-3-phosphate (G3P), mitochondria from luzindole-treated animals had significantly lower *state 3* respiration rates using succinate as a fuel during hibernation (Figure 5.1A, T-test, $n = 5$, $P < 0.05$), but not in the summer (Figure 5.1B, T-test, $n = 5$, $P = 0.12$). There were no significant differences between groups using G/M or G3P as a fuel in the hibernating animals. *State 3* respiration rates with G3P

were significantly higher in the vehicle-treated animals in the summer group (Figure 5.1B).

Additionally, *state 4* (non-phosphorylating; maximal) rates were measured to assess respiratory control ratios (RCRs). *State 4* respiration is the maximal respiration rate of isolated mitochondria that has no influence on ATP synthesis (Chance & Williams, 1955). The RCR of isolated mitochondria is the ratio between *state 3* and *state 4*, and is an indicator of coupling efficiency between substrate oxidation and ATP synthesis (Chance & Williams, 1955; Zhang et al., 2012). Luzindole-treated animals tended to have lower RCRs for all fuels during hibernation, but the effect was not significant (Table 5.1).

Mitochondrial Membrane Potential

The kinetics of proton leak were also determined for isolated brain mitochondria by the simultaneous measurement of membrane potential ($\Delta\Psi_m$) and *state 4* respiration rate. There was no significant change in maximum $\Delta\Psi_m$ or *state 4* respiration rate between groups in either hibernation or summer, but the trend in hibernation was that luzindole-treated animals had a lower maximum $\Delta\Psi_m$ than vehicle-treated animals (Table 5.2, Figure 5.2). The highest $\Delta\Psi_m$ shared between the two groups during hibernation was approximately 207 mV (Figure 5.2), and at this shared $\Delta\Psi_m$, proton leak is higher in luzindole-treated animals compared to vehicle-treated animals. However, there was no significant change in proton leak rate at any of the shared $\Delta\Psi_m$ values, suggesting that proton permeability of the mitochondrial membrane did not change between luzindole

and vehicle-treated animals in hibernation. The proton leak curves of the two experimental groups in summer look virtually identical (Figure 5.2), indicating that luzindole treatment had no effect. However, there does appear to be a clear seasonal change in proton kinetics between hibernation and summer in the brain (Figure 5.2).

## Section 5.1 Figures & Tables

**Figure 5.1. *State 3* respiration rates in brain mitochondria.** (A) *State 3* respiration rates at mid-arousal from hibernation in brain mitochondria from animals treated with luzindole (gray) or vehicle (black). Luzindole-treated animals had significantly lower respiration rates with succinate (*T-test, $P = 0.019$). (B) *State 3* respiration rates during summer in brain mitochondria from animals treated with luzindole (gray) or vehicle (black). Luzindole-treated animals had significantly lower respiration rates with G3P (*T-test, $P = 0.0496$). Number of animals (n) for each group is listed at the bottom of the respective bar. Error bars represent standard error of the mean. Abbreviations: G/M, glutamate/malate; SUC, succinate; G3P, glycerol-3-phosphate.

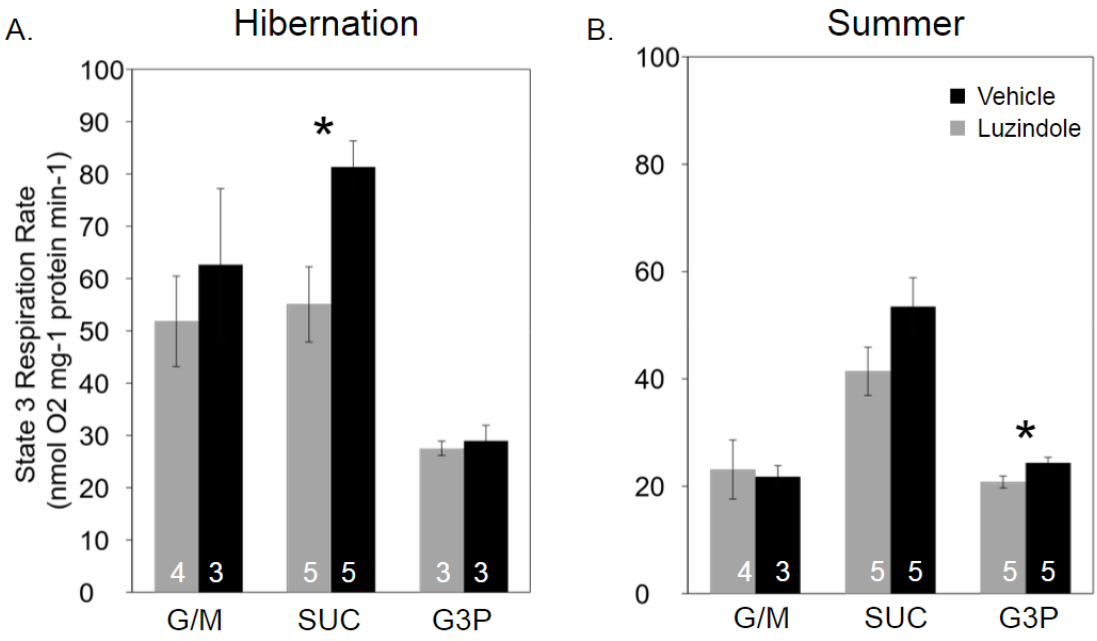

**Figure 5.2. Kinetic response of proton leak according to mitochondrial membrane potential ($\Delta\Psi_m$) in ground squirrel brain mitochondria during hibernation (triangles) and summer (circles).** Luzindole-treated animals are shown in black and vehicle-treated animals are shown in gray. Proton leak kinetics were initiated by inducing *state 4* respiration with the addition of 10 mM succinate. The kinetics of proton leak were determined by inhibiting succinate oxidation stepwise by titrating 0.3 mM malonate until a complete inhibition was obtained, and then measuring this effect on $\Delta\Psi_m$ No significant effect of treatment is seen in either season, but luzindole-treated animals tended to have lower membrane potential during hibernation. Error bars were omitted for clarity. Abbreviations: VEH, vehicle; LUZ, luzindole.

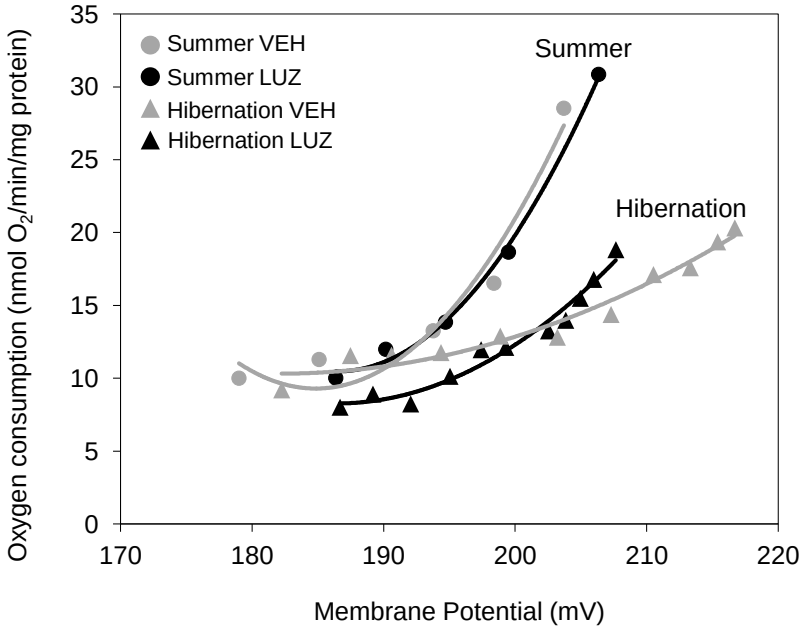

**Table 5.1. Respiratory control ratios (RCRs) for isolated brain mitochondria respiration experiments.** Data are represented as means ± standard error. RCRs are calculated as *state 3* respiration ÷ *state 4* respiration. For the statistical analysis, P-values were obtained with a Student's t-test between the two groups. $P < 0.05$ was considered significant. Abbreviations: G/M, glutamate/malate; SUC, succinate; G3P, glycerol-3-phosphate.

| | **Luzindole** | **Vehicle** | **P-value** |
|---|---|---|---|
| Hibernation (G/M) | 3.54 ± 0.58 | 5.19 ± 0.69 | 0.13 |
| Hibernation (SUC) | 2.83 ± 0.26 | 3.83 ± 0.42 | 0.08 |
| Hibernation (G3P) | 2.67 ± 0.43 | 3.27 ± 1.05 | 0.62 |
| Summer (G/M) | 2.78 ± 0.90 | 3.08 ± 0.44 | 0.74 |
| Summer (SUC) | 1.85 ± 0.13 | 1.85 ± 1.13 | 0.99 |
| Summer (G3P) | 1.37 ± 0.05 | 1.42 ± 0.11 | 0.68 |

**Table 5.2. Bioenergetics of brain mitochondria.** Data are represented as means ± standard error. For the statistical analysis, P-values were obtained with a Student's t-test between the two groups. $P < 0.05$ was considered significant. Mitochondrial membrane potentials ($\Delta\Psi_m$) are shown in mV. Respiration rates are shown in nmol $O_2$ $mg^{-1}$ protein $min^{-1}$.

| | **Luzindole** | **Vehicle** | **P-value** |
|---|---|---|---|
| Hibernation State 4 $\Delta\Psi_m$ | 207.66 ± 3.53 | 216.71 ± 1.97 | 0.056 |
| Hibernation State 4 Respiration | 18.83 ± 2.00 | 20.32 ± 1.40 | 0.56 |
| Summer State 4 $\Delta\Psi_m$ | 206.35 ± 4.35 | 203.70 ± 8.05 | 0.78 |
| Summer State 4 Respiration | 30.86 ± 4.00 | 28.54 ± 5.55 | 0.74 |

## SECTION 5.2: DISCUSSION

### Introduction

This work investigated the effect of the competitive melatonin receptor antagonist luzindole on brain mitochondrial function in a hibernating mammal during arousal from torpor. Additionally, we investigated luzindole's effect on mitochondrial function in the summer, after completion of the hibernation season.

### Melatonin Receptor Signaling is Important for Optimal Mitochondrial Function

In this study, we show that melatonin receptor appears to be important for optimal mitochondrial function in the whole brain during arousal from torpor. Here, we report that disruption of melatonin receptor signaling during arousal from torpor results in decreased mitochondrial function, specifically including a significant decrease in the *state 3* respiration rates of luzindole-treated animals when using succinate as a fuel. We also see a decrease in mitochondrial membrane potential with luzindole treatment, although this trend is not significant, potentially due to our small sample size.

Melatonin is known to protect mitochondria (Acuna-Castroviejo et al., 2001), which is particularly evident in research in animal models of neurological disorders. Treatment with melatonin ameliorated mitochondrial dysfunction associated with Alzheimer's disease by restoring membrane potential and respiration rates in young mice (Dragicevic et al., 2011). Luzindole partially blocked the ability of melatonin to restore mitochondrial function, indicating that melatonin receptors play a role in mitochondrial protection. Melatonin also slowed disease progression in a mouse model of Huntington's

Disease (HD) and this study also showed that melatonin receptor expression decreased in HD mice, suggesting that depletion of melatonin receptor signaling enhances the disease phenotype (Wang et al., 2011). Additionally, previous work has shown that melatonin protects mitochondria by antagonizing apoptotic signaling, as mentioned previously, an effect that is reversed by luzindole (Radogna et al., 2008). Our findings with the hibernator, which produces melatonin naturally during arousal from hibernation (Florant et al., 1984; Larkin et al., 2015; Stanton et al., 1986), supports this work by functionally demonstrating that disrupting melatonin receptor signaling upon arousal from torpor reduces mitochondrial function.

It is important to state that the effect of luzindole is seen in mitochondria isolated from the whole brain. It is possible that the effect of melatonin receptor signaling on whole brain mitochondrial respiration and membrane potential is not necessarily just to protect the mitochondria, but to actually enhance and improve mitochondrial function during arousal in the brain, effectively allowing the hibernator's mitochondria to perform better than the mitochondria of a non-hibernating mammal in the same conditions. This idea is supported in part by the summer experiments, showing both that luzindole administration has no effect on mitochondrial function compared to vehicle and that the summer respiration rates and membrane potentials overall are lower than what is seen in hibernation (Figure 5.1, Figure 5.2, Table 5.2). This is also supported by the ability of melatonin to restore mitochondrial function in a mouse model of Alzheimer's disease (Dragicevic et al., 2011). Additionally, previous work showed that melatonin administration stimulated mitochondrial respiration in rat brain (Martín et al., 2000),

however, it is not known whether this effect is receptor-mediated. Arousal is a very energy costly event (Lyman et al., 1982), requiring a considerable amount of energy generated by the mitochondria. It is possible that melatonin production upon arousal from torpor functions to help the brain mitochondria work harder and more efficiently during a period of extreme energy need.

# CHAPTER 6: Conclusions

Together, these investigations improve our understanding of the metabolic feats in a hibernator. Specifically, these studies on mitochondrial function provide additional insight into the overall metabolic system of the thirteen-lined ground squirrel. Both brown adipose tissue and the brain are major metabolic tissues that contribute to the overall energetic needs and metabolism of the thirteen-lined ground squirrel. Unlike other tissues, where metabolism may be suppressed during torpor, maintenance of both BAT and brain metabolism at some reduced level is critical because they are necessary for adaptive thermogenesis and the regulation of hibernation, respectively (Cannon & Nedergaard, 2004; Drew et al., 2007).

Although the basis of this study measured *in vitro* mitochondrial dynamics, a more complete metabolic picture was constructed due to the integration of transcriptomes, mitoproteome, and functional assessments of BAT and brain mitochondria. Functional analysis on mitochondrial bioenergetics showed increased respiratory capacity of both BAT and brain mitochondria during hibernation. These results, along with previous findings, suggest that hibernator BAT and brain contain a streamlined mechanism capable of efficient and rapid heat and ATP production and their subsequent utilization during torpor and arousal cycles of hibernation.

Future studies in BAT mitochondria should consist of identifying and characterizing novel protein isoforms, such as alternative splice variants, single amino acids variants, mutations, and post-translational modifications of mitochondrial proteins. Careful analysis of these amino acid variants may provide essential underpinnings into the hibernation phenotype and may aid in better understanding how BAT function is

maintained throughout hibernation. Additionally, future functional studies involving various fuels, such as fatty acid derivatives, should be conducted to investigate if specific substrates at different temperatures play a role in the overall thermogenic capacity of BAT mitochondria across the year. Even assessing coupled BAT mitochondria may provide mechanistic insight of BAT and may aid in understanding the overall mitochondrial metabolism of a natural hibernator.

Lastly, future investigation in brain mitochondria should focus on the roles temperature and substrate oxidation play on the enhanced metabolic activity of brain mitochondria during hibernation. Perhaps specific substrates, such as fatty acid derivatives, at different temperatures play a role in the overall oxidative capacity of brain mitochondria across the year. Furthermore, it is important to state that this thesis focused on seasonal changes of mitochondrial bioenergetics from mitochondria isolated from the whole brain. Measuring mitochondrial bioenergetics in separate regions of the brain may aid in better understanding of how different regions of a hibernator's brain adapt to the extreme physiological conditions associated with the hibernation phenotype.

# CHAPTER 7: Literature Cited

Acuna-Castroviejo, D. et al., 2001. Melatonin, mitochondria, and cellular bioenergetics. *Journal of Pineal Research*, 30, pp.65–74.

Andrews, M.T. et al., 2009. Adaptive mechanisms regulate preferred utilization of ketones in the heart and brain of a hibernating mammal during arousal from torpor. *American Journal of Physiology - Regulatory, Integrative and Comparative Physiology*, 296(2), pp.R383–R393.

Andrews, M.T., 2007. Advances in molecular biology of hibernation in mammals. *BioEssays*, 29(5), pp.431–440.

Andrews, M.T., 2004. Genes controlling the metabolic switch in hibernating mammals. *Biochemical Society Transactions*, 32(6), pp.1021–1024.

Andrews, M.T. et al., 1998. Low-temperature carbon utilization is regulated by novel gene activity in the heart of a hibernating mammal. *Proceedings of the National Academy of Sciences*, 95(14), pp.8392–8397.

Aquila, H., Link, T.A. & Klingenberg, M., 1985. The uncoupling protein from brown fat mitochondria is related to the mitochondrial ADP/ATP carrier. Analysis of sequence homologies and of folding of the protein in the membrane. *The EMBO Journal*, 4(9), pp.2369–2376.

Armstrong, C. & Staples, J.F., 2010. The role of succinate dehydrogenase and oxaloacetate in metabolic suppression during hibernation and arousal. *Journal of Comparative Physiology. B, Biochemical, Systemic, and Environmental Physiology*, 180(5), pp.775–783.

Barger, J.L. et al., 2003. Tissue-specific depression of mitochondrial proton leak and substrate oxidation in hibernating arctic ground squirrels. *American Journal of Physiology - Regulatory, Integrative and Comparative Physiology*, 284(5), pp.R1306–R1313.

Barnes, B.M., 1989. Freeze avoidance in a mammal: body temperatures below 0 degree C in an Arctic hibernator. *Science*, 244(4912), pp.1593–1595.

Bieber, C. et al., 2014. Body mass dependent use of hibernation: why not prolong the active season, if they can? C. Franklin, ed. *Functional Ecology*, 28(1), pp.167–177.

Bittman, E.L., Thomas, E.M. & Zucker, I., 1994. Melatonin binding sites in sciurid and hystricomorph rodents: Studies on ground squirrels and guinea pigs. *Brain Research*, 648(1), pp.73–79.

Boss, O., Muzzin, P. & Giacobino, J.P., 1998. The uncoupling proteins, a review. *European Journal of Endocrinology*, 139(1), pp.1–9.

Bouillaud, F., Weissenbach, J. & Ricquier, D., 1986. Complete cDNA-derived amino acid sequence of rat brown fat uncoupling protein. *The Journal of Biological Chemistry*, 261(4), pp.1487–1490.

Boveris, A. & Chance, B., 1973. The mitochondrial generation of hydrogen peroxide. General properties and effect of hyperbaric oxygen. *The Biochemical Journal*, 134(3), pp.707–716.

Brand, M. et al., 1994. The causes and functions of mitochondrial proton leak. *Biochimica et Biophysica Acta (BBA) - Bioenergetics*, 1187(2), pp.132–139.

Brand, M.D., 2011. The sites and topology of mitochondrial superoxide production. *Experimental Gerontology*, 45(7-8), pp.466–472.

Brand, M.D., 2000. Uncoupling to survive? The role of mitochondrial inefficiency in ageing. *Experimental Gerontology*, 35(6-7), pp.811–820.

Bratincsak, A. et al., 2007. Morphological characterization of spinal cord dorsal horn lamina I neurons projecting to the parabrachial nucleus in the rat. *The Journal of Comparative Neurology*, 504(3), pp.287–297.

Breitwieser, G.E., 2002. Beta-Adrenergic potentiation of endoplasmic reticulum calcium release in brown fat cells. *American Journal of Physiology*, 282, pp.C980–C1981.

Van Breukelen, F. & Martin, S.L., 2002. Molecular adaptations in mammalian hibernators: unique adaptations or generalized responses? *Journal of Applied Physiology*, 92, pp.2640–2647.

Broekemeier, K.M., Dempsey, M.E. & Pfeiffer, D.R., 1989. Cyclosporin A is a potent inhibitor of the inner membrane permeability transition in liver mitochondria. *The Journal of Biological Chemistry*, 264(14), pp.7826–7830.

Brown, J.C.L. et al., 2013. Regulation of succinate-fuelled mitochondrial respiration in liver and skeletal muscle of hibernating thirteen-lined ground squirrels. *The Journal of Experimental Biology*, 216(Pt 9), pp.1736–1743.

Buck, M.J., Squire, T.L. & Andrews, M.T., 2002. Coordinate expression of the PDK4 gene: a means of regulating fuel selection in a hibernating mammal. *Physiological Genomics*, 8(1), pp.5–13.

Burlington, R.F., Therriault, D.G. and Hubbard, R.W., 1969. Lipid changes in isolated brown fat cells from hibernating and aroused thirteen-lined ground squirrels (Citelus tridecemlineatus). *Comparative Biochemistry and Physiology*, 29(May 1967), pp.431–437.

Cannon, B., 1977. The Mitochondiral ATPase of brown adipose tissue  Purification and comparison with the mitochondrial ATPase from Beef Heart. *FEBS Letters*, 76(2), pp.284–289.

Cannon, B. & Nedergaard, J., 2004. Brown adipose tissue: function and physiological significance. *Physiological Reviews*, 84(1), pp.277–359.

Cannon, B. & Nedergaard, J., 2008. Studies of thermogenesis and mitochondrial function in adipose tissues. *Methods in Molecular Biology (Clifton, N.J.)*, 456(1), pp.109–121.

Carey, H.V., Andrews, M.T. & Martin, S.L., 2003. Mammalian hibernation: cellular and molecular responses to depressed metabolism and low temperature. *Physiological Reviews*, 83(4), pp.1153–1181.

Carey, H.V., Andrews, M.T., and Martin, S.L., 2003. Mammalian hibernation: cellular and molecular responses to depressed metabolism and low temperature. *Physiological Reviews*, 83, pp.1153–1181.

Carroll, J. et al., 2006. Bovine complex I is a complex of 45 different subunits. *Journal of Biological Chemistry*, 281(43), pp.32724–32727.

Chaffee, R.R. et al., 1966. Biochemistry of brown fat and liver of hibernating golden mantled ground squirrels (Citellus lateralis). *Canadian Journal of Physiology and Pharmacology*, 44(2), pp.217–223.

Chaffee, R.R., Allen, J.R., Cassuto, Y. and Smith, R.E., 1964. Biochemistry of brown fat and liver of cold-acclimated hamsters. *American Journal of Physiology*, 207, pp.1211–1214.

Chance, B. & Williams, G.R., 1955. Respiratory enzymes in oxidative phosphorylation: III. The steady state. *Journal of Biological Chemistry*, 217, pp.409–427.

Chaudhry, A. & Granneman, J.G., 1999. Differential regulation of functional responses by beta-adrenergic receptor subtypes in brown adipocytes. *The American Journal of Physiology*, 277(1 Pt 2), pp.R147–R153.

Chung, D. et al., 2011. Mitochondrial respiration and succinate dehydrogenase are suppressed early during entrance into a hibernation bout, but membrane remodeling

is only transient. *Journal of Comparative Physiology. B, Biochemical, Systemic, and Environmental Physiology*, 181(5), pp.699–711.

Clark, L.C. et al., 1953. Continuous recording of blood oxygen tensions by polarography. *Journal of Applied Physiology*, 6(3), pp.189–193.

Dave, K.R., Christian, S.L., Perez-Pinzon, M.A. and Drew, K.L., 2012. Neuroprotection : Lessons from hibernators. *Comparative Biochemistry and Physiology Part B: Biochemistry and Molecular Biology*, 162, pp.1–9.

Divakaruni, A.S. & Brand, M.D., 2011. The regulation and physiology of mitochondrial proton leak. *Physiology*, 26, pp.192–205.

Dragicevic, N. et al., 2011. Melatonin treatment restores mitochondrial function in Alzheimer's mice: a mitochondrial protective role of melatonin membrane receptor signaling. *Journal of Pineal Research*, 51(1), pp.75–86.

Drew, K.L. et al., 2007. Central nervous system regulation of mammalian hibernation: implications for metabolic suppression and ischemia tolerance. *Journal of Neurochemistry*, 102(6), pp.1713–1726.

Drew, K.L. et al., 2004. Hypoxia tolerance in mammalian heterotherms. *The Journal of Experimental Biology*, 207(Pt 18), pp.3155–3162.

Eddy, S.F. & Storey, K.B., 2004. Up-regulation of fatty acid-binding proteins during hibernation in the little brown bat, Myotis lucifugus. *Biochimica et Biophysica Acta (BBA) - Gene Structure and Expression*, 1676(1), pp.63–70.

Efremov, R.G., Baradaran, R. & Sazanov, L.A., 2010. The architecture of respiratory complex I. *Nature*, 465(7297), pp.441–445.

Epperson, L.E. et al., 2010. Seasonal protein changes support rapid energy production in hibernator brainstem. *Journal of Comparative Physiology B*, 180(4), pp.599–617.

Fedorenko, A., Lishko, P.V. & Kirichok, Y., 2012. Mechanism of fatty-acid-dependent UCP1 uncoupling in brown fat mitochondria. *Cell*, 151(2), pp.400–413.

Florant, G.L. et al., 1984. Plasma melatonin concentrations in hibernating marmots: absence of a plasma melatonin rhythm. *American Journal of Physiology - Regulatory, Integrative and Comparative Physiology*, 247(6), pp.R1062–R1066.

Foss, E.J. et al., 2011. Genetic variation shapes protein networks mainly through non-transcriptional mechanisms. *PLoS Biology*, 9(9), e1001144.

Frerichs, K.U. et al., 1994. Local cerebral blood flow during hibernation, a model of natural tolerance to "cerebral ischemia". *Journal of Cerebral Blood Flow and Metabolism*, 14(2), pp.193–205.

Von Gall, C., Stehle, J.H. & Weaver, D.R., 2002. Mammalian melatonin receptors: Molecular biology and signal transduction. *Cell and Tissue Research*, 309(1), pp.151–162.

Gallagher, K. & Staples, J.F., 2013. Metabolism of brain cortex and cardiac muscle mitochondria in hibernating 13-lined ground squirrels Ictidomys tridecemlineatus. *Physiological and Biochemical Zoology*, 86(1), pp.1–8.

Geiser, F., 1998. Evolution of daily torpor and hibernation in birds and mammals: importance of body size. *Clinical and Experimental Pharmacology and Physiology*, 25(9), pp.736-740.

Geiser, F., 2004. Metabolic rate and body temperature reduction during hibernation and daily torpor. *Annual Review of Physiology*, 66, pp.239–274.

Geiser, F., 1988. Reduction of metabolism during hibernation and daily torpor in mammals and birds: temperature effect or physiological inhibition? *Journal of Comparative Physiology B*, 158(1), pp.25–37.

Geiser, F. & Körtner, G., 2010. Hibernation and daily torpor in Australian mammals. *Australian Zoologist*, 35(2), pp.204-215.

Gomes, L.C., Di Benedetto, G. & Scorrano, L., 2011. During autophagy mitochondria elongate, are spared from degradation and sustain cell viability. *Nature Cell Biology*, 13(5), pp.589–598.

Grabek, K.R., Martin, S.L. & Hindle, A.G., 2015. Proteomics approaches shed new light on hibernation physiology. *Journal of Comparative Physiology B*, DOI 10.1007/s00360–015–0905–9.

Gry, M. et al., 2009. Correlations between RNA and protein expression profiles in 23 human cell lines. *BMC Genomics*, 10(1), p.365.

Guppy, M. & Withers, P., 1999. Metabolic depression in animals: physiological perspectives and biochemical generalizations. *Biological Reviews of the Cambridge Philosophical Society*, 74(1), pp.1–40.

Hampton, M. et al., 2011. Deep sequencing the transcriptome reveals seasonal adaptive mechanisms in a hibernating mammal. *PLoS ONE*, 6(10), e27021.

Hampton, M., Melvin, R.G. & Andrews, M.T., 2013. Transcriptomic analysis of brown adipose tissue across the physiological extremes of natural hibernation. *PLoS ONE*, 8(12), e85157.

Hampton, M., Nelson, B.T. & Andrews, M.T., 2010. Circulation and metabolic rates in a natural hibernator : an integrative physiological model. *American Journal of Physiology - Regulatory, Integrative and Comparative Physiology*, 299, pp.1478–1488.

Harris, J.J., Jolivet, R. & Attwell, D., 2012. Synaptic energy use and supply. *Neuron*, 75(5), pp.762–777.

Heaton, G.M. et al., 1978. Brown-adipose-tissue mitochondria: photoaffinity labelling of the regulatory site of energy dissipation. *European Journal of Biochemistry / FEBS*, 82(2), pp.515–521.

Henry, P.G. et al., 2007. Brain energy metabolism and neurotransmission at near-freezing temperatures: In vivo 1H MRS study of a hibernating mammal. *Journal of Neurochemistry*, 101(6), pp.1505–1515.

Hindle, A.G. & Martin, S.L., 2013. Cytoskeletal regulation dominates temperature-sensitive proteomic changes of hibernation in forebrain of 13-lined ground squirrels. *PLoS ONE*, 8(8), e71627.

Hindle, A.G. & Martin, S.L., 2014. Intrinsic circannual regulation of brown adipose tissue form and function in tune with hibernation. *American Journal of Physiology - Endocrinology and Metabolism*, 306, pp.E284–E299.

Hook, E. & Guzman, E.S., 1941. The respiration of brown adipose tissue and kidney of the hibernating and non-hibernating ground squirrel. *American Journal of Physiology*, 133, pp.56–63.

Houstěk, J., Cannon, B. & Lindberg, O., 1975. Gylcerol-3-phosphate shuttle and its function in intermediary metabolism of hamster brown-adipose tissue. *European Journal of Biochemistry / FEBS*, 54(1), pp.11–18.

Huang, D.W. et al., 2007. The DAVID Gene Functional Classification Tool: a novel biological module-centric algorithm to functionally analyze large gene lists. *Genome Biology*, 8(9), p.R183.

Huang, D.W., Sherman, B.T. & Lempicki, R.A., 2009. Systematic and integrative analysis of large gene lists using DAVID bioinformatics resources. *Nature Protocols*, 4(1), pp.44–57.

Kelly, D.P. & Scarpulla, R.C., 2004. Transcriptional regulatory circuits controlling mitochondrial biogenesis and function. *Genes and Development*, 18(4), pp.357–368.

Kemp, T.S., 2006. The origin of mammalian endothermy: a paradigm for the evolution of complex biological structure. *Zoological Journal of the Linnean Society*, 147(4), pp.473–488.

Korshunov, S.S., Skulachev, V.P. & Starkov, A.A., 1997. High protonic potential actuates a mechanism of production of reactive oxygen species in mitochondria. *FEBS Letters*, 416(1), pp.15–18.

Lambert, A.J. & Brand, M.D., 2004. Superoxide production by NADH:ubiquinone oxidoreductase (complex I) depends on the pH gradient across the mitochondrial inner membrane. *The Biochemical Journal*, 382(Pt 2), pp.511–517.

Larkin, J.E., Yellon, S.M. & Zucker, I., 2015. Melatonin production accompanies arousal from daily torpor in Siberian hamsters. *Physiological and Biochemical Zoology*, 76(4), pp.577–585.

Larson, J. et al., 2014. No oxygen? No problem! Intrinsic brain tolerance to hypoxia in vertebrates. *The Journal of Experimental Biology*, 217(Pt 7), pp.1024–1039.

Laursen, W.J. et al., 2015. Neuronal UCP1 expression suggests a mechanism for local thermogenesis during hibernation. *Proceedings of the National Academy of Sciences*, 112(5), pp.1607–1612.

Li, L. et al., 2011. Mitochondrial biogenesis and peroxisome proliferator–activated receptor-gamma coactivator-1 alpha (PGC-1 alpha) deacetylation by physical activity. *Diabetes*, 60(January), pp.157–167.

Li, Z. & Graham, B.H., 2012. Measurement of mitochondrial oxygen consumption using a clark electrode. *Methods in Molecular Biology*, 837, pp.63–72.

Liesa, M. & Shirihai, O.S., 2013. Mitochondrial dynamics in the regulation of nutrient utilization and energy expenditure. *Cell Metabolism*, 17(4), pp.491–506.

Lin-Moshier, Y. et al., 2013. Re-evaluation of the role of calcium homeostasis endoplasmic reticulum protein (CHERP) in cellular calcium signaling. *Journal of Biological Chemistry*, 288(1), pp.355–367.

Lipton, P., 1999. Ischemic cell death in brain neurons. *Physiological Reviews*, 79(4), pp.1431–1568.

Liu, S. Sen, 1997. Generating, partitioning, targeting and functioning of superoxide in mitochondria. *Bioscience Reports*, 17(3), pp.259–272.

Locke, R.M., Rial, E. & Nicholls, D.G., 1982. The acute regulation of mitochondrial proton conductance in cells and mitochondria from the brown fat of cold-adapted and warm-adapted guinea pigs. *European Journal of Biochemistry / FEBS*, 129(2), pp.381–387.

Lotz, C. et al., 2014. Characterization, design, and function of the mitochondrial proteome: from organs to organisms. *Journal of Proteome Research*, 13(2), pp.433–446.

Lowell, B.B. & Spiegelman, B.M., 2000. Towards a molecular understanding of adaptive thermogenesis. *Nature*, 404(6778), pp.652–660.

Lutfalla, G. & Uze, G., 2006. Performing quantitative reverse-transcribed polymerase chain reaction experiments. *Methods in Enzymology*, 410, pp.386–400.

Lyman, C.P. et al., 1982. *Hibernation and Torpor in Mammals and Birds.*, New York: Academic Press.

Ma, Y.L. et al., 2005. Absence of cellular stress in brain after hypoxia induced by arousal from hibernation in Arctic ground squirrels. *American Journal of Physiology - Regulatory, Integrative and Comparative Physiology*, 289(5), pp.R1297–R1306.

MacDonald, J.A. & Storey, K.B., 2005. Temperature and phosphate effects on allosteric phenomena of phosphofructokinase from a hibernating ground squirrel (Spermophilus lateralis). *FEBS Journal*, 272(1), pp.120–128.

Magariños, A.M. et al., 2006. Rapid and reversible changes in intrahippocampal connectivity during the course of hibernation in European hamsters. *Proceedings of the National Academy of Sciences*, 103(49), pp.18775–18780.

Maginniss, L.A. & Milsom, W.K., 1994. Effects of hibernation on blood oxygen transport in the golden-mantled ground squirrel. *Respiration Physiology*, 95(2), pp.195–208.

Malatesta, M. et al., 2001. Fine structural modifications of liver, pancreas and brown adipose tissue mitochondria from hibernating, arousing and euthermic dormice. *Cell Biology International*, 25(2), pp.131–138.

Malik, A.N. et al., 2011. Mitochondrial DNA as a non-invasive biomarker: accurate quantification using real time quantitative PCR without co-amplification of

pseudogenes and dilution bias. *Biochemical and Biophysical Research Communications*, 412(1), pp.1–7.

Martín, M. et al., 2000. Melatonin-induced increased activity of the respiratory chain complexes I and IV can prevent mitochondrial damage induced by ruthenium red in vivo. *Journal of Pineal Research*, 28(4), pp.242–248.

McKee, G. & Andrews, J.F., 1990. Brown adipose tissue lipid is the main source of energy during arousal of the golden hamster (Mesocricetus auratus). *Comparative Biochemistry and Physiology. A, Comparative Physiology*, 96(4), pp.485–488.

de Meis, L., 2003. Brown adipose tissue Ca2+-ATPase: uncoupled ATP hydrolysis and thermogenic activity. *Journal of Biological Chemistry*, 278(43), pp.41856–41861.

Melvin, R.G. & Andrews, M.T., 2009. Torpor induction in mammals: recent discoveries fueling new ideas. *Trends in Endocrinology and Metabolism*, 20(10), pp.490–498.

Mitchell, P. & Moyle, J., 1967. Chemiosmotic hypothesis of oxidative phosphorylation. *Nature*, 213(5072), pp.137–139.

Mráček, T., Drahota, Z. & Houštěk, J., 2013. The function and the role of the mitochondrial glycerol-3-phosphate dehydrogenase in mammalian tissues. *Biochimica et Biophysica Acta*, 1827(3), pp.401–410.

Murphy, M.P., 2009. How mitochondria produce reactive oxygen species. *The Biochemical Journal*, 417(1), pp.1–13.

Nedergaard, J. et al., 2001. UCP1 : the only protein able to mediate adaptive non-shivering thermogenesis and metabolic ine ¤ ciency. *Biochimica et Biophysica Acta*, 1504, pp.82–106.

Nedergaard, J. & Cannon, B., 1984. Preferential utilization of brown adipose tissue lipids during arousal from hibernation in hamsters. *The American Journal of Physiology*, 247(3 Pt 2), pp.R506–R512.

Nelson, C.J. et al., 2008. *Lehninger Principles of Biochemistry* Fifth., London.

Nicholls, D.G., 2005. Mitochondria and calcium signaling. *Cell Calcium*, 38(3-4 SPEC. ISS.), pp.311–317.

Nicholls, D.G., 2009. Mitochondrial calcium function and dysfunction in the central nervous system. *Biochimica et Biophysica Acta*, 1787(11), pp.1416–1424.

Nicholls, D.G., 1974. The influence of respiration and ATP hydrolysis on the proton-electrochemical gradient across the inner membrane of rat-liver mitochondria as determined by ion distribution. *European Journal of Biochemistry / FEBS*, 50(1), pp.305–315.

Nicholls, D.G. & Ferguson, S.J., 2013. *Bioenergetics 4* Fourth., Elsevier Ltd.

Nicholls, D.G. & Locke, R.M., 1984. Thermogenic mechanisms in brown fat. *Physiological reviews*, 64(1), pp.1–64.

Nicholls, D.G. & Rial, E., 1999. A history of the first uncoupling protein, UCP1. *Journal of Bioenergetics and Biomembranes*, 31(5), pp.399–406.

Nie, L. et al., 2007. Integrative analysis of transcriptomic and proteomic data: challenges, solutions and applications. *Critical Reviews in Biotechnology*, 27(2), pp.63–75.

Von der Ohe, C.G. et al., 2007. Synaptic protein dynamics in hibernation. *The Journal of Neuroscience*, 27(1), pp.84–92.

Von der Ohe, C.G. et al., 2006. Ubiquitous and temperature-dependent neural plasticity in hibernators. *The Journal of Neuroscience*, 26(41), pp.10590–10598.

Ohkawa, K.I., Vogt, M.T. & Farber, E., 1969. Unusually high mitochondrial alpha glycerophosphate dehydrogenase activity in rat brown adipose tissue. *Journal of Cell Biology*, 41(2), pp.441–449.

Palmeira, C.M. & Rolo, A.P., 2012. Mitochondiral membrane potential (DY) fluctuations associated with the metabolic states of mitochondria. *Methods in Molecular Biology*,810, pp. 89–101.

Pamenter, M.E., 2014. Mitochondria: A multimodal hub of hypoxia tolerance. *Canadian Journal of Zoology*, 92, pp.569–589.

Pandi-Perumal, S.R. et al., 2008. Physiological effects of melatonin: Role of melatonin receptors and signal transduction pathways. *Progress in Neurobiology*, 85(3), pp.335–353.

Pascal, L.E. et al., 2008. Correlation of mRNA and protein levels: cell type-specific gene expression of cluster designation antigens in the prostate. *BMC Genomics*, 9, p.246.

Popov, V.I. & Bocharova, L.S., 1992. Hibernation-induced structural changes in synaptic contacts between mossy fibres and hippocampal pyramidal neurons. *Neuroscience*, 48(1), pp.53–62.

Popov, V.I., Bocharova, L.S. & Bragin, A.G., 1992. Repeated changes of dendritic morphology in the hippocampus of ground squirrels in the course of hibernation. *Neuroscience*, 48(1), pp.45–51.

Radogna, F. et al., 2007. Melatonin antagonizes apoptosis via receptor interaction in U937 monocytic cells. *Journal of Pineal Research*, 43(2), pp.154–162.

Radogna, F. et al., 2008. Melatonin antagonizes the intrinsic pathway of apoptosis via mitochondrial targeting of Bcl-2. *Journal of Pineal Research*, 44(3), pp.316–325.

Reiter, R.J., Tan, D.X. & Fuentes-Broto, L., 2010. Melatonin: a multitasking molecule. *Progress in Brain Research*, 181, pp.127–151.

Ridley, R.G. et al., 1986. Complete nucleotide and derived amino acid sequence of cDNA encoding the mitochondrial uncoupling protein of rat brown adipose tissue: lack of mitochondrial targeting presequence. *Nucleic Acids Research*, 14, pp.4025–4035.

Ross, A.P. et al., 2006. Persistent tolerance to oxygen and nutrient deprivation and N-methyl-D-aspartate in cultured hippocampal slices from hibernating Arctic ground squirrel. *Journal of Cerebral Blood Flow and Metabolism*, 26, pp.1148–1156.

Ruf, T. & Geiser, F., 2014. Daily torpor and hibernation in birds and mammals. *Biological Reviews*.

Russell, R.L. et al., 2010. Extensive use of torpor in 13-lined ground squirrels in the fall prior to cold exposure. *Journal of Comparative Physiology. B, Biochemical, Systemic, and Environmental Physiology*, 180(8), pp.1165–1172.

Russeth, K.P., Higgins, L. & Andrews, M.T., 2006. Identification of proteins from non-model organisms using mass spectrometry: Application to a hibernating mammal. *Journal of Proteome Research*, 5(4), pp.829–839.

Schwartz, C. & Andrews, M.T., 2013. *Circannual transitions in gene expression: lessons from seasonal adaptations.* 1st ed., Elsevier Inc.

Schwartz, C., Hampton, M. & Andrews, M.T., 2015. Hypothalamic gene expression underlying pre-hibernation satiety. *Genes, Brain and Behavior*, 14(3), pp.310–318.

Schwartz, C., Hampton, M. & Andrews, M.T., 2013. Seasonal and regional differences in gene expression in the brain of a hibernating mammal. *PLoS ONE*, 8(3), e58427.

Serviddio, G. and Sastre, J., 2010. Measurement of mitochondrial membrane potential and proton leak D. Armstrong, ed. *Advanced Protocols in Oxidative Stress II*, 594(3), pp.107–121.

Severinghaus, J.W. & Astrkup, P.B., 1986. History of blood gas analysis. IV. Leland Clark's oxygen electrode. *Journal of Clinical Monitoring*, 2(2), pp.125–139.

Shibao, C. et al., 2007. Autonomic contribution to blood pressure and metabolism in obesity. *Hypertension*, 49(1), pp.27–33.

Silva, A.M. & Oliveira, P.J., 2012. Mitochondrial Bioenergetics. *Methods in Molecular Biology*, 810, pp.7–8.

Silva, J.E., 2006. Thermogenic mechanisms and their hormonal regulation. *Physiological Reviews*, 86(2), pp.435–464.

Skulachev, V.P., 1998. Uncoupling: New approaches to an old problem of bioenergetics. *Biochimica et Biophysica Acta - Bioenergetics*, 1363(2), pp.100–124.

Snapp, B.D. & Heller, H.C., 1981. Suppression of metabolism during hibernation in ground squirrels (Citellus lateralis). *Physiological Zoology*, 54(3), pp.297–307.

de Sousa Abreu, R. et al., 2009. Global signatures of protein and mRNA expression levels. *Molecular BioSystems*, 5(12), pp.1512–1526.

Stanton, T.L., Craft, C.M. & Reiter, R.J., 1986. Pineal melatonin: circadian rhythm and variations during the hibernation cycle in the ground squirrel, Spermophilus lateralis. *The Journal of Experimental Zoology*, 239(2), pp.247–254.

Staples, J.F., 2011. Maintaining metabolic balance in mammalian hibernation and daily torpor. In A. Nowakowska & M. Caputa, eds. *Hypometabolism: Strategies of Survival in Vertebrates and Invertebrates*. Kerala, India: Research Singpost, pp. 95–115.

Staples, J.F., 2014. Metabolic suppression in mammalian hibernation: the role of mitochondria. *The Journal of Experimental Biology*, 217(Pt 12), pp.2032–2036.

Staples, J.F. & Brown, J.C.L., 2008. Mitochondrial metabolism in hibernation and daily torpor: a review. *Journal of Comparative Physiology. B, Biochemical, Systemic, and Environmental Physiology*, 178(7), pp.811–27.

Storey, K.B. & Storey, J.M., 2010. *Metabolic Rate Depression : The Biochemistry of mammalian hibrnation* 1st ed., Elsevier Inc.

Storey, K.B. & Storey, J.M., 2004. Metabolic rate depression in animals: transcriptional and translational controls. *Biological reviews of the Cambridge Philosophical Society*, 79(1), pp.207–233.

Tan, D.X. et al., 2007. One molecule, many derivatives: A never-ending interaction of melatonin with reactive oxygen and nitrogen species? *Journal of Pineal Research*, 42(1), pp.28–42.

Tan, D.X. et al., 2005. Physiological ischemia/reperfusion phenomena and their relation to endogenous melatonin production. *Endocrine*, 27(2), pp.149–158.

Walker, J.M. et al., 1977. Sleep and hibernation in ground squirrels (Citellus spp): electrophysiological observations. *American Journal of Physiology – Regulatory, Integrative and Comparative Physiology*, 233(5), pp.R213–R221.

Wang, X. et al., 2011. The melatonin MT1 receptor axis modulates mutant huntingtin-mediated toxicity. *Journal of Neuroscience*, 31(41), pp.14496–14507.

Wang, Z. et al., 2012. Cytoprotective effects of melatonin on astroglial cells subjected to palmitic acid treatment in vitro. *Journal of Pineal Research*, 52(2), pp.253–264.

Yang, F. et al., 2012. High-pH reversed-phase chromatography with fraction concatenation for 2D proteomic analysis. *Expert Review of Proteomics*, 9(2), pp.129–134.

Yin, S. et al., 2013. Quantitative evaluation of the mitochondrial proteomes of drosophila melanogaster adapted to extreme oxygen conditions. *PLoS ONE*, 8(9), pp.1–13.

Youle, R.J. & van der Bliek, A.M., 2012. Mitochondrial fission, fusion, and stress. *Science*, 337(6098), pp.1062–1065.

Zhang, J. et al., 2012. Measuring energy metabolism in cultured cells, including human pluripotent stem cells and differentiated cells. *Nature Protocols*, 7(6), pp.1068–1085.

Zhang, Y. et al., 2014. Critical roles of mitochondria in brain activities of torpid Myotis ricketti bats revealed by a proteomic approach. *Journal of Proteomics*, 105, pp.266–284.

Zhao, H.W. et al., 2006. Decreased NR1 phosphorylation and decreased NMDAR function in hibernating arctic ground squirrels. *Journal of Neuroscience Research*, 84(2), pp.291–298.

Zhao, J.J. et al., 2014. Increased Na+ /Ca2+ exchanger activity promotes resistance to excitotoxicity in cortical neurons of the ground squirrel (a hibernator). *PLoS ONE*, 9(11), pp.1–20.

Zhou, S. et al., 2001. Cumulative and irreversible cardiac mitochondrial dysfunction induced by doxorubicin. *Cancer Research*, 61, pp.771–777.

**APPENDIX A. Differentially expressed proteins in BAT mitochondria between torpor, IBA, and spring.** 106 BAT mitochondrial proteins were differentially expressed according to the criteria outlined in the Materials and Methods section (Chapter 2). In this proteomic study, the hibernation time point (HIB) is a combination of data from torpor TOR and IBA. 56 proteins showed highest expression in HIB compared to SP, while 48 proteins showed highest expression in SP compared to HIB. The order of the protein list corresponds to protein abundance, with proteins at the top of the list containing more confidentially identified peptides. Differential expression patters are in comparison to spring time point.

| Protein | Description | Differential Expression |
|---|---|---|
| LRPPRC | leucine-rich PPR-motif containing | Lower in IBA |
| IMMT | inner membrane protein | Higher in TOR |
| ACO2 | aconitase 2 | Lower in IBA |
| HADHA | trifunctional protein, alpha subunit | Higher in TOR |
| PC | pyruvate carboxylase | Higher in TOR |
| ACADVL | acyl-CoA dehydrogenase, very long chain | Lower in IBA |
| OGDH | oxoglutarate dehydrogenase | Higher in TOR |
| GPD2 | glycerol-3-phosphate dehydrogenase 2 | Lower in IBA |
| ACAA2 | acetyl-CoA acyltransferase 2 | Higher in TOR |
| CPT2 | carnitine palmitoyltransferase 2 | Higher in TOR |
| HSPD1 | heat shock 60kDa protein 1 | Lower in IBA & Higher in TOR |
| HADHB | trifunctional protein, beta subunit | Higher in TOR |
| ACSL1 | acyl-CoA synthetase long-chain family member 1 | Higher in TOR |
| LARS2 | leucyl-tRNA synthetase 2 | Lower in IBA & Higher in TOR |
| IDH2 | isocitrate dehydrogenase 2 | Higher in TOR |
| HSDL2 | hydroxysteroid dehydrogenase like 2 | Lower in IBA |
| ADCK3 | aarF domain containing kinase 3 | Higher in TOR |
| ETFDH | electron-transferring-flavoprotein dehydrogenase | |

| | | |
|---|---|---|
| ACAD10 | acyl-CoA dehydrogenase family, member 10 | Lower in IBA |
| CS | citrate synthase | Lower in IBA |
| SDHA | succinate dehydrogenase complex, subunit A | Higher in TOR |
| CRAT | carnitine O-acetyltransferase | Lower in IBA |
| LONP1 | lon peptidase 1 | Higher in TOR |
| ALDH6A1 | aldehyde dehydrogenase 6 family, member A1 | Lower in IBA |
| PCCA | propionyl CoA carboxylase, alpha polypeptide | Lower in IBA |
| TRAP1 | TNF receptor-associated protein 1 | Lower in IBA |
| PCK2 | phosphoenolpyruvate carboxykinase 2 | Lower in IBA |
| HADH | hydroxyacyl-CoA dehydrogenase | Higher in IBA & TOR |
| ACADS | acyl-CoA dehydrogenase, C-2 to C-3 short chain | Higher in TOR |
| PHB2 | prohibitin 2 | Higher in TOR |
| SUCLG2 | succinyl-CoA ligase [GDP-forming] beta subunit | Higher in TOR |
| DECR1 | 2,4-dienoyl-CoA reductase | Lower in IBA |
| AIFM1 | apoptosis-inducing factor, 1 | Higher in TOR |
| ECHS1 | enoyl-CoA hydratase, short chain,1 | Higher in TOR |
| IDH3B | isocitrate dehydrogenase 3 beta | Higher in TOR |
| TIM44 | translocase of inner mitochondrial membrane 44 | Higher in TOR |
| CPT1B | carnitine palmitoyltransferase 1B | Higher in TOR |
| SHMT2 | serine hydroxymethyltransferase 2 | Higher in IBA & TOR |
| SAMM50 | sorting and assembly machinery component 50 | Lower in IBA |
| HSD17B4 | hydroxysteroid (17-beta) dehydrogenase 4 | Higher in TOR |
| ETFA | electron-transfer-flavoprotein, alpha polypeptide | Higher in IBA |
| SDHB | succinate dehydrogenase complex, subunit B | Lower in IBA |

| | | |
|---|---|---|
| ETFB | electron-transfer-flavoprotein, beta polypeptide | Lower in IBA |
| GOT2 | glutamic-oxaloacetic transaminase 2 | Lower in IBA |
| PCCB | propionyl CoA carboxylase, beta polypeptide | Higher in TOR |
| ECH1 | enoyl CoA hydratase 1 | Lower in IBA |
| CKMT1B | creatine kinase U-type, mitochondrial isoform X2 | Lower in IBA |
| ACAT1 | acetyl-CoA acetyltransferase 1 | Higher in IBA & TOR |
| SLC25A12 | solute carrier family 25, member 12 | Lower in IBA |
| LAP3 | leucine aminopeptidase 3 | Lower in IBA |
| ACSS1 | acyl-CoA synthetase short-chain family member 1 | Lower in IBA |
| PMPCA | mitochondrial-processing peptidase subunit alpha | Lower in IBA |
| NLRX1 | NLR family member X1 | Higher in TOR |
| SLC25A20 | solute carrier family 25, member 20 | Higher in TOR |
| SLC25A11 | solute carrier family 25, member 11 | Higher in TOR |
| ABCB8 | ATP-binding cassette, sub-family B member 8 | Higher in IBA & TOR |
| SUCLG1 | succinate-CoA ligase, alpha subunit | Higher in TOR |
| PLIN1 | Perilipin 1 | Lower in IBA |
| IDH3G | isocitrate dehydrogenase, subunit gamma | Lower in IBA & TOR |
| MLYCD | malonyl-CoA decarboxylase | Higher in TOR |
| PDHX | pyruvate dehydrogenase complex, component X | Lower in IBA |
| MUT | methylmalonyl-CoA mutase | Higher in TOR |
| ALDH4A1 | aldehyde dehydrogenase 4 family, member A1 | Lower in IBA |
| ALDH9A1 | aldehyde dehydrogenase 9 family, member A1 | Lower in IBA |
| AK3 | adenylate kinase 3 | Lower in IBA |
| AMACR | alpha-methylacyl-CoA racemase | Higher in TOR |

| | | |
|---|---|---|
| ACSS3 | acyl-CoA synthetase short-chain family member 3 | Higher in TOR |
| AK2 | adenylate kinase 2 | Lower in IBA |
| QIL1 | chromosome 19 open reading frame 70 | Higher in TOR |
| MECR | mitochondrial trans-2-enoyl-CoA reductase | Higher in TOR |
| SLC4A1 | solute carrier family 4, member 11 | Higher in TOR |
| ECI2 | enoyl-CoA delta isomerase 2 | Lower in IBA |
| NNT | nicotinamide nucleotide transhydrogenase | Lower in IBA |
| GSTZ1 | glutathione transferase zeta 1 | Higher in TOR |
| VDAC2 | voltage-dependent anion channel 2 | Higher in TOR |
| GCDH | glutaryl-CoA dehydrogenase | Higher in TOR |
| PRDX3 | peroxiredoxin 3 | Lower in IBA |
| DNAJC11 | DnaJ (Hsp40) homolog, subfamily C, member 11 | Lower in IBA |
| BCKDHA | branched chain keto acid dehydrogenase E1, alpha | Higher in TOR |
| NDUFA7 | NADH dehydrogenase 1 alpha subcomplex, 7 | Lower in IBA |
| SLC25A3 | solute carrier family 25, member 3 | Lower in IBA |
| MTCH2 | mitochondrial carrier 2 | Lower in IBA |
| CYCS | cytochrome c, somatic | Higher in TOR |
| ALDH7A1 | alpha-aminoadipic semialdehyde dehydrogenase | Higher in TOR |
| DBT | dihydrolipoamide branched chain transacylase E2 | Lower in IBA |
| DHRS4 | dehydrogenase/reductase member 4 | Lower in IBA |
| PITRM1 | pitrilysin metallopeptidase 1 | Lower in IBA |
| SLC25A11 | solute carrier family 25, member 11 | Higher in TOR |
| IVD | isovaleryl-CoA dehydrogenase | Higher in TOR |
| ACSM5 | acyl-CoA synthetase medium-chain family member 5 | Lower in IBA |

| | | |
|---|---|---|
| TMEM143 | transmembrane protein 143 | Lower in IBA |
| OAT | ornithine aminotransferase | Higher in TOR |
| LACTB | lactamase, beta | Lower in IBA & TOR |
| ACSF2 | acyl-CoA synthetase family member 2 | Higher in IBA & TOR |
| NUDT13 | nudix-type motif 13 | Lower in IBA |
| TIMM50 | translocase of inner mitochondrial membrane 50 | Higher in TOR |
| CISD3 | CDGSH iron sulfur domain 3 | Higher in TOR |
| AASS | aminoadipate-semialdehyde synthase | Higher in TOR |
| PMPCB | peptidase beta | Lower in IBA |
| ACTB | actin, beta | Higher in TOR |
| PDPR | pyruvate dehydrogenase phosphatase regulatory subunit | Lower in IBA |
| TSFM | Ts translation elongation factor | Higher in TOR |
| EHD2 | EH domain-containing 2 | Higher in TOR |
| COQ10B | coenzyme Q10 homolog B | Lower in IBA |
| D2HGDH | D-2-hydroxyglutarate dehydrogenase | Higher in TOR |
| | | Higher in TOR |